University of Rome "Tor Vergata"
Department of electronic engineering

Doctorate in

Sensorial and learning systems engineering

Title of the thesis

Analytical System with Familiar Devices

XIX Cycle

Candidate

Adriano Alimelli

Supervisor

Corrado Di Natale

Acknowledgments

First of all, I would like to give my special thanking to the Doctorate Coordinator, Prof. R. Marino, to my Doctorate Supervisor Prof. C. Di Natale, to Prof. A. D'Amico and Prof. R. Paolesse from our University for their important contribution to this thesis.

I wish also to thank Prof. I. Lundstrom and Prof. D. Filippini for giving me the possibility to establish a continuous and fruitful collaboration with the *Department of Physics of University of Linkoping, Sweden.*

I would like to also thank Dr. G. Ciolfi and Dr. S. Moretti from *Isituto Sperimentale per l'Enologia,* Velletri (Rome) for the contribution to the experiments on wines, and *Ginevri s.r.l* from Pavona (Rome) for the contribution to the experiments on bilirubin.

I'm deeply indebted with all my friends from laboratories of *Electronic Engineering* and *Sciences and Chemical Technologies* Departments, and *CNR-IMM,* where I've been able to perform the most part of my work.

Index

Chapter 2

Chemical-Interactive-Materials: Porphyrins, related Metal complexes and TetraPyrrolic Compounds

Chapter 3

CSPT-Enose mode based Chemical Sensor Array

Chapter 4

CSPT-Spectroscopy mode: Wine Optical Properties detection and Bilirubin analysis

Chapter 5

Further Applications

Preface

In the last few years there has been a huge demand to monitor different chemical environments, such as for example urban indoor and outdoor atmospheres, food aromas, etc. Chemical sensors are among the most promising devices to be exploited for these kind of applications.

The structure of a generic chemical sensor can be ideally divided in two subunits: the sensing material and the transducer.

The Chemical Interactive Material (CIM) interacts with the chemical species present in the environment by changing some of its physico-chemical properties, while the transducer transforms these variations in a readable signal, generally an electric signal.

Then, one of the possibility, of course much rising, to developing a chemical sensor is to exploit the optical proprieties of the CIMs.

Indeed, optical properties of sensitive layers are very interesting to fabricate chemical sensors because the optical properties, such as absorbance and fluorescence, are strongly influenced by the interaction with guest molecules. Nonetheless, the chemical practice of this approach is badly balanced by the transducer counterpart. Indeed, traditional optical instrumentations of high quality are usually bulky and expensive.

For example, the measure of fluorescence for analytical purposes is rather limited by the relative complexity and cost of the opto-electronic setup although the miniaturization efforts have reduced the complexity and the cost of such instrumentations, the application of optical methods, although encouraging, has been hindered by the relative high cost of the instrumentation.

On the other side in the last decade, in spite of the high cost of optical instruments, we assisted to a fast growth of performance in fields as consuming electronics, giving rise to a number of low-cost advanced optical equipments such as digital scanners, cameras, and screens whose characteristics largely fit the requirements necessary to capture change of

optical properties of sensitive layers in many practical applications, that could be usefully exploited in routine analysis.

A first demonstration in this direction was given by Suslick and colleagues when they shown how a simple flatbed digital scanner could be converted into a powerful analytical instrument for the detection of subtle colour changes in chemical dyes for the detection of volatile compounds. More recently Filippini and Lundström showed that a combination of a computer monitor and an inexpensive web cam may be turned into a sort of spectrophotometer instrument. This last technique, known as Computer Screen Photo assisted Technique (CSPT) is based on the fact that a computer screen can be easily programmed to display millions of colour, combining wavelengths in the optical range. Compared with the use of digital scanner, to probe the sample with a variable combination of wavelengths instead of use the white light of scanners, gives the possibility to perform a spectroscopy measurement combining absorbance and fluorescence of samples. Due to the large diffusion of portable computers, PDAs, and cellular phones all endowed with colour screen, camera, and an even more extended computation capabilities, the application of the CSPT concept may be foreseen as to give rise to a sort of ubiquitous analytical capacity.

Then CSPT could in principle be used to detect general parameters related to the absorbance-emission spectra of every material under observation.

In this Thesis, we show the possibility to use this very simple platform, based on computer screen and a web cam (CSPT), in two different configuration (Enose-mode and Spectroscopy mode), for very different kind of applications.

In fact, in the first case, we present a chemical gas sensor array where the optical features of layers of chemicals are transduced by CSPT-Enose mode (Chapter 3 and 4); while in the second case we highlight the potentiality to use the CSPT such as a spectrophotometer, to directly optical characterize the compounds that we are observing (Chapter 5).

INTRODUCTION

In the last years there has been a huge progress in Chemical Optical Sensors, nowadays optical sensors are used in numerous scientific and technical applications. The recent increase of the exploitation of optical sensors in research and development, in automation and many kinds of measuring systems has made impossible describing in details all chemical optical sensors in few pages but only giving an introductory overview. There are also a large a variety of different components that are used in sensor technology: light sources, detectors and different kinds of optical parts. The availability of semiconductor light sources, detectors, fibre and integrated optics and image sensors has provided us with revolutionary opportunities for new and even, in some cases, low cost optical sensors. Furthermore different detection schemes depending on wavelength, phase and pulsetime. For all these reasons only some of the main sensors will be shown, providing knowledge on a variety of optical sensor techniques: in fact the unique aim of this survey is giving a concise collection of knowledge to this highly interdisciplinary field, an ideal starting point and a source of information.

OPTICAL RADIATION

The Optical radiation is part of electromagnetic radiation, which extends over a continuous spectrum and is embedded approximately from wavelengths of 1 nm to 1 mm, the range between X-rays and radio waves, as shown in Figure 1. The propagation of electromagnetic waves is completely described by a system of differential equations, known as Maxwell's equations, and by the electromagnetic properties of the medium. The electromagnetic radiation has a continuous spectrum; the different spectral range are fixed by convention and there exists no discontinuity in the spectrum.

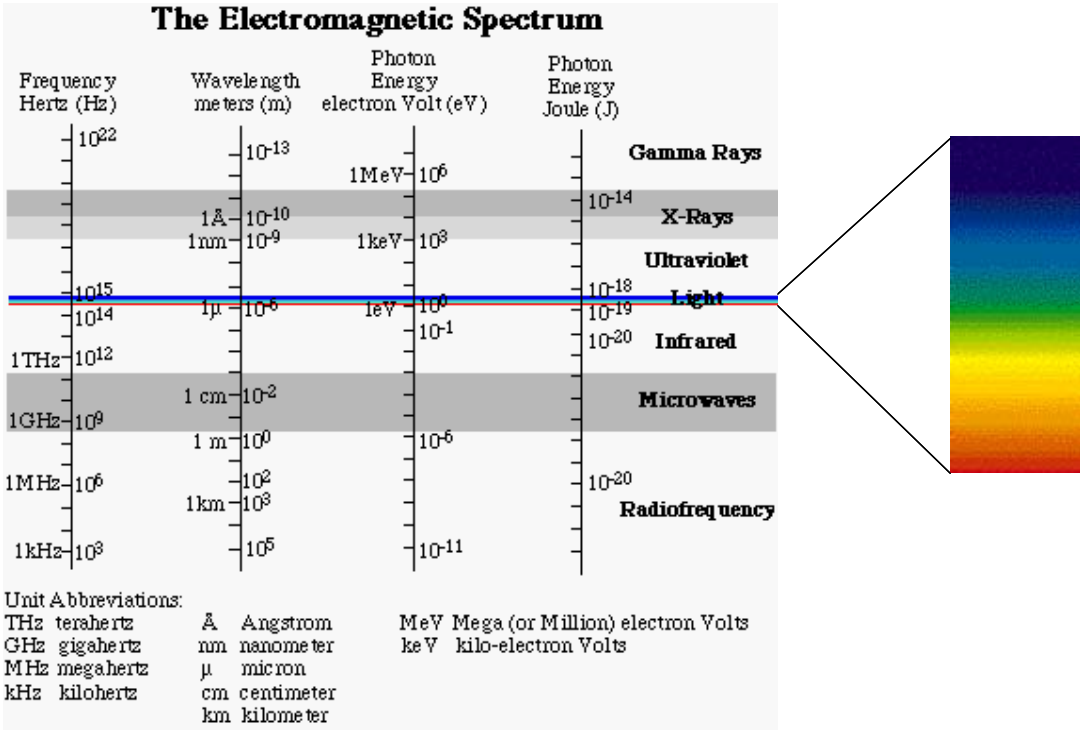

Figure 1: The electromagnetic Spectrum.

The basic laws of electromagnetism were found by Coulomb, Ampère, Gauss, Faraday, Biot and Savart. Maxwell combined the different observations to a consistent set of differential equations by introducing four vector fields, which depend on space and time.

For the purposes of this Thesis, it is not important describing in details the propagation laws of optical radiations and the optical components that are used in systems like sensors to collect, distribute, modify or analyze optical radiation, but the aim is showing an overview of the main techniques used in chemical optical sensing.

OPTICAL SENSORS

Optical sensing became a key technique for many measuring tasks, so a growing numbers of chemical optical sensors are continuously developed. In general optical sensors are devices that measure the modulation of a light property, i.e. they can measure absorbance, fluorescence, reflectance, refractive index, interference, polarization and scattering. Optical sensors are formed by 4 or 3 components:

1. *Light source* (such as solid state laser, laser diode, light emitted diode (LED) etc, for investigating the sensor;
2. *Optics* for guiding light to and from the Sensor;
3. *Detector* (such as photodiode, CMOS detector, charge coupled device (CCD) camera etc)for detecting the light signal coming from the sensor;
4. The *Sensor*.

There are two many kinds of optical sensors:

- Intrinsic and
- Extrinsic.

In the first case the chemical species that must be measured, are themselves the sensors so only three components are required inasmuch as the sensor transduction mechanism is intrinsic to the molecule. In fact some organic molecules absorb light at particular wavelengths and/or fluoresce and therefore emit light at specific wavelengths. In this way we can detect directly these kind of molecules simply by measuring absorbance and/or fluorescence at their absorption and emission wavelengths.

In the second case, the most optical sensors, an sensing material, that changes the optical properties, is employed. These species can be very different, polymers, dyes, porphyrins and all the materials that can interact with the analytes changing or modulating optical signals. Besides a lot of substrates can be used for optical sensors such as glass slides, polymeric films etc.

A wide range of light-based chemical sensors have been developed using a variety of different devices and materials, then in the next paragraphs will be shown some of the key approaches for building optical sensors highlighting every time the different waveguides used, the several sensing materials exploited and the optical transduction mechanisms. The huge possibility of developing optical chemical sensors, for example matching different sensing materials with several waveguides, it has made impossible finding a key to separately classify the different methods used or the single applications developed , but only giving an brief overview.

FIBRE-OPTIC APPLICATIONS

Central to many optical chemical sensors is the exploitation of one of the several available waveguides. Fibre-optics, capillary tubes and planar waveguides all use the phenomenon of total internal reflection. The increasing use of optical fibres along with photosensors and optical transducers has led to the development of a range of devices that are specially intended for chemical optical sensors. The development of optical sensors became feasible with the availability of optical fibers in the visible range. Recent developments are concerned with the extension of the visible spectral range to include fiber-optic sensors in the UV, near-and mud-IR range. Apart from fiber optical sensors, there is also an interest in sensors based on planar optics.

One of the more interesting methods to employ for building a chemical optical sensors is the fluorescence, because of well separated excitation and emission spectrum, high quantum yield, and intrinsic sensitivity. Fluorophores are molecules that absorb light at specific wavelengths and emit light a longer wavelengths. This difference in wavelengths and thus in energy is due to the Stoke's shift and represents vibrational relaxation and other energy losses [1]. Quantum yield or quantum efficiency is how well absorbed photons are converted to emitted photons.

In general, fiber optical sensors generate an optical signal in proportion to the analyte concentration. The application of optical fibre sensing technique to chemical and biochemical sensing, with applications in industrial plant and to a large range of biomedical functions, is one of the fastest growing areas in opto-electronics. There are essentially two main techniques currently under investigation:

- The first uses a multimode fibre to convey light to a sample region, where it either suffers spectrally-dependent absorption or causes fluorescence in the chemical sample (or CIM). The absorption/fluorescence spectra are then monitored via the light returning in the same, or other, fibre.

▪ The second technique involves coating the tip of a fibre with a material which reacts more or less selectively with an analyte present in a sample, in a predictable way, to provide measurable changes in the optical properties of the material. These changes may again be in the absorption/reflection spectra, or in the nature of the fluorescence. Furthermore if the indicator is immobilized on the core of a waveguide, the measurement of evanescent waves is feasible for determination of analyte.

The fibre tips, in both the above cases, are sometimes referred to as "optodres" or "optodes". The simplest type of optical fiber sensor involves coupling an optical fibre to a spectrophotometer. With this device, the color of fluorescence of solutions or of bio-chemical matter can be measured. In this case, the waveguide merely serves to transfer the radiation. Instead of a photometer the fibers may be linked by means of a optoelectronic circuit; in this case, the light source can be a light emitted diode (LED) and the detector a photodiode.

In order to illustrate the applicability of fiber-optical sensors some fundamentals of waveguides are considered.

Fibre cable consists of a core (the waveguides) and a cladding both made from glass, quartz, or plastic. The cables diameters range from 0.05 μm to 0.6 cm. The light propagates down a single fibre or a fiber bundle. The bundle can be arranged randomly or in a fixed position at the input and output of the fiber. When light reaches the waveguide, part of it is transmitted and part is totally reflected.

For the total reflection of light to occur, a critical angle θ is necessary, and the refractive index of the core $n1$ has to be higher than the refractive index of the *cladding* $n2$. The refractive index of the glass core is ~ 1.6 and that of glass cladding ~ 1.5. For measurements in the mid-IR range other materials are necessary. The critical angle θ is determined by the *numerical aperture (NA)* of the waveguide. *NA* depends on the refractive index of the core $n1$ and of the cladding $n2$:

$$NA = \sin\theta = \sqrt{n_1^2 - n_2^2}$$

The larger the numerical aperture, the more light the waveguide can capture and transmit.

There are many examples of application that involve fibre-optics in optical chemical sensing. Walt [2] et al. first combined fiber-optics with fluorescent dyes for measuring of organic compounds in 1991. They had used a polarity-sensitive, solvatochromic dye Nile Red. Other research groups have also exploited fluorence-based technique for vapor sensing. There are some mechanisms that give florescent properties to dye. One of these is TICT, twisted intramolecular charge transfer, excited state. Exploiting this mechanism Orellana [3] has been able to demonstrate the reversible measurement of various alcohols by absorbing these particular dyes to silica gel and immobilizing the resulting gel at the tip of an optical fibre. Since these first experiences an increasing number of research groups have begun to incorporate betaine dyes onto the end of optical fibres in various ways to develop chemical sensors.

The sensors based on solvatochromic dyes embedded in polymers have been exploited to develop a cross-reactive vapor sensors array by Dickinson [4]. In this device, Nile Red was immobilized within different polymers, which were dip coated onto the ends of individual optical fibres. Nineteen sensors were bundled into an array format. Upon exposure to an organic vapor, each polymer sensor absorbed vapor according to its partition coefficient for that vapor. The change in each sensor's fluorescence spectrum depended on how much vapor partitioned into that sensor as well as the difference between the vapor's and polymer's polarities. Fluorescence detection was accomplished by using a two-dimensional detector, a CCD camera, so that we could acquire fluorescent signals from all the sensors in the array simultaneously. To simplify signal detection, the fluorescence was collected at a single wavelength by interposing an emission filter between the fiber and the CCD chip. Some of the polymers exhibited a swelling effect in which the polymer volume increased as vapor partitioned into it. Therefore, the response of each sensor is due to a combination of vapor partitioning into the polymer, polarity differences between the polymer and the vapor, but also polymer swelling. But, because this deposition method ,there were a

lack of reproducibility of the sensing films. To avoid this effect has been exploited the difference in materials composition between clads and cores, that provides a method for selectively etching the cores. When the polished distal tip of a custom optical imaging fiber array is placed into an acid etchant, the cores etch at a faster rate than the clads leading to an array of wells. At the bottom of each well is the distal face of an optical fiber. In this way, each well is "optically wired" to its own individual optical fiber. We discovered that latex or silica beads, matched in size to the dimensions of the individual wells, would spontaneously assemble into each well in a highly efficient self-organizing fashion. This approach could be used to create sensor arrays based on polymeric microspheres. Microspheres sensors can be created by taking monodisperse polymeric microspheres and swelling them in a suitable organic solvent containing dissolved Nile Red [5]. Upon removal from the solvent, evaporation of residual solvent occurs resulting in Nile Red being trapped within the polymeric matrix. Another class of bead sensors uses surface modified silica beads to which Nile Red is adsorbed. Many different bead types can be prepared out of a variety of polymers and surface functional groups. To create a sensing array, the desired individual bead types are mixed, i.e. 100 milligrams of beads contains approximately 10 billion beads. Then, the beads are randomly distributed onto the distal face of an etched imaging fiber such that one bead occupies each well. In order to register the position of each bead in the array after fabrication, the fiber is connected to the optical imaging system and a vapor is pulsed onto the fiber's sensor end and a registration protocol as "self-encoding" is used to identify them.

All the sensor beads of a particular type give virtually identical responses because they are all prepared at the same time. Another important feature of these cross-reactive optical arrays is the built-in redundancy of each of the sensors: replicates provide significant advantages in terms of signal-to-noise. The microsphere arrays also have several other advantages such as flexibility of array types, scalability, and simple manufacturing. The major limitation with fluorescent dyes for optical sensor arrays is photobleaching: upon exposure to light, any indicating material loses its intensity

because of photooxidation. Nevertheless all the limitations due to their short history, this kind of “optical electronic” noses are very interesting for very point of views.

Another possibility is the exploitation of host-guest supramolecular chemistry for sensing. Host compounds that trap guest molecules have been used for detecting solvent vapors [6]. These host materials surround the guest vapor molecules and form inclusion complexes with specific crystal structures that show both wavelengths shift and quantum intensity changes in their emission spectra. This bathochromic shifts are due to various energy losses relative to increased packing density.

Another possible approach is the exploitation of chemiluminescence based sensors that used chemically reactive materials capable of directly emitting photons following oxidation, without using an excitation source to generate the emission signal. In this way becomes possible simplify the instrumentation. This technique has been used to detect oxygen, metal ion and organic vapors (chlorinated hydrocarbons, hydrazine and ammonia [7]). The reagent luminol was used to detect oxidants, while a $Ru(bpy)_3^{3+}$ complex was used for reductants. Luminol sensing capacity was expanded to halogenated hydrocarbons by the addition of an in-line heated platinum filament used as a pre-oxidative step.

COLORIMETRIC TECHNIQUES

These sensors are able to measure indicator color changes. They can measure changes in absorbance and/or in local refractive index. There have been developed a lot of vapor sensors using colorimetric techniques. One of these was done by Wohltjen et al. [8] that developed a reversible capillary tube for detecting ammonia, hydrazine and pyridine, by coating a glass capillary with an oxazine perchlorate dye film. This dye upon exposure to these volatile compounds changes its color and then its transmission property. This change is revealed by using a simple phototransistor. Stetter, Maclay and Ballantine [9], in similar vay, detected and quantify H2S and HCl acid vapors down to 10 ppb level by using a coating of bromothymol.

Even commercial thermal printer papers have been exploited to measure solvent vapors. Wolfbeis and coworkers [10] showed that these materials have reversible interactions with solvent vapors, and when they were being exposed to ether they produced a black color or a dark blue. Were developed sensors for detecting typical laboratory solvents (i.e. alcohol, acetates etc) by incorporating these papers into various optical devices and monitoring light absorption at 605 nm.

Polymers are another class of compounds most exploited in optical vapor sensing for their differential vapors sorption and binding properties as well as their emissive properties. An example is a amine-containing poly(vinylchloride) membranes based sensor that detects 2,4-dinitrotoluene (DNT), a compound commonly present in land mines [11]. Absorption into the polymer generates a complex with an absorbance at 430 nm that is monitored over time to detect DNT level.

Therefore the importance of sensing material is clear in all of these different methods. Also inorganic compounds are successfully exploited as sensing materials. Mann et al. [12] have demonstrated shifts in maximum absorption and emission wavelengths of platinum and palladium isocyanide complexes upon exposure to VOCs. For example the Pt-Pt compound $[Pt(p\text{-}C_{10}H_{21}PhNC)_4][Pt(CN)_4]$, was used to detect CHCl3.

Photostability and an insensitivity to water vapor make inorganic materials particularly attractive for incorporation into an electronic nose sensing device. Metalloporphyrins, as will be shown in detail in Second Chapter, are good inorganic sensing materials as they are well-characterized, stable and easily modifiable by a wide range of central metals and/or external substituents. D'Amico and colleagues [13] have developed a device for distinguishing between six different liquors by monitoring absorbance changes with a simple LED and photodetector system exploiting an array of cross-sensitive metalloporphyrins.

Suslick and Rakow [14] also exploited an array of different metalloporphyrins, in this experience with an inexpensive and consumer device, a flatbed scanner. This array was formed by spotting these CIMs onto silica TLC plates. The measure has been performed by simply color subtracting of the array imaging before and after vapor exposure, acquired by the scanner. 15 minutes exposures were used to ensure maximum array response, good reversibility, reproducibility and sensitivity. These two previous examples of optical sensors are the precursors of further opto-electronic noses.

SURFACE PLASMON RESONANCE

Coordination polymers can be also exploited as sensing layers in a Surface Plasmon Resonance (SPR) setup for detecting ethanol, water, toluene, benzene and acetonitrile [15]. The SPR method exploits the delocalized conducting electron clouds found at the surface of metal films such as gold or silver. These electron clouds maintain a collective wave vector parallel to the interface. Therefore, by lighting with a particular wavelength and polarization at the interface, any changes in the refractive index at the surface, caused by the sorption of vapor molecules into a polymer network at the surface, can be measured in real-time by monitoring the illumination angle needed to give a minimum in the measured reflected light. Otherwise a white light source can be used to investigate the wavelength at which the SPR occurs [16]. The refractive index change could be correlated with the swelling swelling and increased density of the polymer due to absorption of the volatile compounds. Abdelghani et al. [17] have exploited the PSR method with an optical fibre. They have coated the core of silica fibre by a 50 nm thick layer of silver and, to protect against oxidation, have assembled alkanethiol layers onto the silver layers. Finally they have chosen a fluorinated siloxane layer because its refractive index, surface tension and gas permeability properties. By this sensor they have detected high ppm level for both the aromatic and chlorinated compounds with very long measure and recovery times.

INTERFERENCE AND REFLECTION BASED TECHNIQUES

Another interesting technique is the use of interference spectroscopy. In fact the analyte-swelled polymer layers have much larger changes in optical thickness then refractive index [18]. In this way Gauglitz et al. have developed Reflectometric Interference Spectroscopy (RIfS) techniques for optical vapor sensing. In this approach, light incident at the interface between two planar optical layers can be reflected from both the top and bottom of a polymer sensing film, setting up an interference pattern that is very sensitive to changes in the optical thickness of the polymer layer. Unfortunately these devices are usually much expensive, even if less expensive RIfS sensors with comparable sensitivity have been developed using four inexpensive LEDs and a single photodiode [19].

The RIfS technique has also been extended to enantiomer discrimination. By depositing polymer solutions containing chiral peptide residues from the 'Chirasil-Val' chromatographic stationary phase, Göpel and colleagues [20] studied the responses of their sensors to several mixtures of (R) and (S) – methyl lactate in varying proportions.

Interference methods have been also applied to porous silicon chips (PSi). Sailor et al. [21] have developed simple chemical etching methods for generating porous silicon films that display both interferometric and photoluminescence properties. In the case of photoluminescence, the quenching can be induced via energy transfer by the adsorption of analyte molecules in the pores of the silicon. Thus, by monitoring emission at a specific wavelength (670nm in this experience), sharp decreases can be observed in intensity as the interaction with analyte vapors becomes. Likewise, adsorption events give rise to refractive index changes that lead to shifts in Fabry-Perot interference fringes, measured as changes in reflectivity. Both of these optical attributes were recently used to measure a range of perfumes and solvent vapors.

Another absorbance-type of vapor sensor is based on simple transmission attenuation through a fibre. Microbending caused by the vapor-induced swelling of siloxane layers adjacent to the fibre results in transmission attenuation [22].

Resonating microcantilevers, such as those used in atomic force microscopy (AFM) for atomic-level imaging, are another creative reflection-based method for chemical sensing . Based on the mass-sensing concepts of resonating piezoelectric crystals (e,g, quartz crystal microbalance (QCM)), the approach uses 180 μm-long cantilevers micromachined into silicon that are sensitive to changes in mass occurring at their surfaces. Several groups have explored coating polymer films onto these cantilevers and measuring small changes in mass loading. The technique uses optical detection by measuring the deflection of an incident laser beam as analyte vapors are adsorbed to the surface.

Another research group [23] developed arrays of differentially-coated cantilevers for detecting alcohols, water vapor and several natural vapors. The array sensor was constituted of eight cantilevers coated with different thin films (platinum, PMMA, alkythiol SAMs and zeolites). They used a single laser and a photo-sensitive device for reading sequentially out the array.

SCANNING LIGHT PULSE TECHNIQUE

Lundstrom et al. [24] have developed an innovative optical technique: the so called Scanning Light-Pulse technique. The light impinges on the surface of a MOSFET coated with a thin metal film and penetrates the metal to induce a photocapacitive current. To maintain a constant current, the applied gate voltage must be varied to sustain a constant surface potential. Changes in the gate voltage are monitored and result in a map of ΔV as a function of position on the sensing surface. In a particular experience for detecting ethanol, hydrogen and ammonia, a MOSFET array was coated by three continuous strips of Pt, Pd, and Ir. The sensor surface was divided into a grid, and a temperature gradient (110 - 180°C) was established down the length of the sensor surface. This temperature gradient provided a different sensitivity and selectivity at each point of the sensor grid. The results of measurements were a map of the changes in voltage (ΔV). In this way image maps of the gases were created. These sensor grids can be applied to identifying gas mixtures, rapid and simultaneous screening of new sensing materials, and mapping spatially inhomogeneous reactions. Light-pulsed sensing combines many types of information, including the catalytic activity of the gate metals, gas flow turbulence, edge effects, etc. While not an optical detection technique, the method demonstrates the utility of employing light combined with electrochemical detection.

All these examples of applications are shown above in Table 1.

Transduction Technique	**Description**
Luminescence	Fiber-optic sensors using polarity sensitive fluorophores such as solvatochromic or TICT dyes.
	Randomly-assembled solvatochromic bead arrays.
	Host-guest supramolecular chemistry: shifts in wavelength and intensity of "fluoroclathrands" based on packing density changes caused by vapors.
	Chemiluminescence-based detection, using luminol and Rubipy dyes.
Colorimetric	Color changes of an oxazine perchlorate dye coated on glass capillaries.
	Bromothymol blue in Nafion polymer layers.
	Thermal printer papers as vapor sensors.
	Inorganic sensing materials (e.g. Pt-Pt compounds): color changes caused by perturbation of stacking in charged complexes.
	Metalloporphyrins: formation of coordination complexes with analytes, and use of different metals for changing sensing properties..
Surface Plasmon Resonance (SPR)	Method for detecting changes in refractive index at a surface.
Interference, reflection	Reflective Interferometric Spectroscopy (RifS) for detecting changes in optical thickness of polymer layers.
	Interference measurements using chemically etched porous silicon chips.
Mass loading	Detecting mass changes on resonating AFM microcantilevers.
Scanning light pulse technique	Detecting voltage changes at a MOSFET surface using light to generate the photocapacitive current.

Table 1: Brief and schematic optical chemical sensors overview.

ADVANTAGES AND DISADVANTAGES OF OPTO CHEMICAL SENSORS

Optical transduction methods based on sensors have a lot of advantages over other sensing methods. First of all most of devices (light sources, optics and detectors) used for optical sensors have been already well developed for other applications. Moreover optical signals are not sensitive to electromagnetic interferences. Light is fast and its attenuation is very low through modern optical fibre, that enables remote sensing over long distances without amplifiers or repeaters. Fluorescence, but in general all the optical measurements, is extremely sensitive and can be exploited to detect lowest concentration levels of molecules. Optical sensing can be multiplexed because different optical signals can be carried and detected simultaneously (i.e. optical fibres).
On the other hand, there also some disadvantages. Optical devices are often much expensive and complex. Optical technique are sometimes sensitive to interference by stray light. Besides fluorescent indicators often are photodegradable. For these reasons a variety of electronic noses have been developed exploiting different optical transduction methods [25].

REFERENCES

[1] J. Lakowicz, Principles of Fluorescence Spectroscopy. Plenum Press, New York, 1982.

[2] S. Barnard, D. R. Walt, Environ. Sci. Technol., 1991, 25, 1301-1304.

[3] G. Orellana et al, Anal.Chem. 1995, 67, 2231 – 2238.

[4] T.A. Dickinson, D.R. Walt, J. White, J.S. Kauer, Anal. Chem., 1997, 69, 3413-3418

[5] T.A. Dickinson, K.L Michael, J.S. Kauer, D.R. Walt, Anal. Chem., 1999, 71, 2192-2198.

[6] T. H. Brehmer, P. P. Korkas, E. Weber, Sensors and Actuators. 1997, 44, 595 – 600.

[7] G. E. Collins, S. L. Rose-Pehrsson, Sensors and Actuators. 1996, 34, 317 – 322

[8] Giuliani et al. Reversible Optical Waveguide Vapor Sensor. United States Patent Number 4,513,087. April 23, 1985.

[9] J.R. Stetter, J. Maclay, D.S. Ballantine, Optical Waveguide Vapor Sensor. United States Patent Number 5,315,673. May 24, 1994.

[10] H. E. Posch, O. S. Wolfbeis, Pusterhofer, J. Talanta. 1988, 35, 89 – 94.

[11] L. Gheorghiu, W. R. Seitz, D. Arbuthnot, J. L. Elkind. SPIE Conference on Environmental Monitoring and Remediation Technologies II. 1999, 3853, 296 – 302.

[12] C. A. Daws, C. L. Exstrom, J. R. Sowa, Jr., K. R. Mann. Chem Mater. 1997, 9, 363 – 368.

[13] A. D'Amico et al. Sensors and Actuators. 1999, 65, 209 – 215.

[14] N.A. Rakow, K.S. Suslick. Nature. 2000, 406, 710 – 713.

[15] R. Casalini et al,. Sensors and Actuators. 1999, 57, 28 – 34.

[16] R.W. Nelson, J.R. Krone, O. Jansson, Anal. Chem., 1997, 69, 4369-4374.

[17] A. Abdelghani et al,. Analytica Chemica Acta. 1997, 337, 225- 232.

[18] K. Spaeth, G. Kraus, G. Gauglitz, Fresenius' J. Anal. Chem., 1997, 357, 292.

[19] R. Reichl, R. Krage, C. Krummel, G. Gauglitz. Applied Spectroscopy. 2000, 54, 583 – 586.

[20] K. Bodenhofer et al. Nature. 1997, 387, 577 – 580.

[21] S. Letant, S. Content, T. Tan, F. Zenhausern, M. Sailor, Sensors & Actuators B¸2000, 69, 193-198.

[22] A. Yasser, B. Lawrence. Sensors. 1996, April, 76 – 77.

[23] H. P. Lang, et al. Appl. Phys. Lett. 1998, 72, 383 – 385.

[24] M. Lofdahl, M. Eriksson, I. Lundstrom Sens. Actuators B, 2000, 70, 77-82.

[25] K.J.Albert, N.S. Lewis, C.L. Schauer, G.A Sotzing, S.E. Stitzel, T.P. Vaid, and D.R. Walt, Chem Reviews, 2000, 100, 2595-2626.

CHAPTER 1

Computer Screen Photo-assisted Technique

INTRODUCTION

A lot of chemical and biochemical analysis make use of visible absorption measurements [1] to read the information they codify. Assays typically are arrays of samples with different transmittance spectra which suffer changes upon target reactions, which are evaluated with dedicated and expensive instruments which minimally comprise a two dimensional position controlled light source of tuneable wavelength and modulated intensity.

Furthermore these kind of assays are not universal, but optimised to identify well defined target processes instead, in this work the evaluation of visible absorption-emission is quite reduced simply using inexpensive and ubiquitous devices which can be universally used for very different sorts of chemical analysis.

In fact, in this Thesis, we especially consider emerging applications as 'home tests' or 'self-tests' where the existing instrumentation is too expensive or complex, making necessary a more versatile and simpler approach.

In tune with this goal here are presented a method to measure visible absorption features by colour recognition using a programmable large area light source provided by broadly available LCD computer screens, working in the simplest case with a web camera as detector, the so called Computer Screen Photo-assisted Technique.

The computer screen photo-assisted technique (CSPT) is a method for optical characterization of absorbing, reflective or fluorescent substances that just utilizes regular computer sets and web cameras as a measuring setup. Due to their versatility and global dissemination, CSPT setups are an attractive alternative for the evaluation of home test; especially considering its natural ability to evaluate complex response patterns suitable with increasingly sophisticated tests for medical [2] or environmental purposes. CSPT is also an imaging technique able to adapt to multiple assay formats providing multiple determinations with a single familiar platform.

1.1. THE COLOUR: THE HUMAN PERCEPTION OF ELECTROMAGNETIC FIELD

To well understand the CSPT work principle, it must be taken in account that the CSPT is essentially a colorimetric technique, for this reason in this Section will be shown some of the fundamentals of the Colour, and its perception by the human beings.

Optical radiation is part of electromagnetic radiation with wavelengths from 1 nm to 1 mm, the range between X-rays and radio waves. According to the vocabulary of the Commission International de l'Eclairage (CIE) [3] optical radiation is divided into many ranges which are shown in Figure 1 in the Introduction Section.

The visible spectrum is the portion of the electromagnetic spectrum that is visible to the human eye. Electromagnetic radiation in this range of wavelengths is called visible light or simply light. There are no exact bounds to the visible spectrum; a typical human eye will respond to wavelengths from 400 to 700 nm, although some people may be able to perceive wavelengths from 380 to 780 nm.

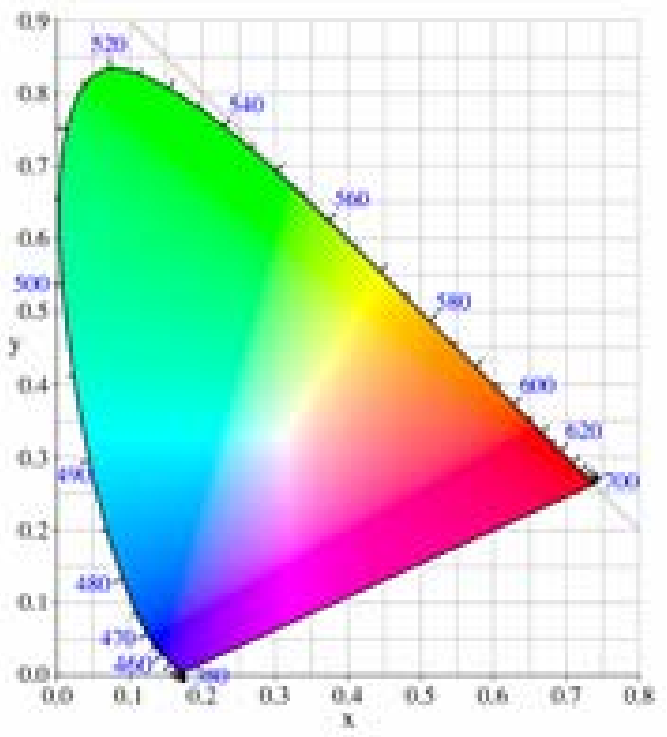

Figure 1.1: The CIE 1931 colour space chromaticity diagram with wavelengths in nanometers. Note that the colors depicted depend on the color space of the device on which you are viewing the image.

In Table 1.1 are reported all the primaries colors and relative wavelengths.

Wavelengths [nm]	**Light color**
380-420	Violet
420-440	Indigo
440-500	Blue
500-520	Cyan
520-565	Green
565-590	Yellow
590-625	Orange
625-740	Red

Table 1.1: The colours of Visible Spectrum and the relative wavelengths.

Newton divided the spectrum for the first time into seven named colors: Red, Orange, Yellow, Green, Blue, Indigo, and Violet; or ROYGBIV. He chose seven colors out of a belief, derived from the ancient Greek philosophers, that there was a connection between the colors, the musical notes, the known objects in the solar system, and the days of the week (Figure 1.2).

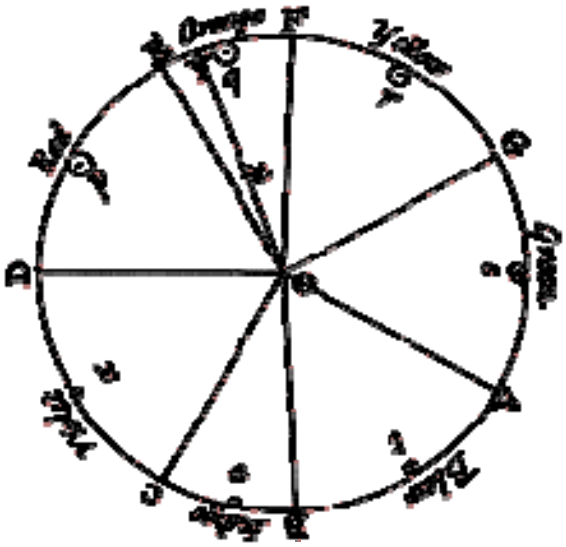

Figure 1.2: Newton's color circle, showing the colors correlated with musical notes and symbols for the planets.

The human eye is relatively insensitive to indigo's frequencies, and some otherwise well-sighted people cannot distinguish indigo from blue and violet. For this reason some commentators have suggested that indigo should not be regarded as a color in its own right but merely as a shade of blue or violet. Some of the explanations of the optical spectrum came from Isaac Newton, when he wrote his Opticks [4] (see Figure 1.3). Newton first used the word *spectrum* (Latin for "appearance" or "apparition") in print in 1671 in describing his experiments in optics. Newton observed that, when a narrow beam of white sunlight strikes the face of a glass prism at an angle, some is reflected and some of the beam passes into and through the glass, emerging as different colored bands. Newton hypothesized that light was made up of "corpuscles" (particles) of different colors, and that the different colors of light

moved at different speeds in transparent matter, with red light moving more quickly in glass than violet light. The result is that red light was bent (refracted) less sharply than violet light as it passed through the prism, creating a spectrum of colors.

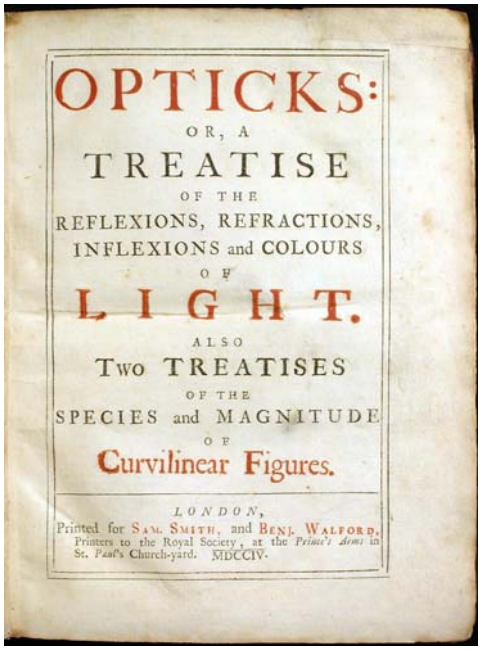
OPTICKS:
OR, A
TREATISE
OF THE
REFLEXIONS, REFRACTIONS,
INFLEXIONS and COLOURS
OF
LIGHT.
ALSO
Two TREATISES
OF THE
SPECIES and MAGNITUDE
OF
Curvilinear Figures.
LONDON,
Printed for SAM. SMITH, and BENJ. WALFORD,
Printers to the Royal Society, at the Prince's Arms in
St. Paul's Church-yard. MDCCIV.

Figure 1.3: Opticks or a treatise of the reflections, refractions, inflections and colours of light

A light-adapted eye typically has its maximum sensitivity at around 555 nm, in the green region of the optical spectrum (see Figure 1.4). The spectrum does not, however, contain all the colors that the human eyes and brain can distinguish. Brown, pink, and magenta are absent, for example, it depends on the particular combination of the wavelengths in the light.

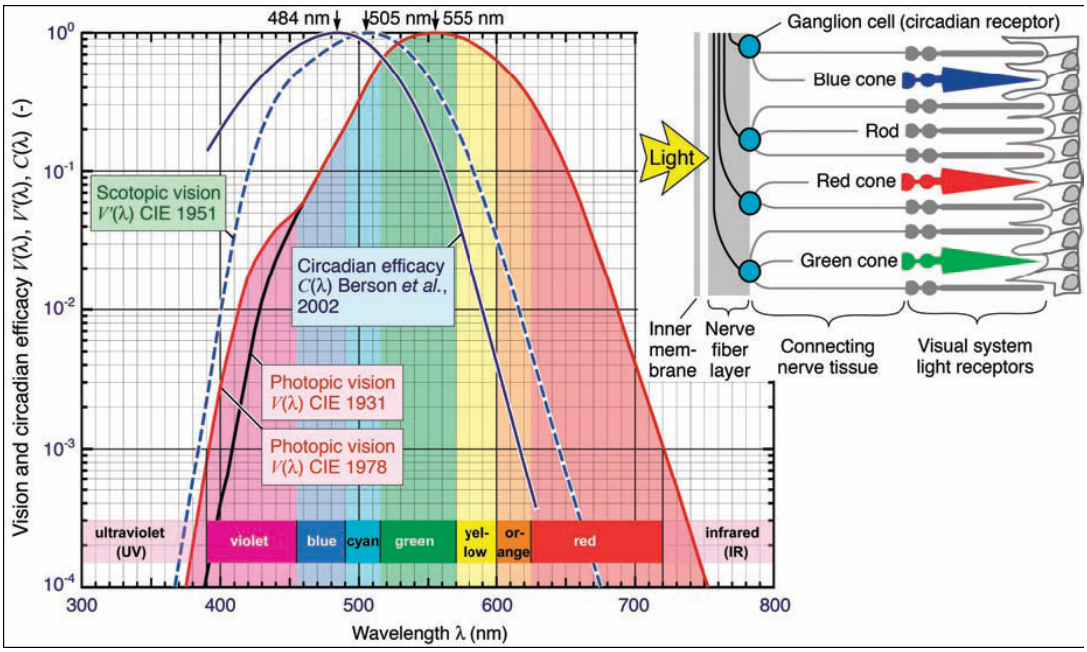

Figure 1.4: CIE eye sensitivity function V(λ) for the photopic vision regime mediated by retinal cone and rod cells. Also shown is the eye sensitivity function for the scotopic vision regime, V (λ), that applies to low ambient light levels, and the circadian efficacy curve C(λ) derived from retinal ganglion cell photoresponse.

Then the colour is the human perception of light.

There are three types of color receptors (known as cone cells) in human beings. This confers trichromatic color vision, so these primates are known as trichromats. In the human eye, the cones are maximally receptive to short, medium, and long wavelengths of light and are therefore usually called S-, M-, and L-cones (Figure 1.5). L-cones are often referred to as the red receptor, but while the perception of red depends on this receptor, microspectrophotometry has shown that its peak sensitivity is in the yellow region of the spectrum. "Scotopic" (dark-adapted) and "photopic" (light-adapted) sensitivities differ; scotopic peak sensitivity (of the rod cells) is at about 500 nm, while photopic sensitivity (of the cone cells) peaks at around 550 nm (Figure 1.7). It is well known that the spectral sensitivity of the cone cell–rich central vision region of the retina is different from the rod cell–rich peripheral vision region of the retina.

Cone cells in the human eye

Cone type	Name	Range	Peak sensitivity
S	β (Blue)	400..500 nm	440 nm
M	γ (Green)	450..630 nm	544 nm
L	ρ (Red)	500..700 nm	580 nm

Figure 1.5: Cone-cells properties.

Recently, a remarkable discovery was made: a fifth type of photoreceptor had first been postulated and then identified in the retina of the human eye, more than 150 years after the discovery of the rod cells and the red-, green-, and blue-sensitive cone cells [5, 6]. The fifth type of photoreceptor, the ganglion cell, had been believed to be merely a nerve interconnection and transmitter cell. Such cells are now believed to be instrumental in the regulation of the human circadian (wake-sleep) rhythm. Because ganglion cells are most sensitive in the blue spectral range (460 to 500 nm, Figure 1.4), they act as a "blue-sky receptor", that is, as a high-color-temperature receptor. The physical process of seeing begins with the absorption of a photon by a pigment called "retinal". We can define a pigment as a substance which is "photoreactive", that is, which absorbs (and possibly re-emits) wavelengths in the visible range. The absorption causes a change in the geometry of the retinal (in the terms of organic chemistry, it changes from a "cis" to an "all-trans" configuration) [7].

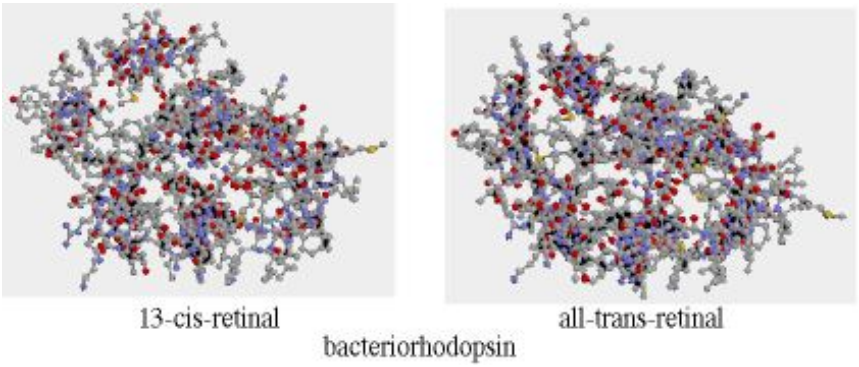

Figure 1.6: Geometry changes of the retina during light sorption.

This change in geometry takes place in about 6 ps. It has the effect of activating an enzyme (phosphodiesterase) which in turn hydrolyzes hundreds of "cylic-GMP" molecules (guanosine 3' - 5' phosphate) which in turn effects the sodium channels in optic nerves, initiating a nerve impulse. (Note that at the level of proteins, geometry defines function; this business of shape-changing, as well as "key and lock" shape fitting, is a ubiquitous signaling mechanism in the world of molecular biology.) The specific protein to which the retinal is linked determines the range of wavelengths to which it is sensitive. Retinal linked to rhodopsin has a peak sensitivity of about 498 nm. Rhodopsin is the protein in human rod cells as well as in many photoactive organisms.

The theories of color try to explain the phenomena of color vision; they are based on Grassmann's law which states that each color can be realized by mixtures of three color stimuli [8, 9] matching the typical human cone responses (and the rod response) (see Figure 1.7)to monochromatic spectral stimuli.

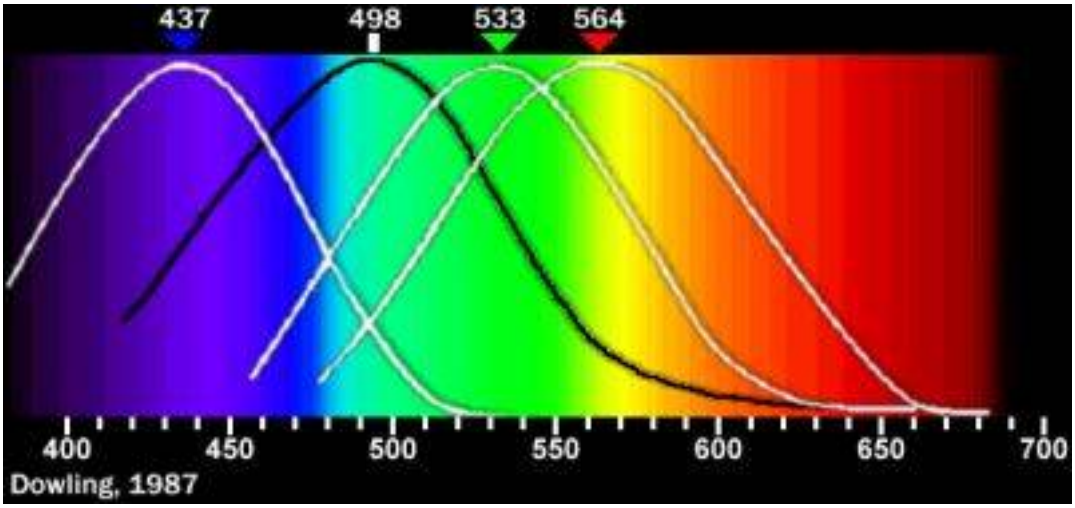

Figure 1.7: Normalized typical human cone responses (and the rod response) to monochromatic spectral stimuli.

1.2. THE CONCEPT

The measuring procedure of CSPT experiments is standard and very simple.
This kind of measurements only involves a desktop computer with a LCD screen and a webcam (in this Thesis a Logitech Quickcam pro 4000 operating at a resolution of 320x240 pixels) in addition to an suitable software that provides to acquisition and data analysis.
During a CSPT measurement the screen illuminates the array with an appropriate sequence of colours, while the webcamera captures the image of the array under analysis in synchronism with the illumination. The result of this data acquisition is a video stream, where regions of interest (ROIs) are selected (white circles in Figure 1.8) and the intensity of the recorded pixels averaged into these regions chosen by us. The procedure is repeated along all 50 (length of the colour sequence) frames, corresponding to an illuminating sequence resembling the human perception of the visible spectrum. In this way a 50 elements vector is obtained for each ROI and camera channel. A fingerprint of the complete array is often constructed by concatenating red, green and blue channel vectors of each ROI and subsequently by collecting the different ROI vectors in a single (*N*M*3)* elements vector, where *N* is the length of the colour sequence, M is the number of the ROIs selected and 3 is the number of camera channel (Red, Green and Blue), as we will see in details in next paragraphs.

1.2.1. LCD Screen as programmable light source

Computer screens are not only our main computer interface, they are also widely configurable solid-state light sources [10]. They are capable of displaying confined areas of arbitrary shape, colour, and intensity that can be two-dimensionally scanned on the screen with 200 μm resolution [11]. All of this is achieved without moving parts and eventually has the possibility of becoming portable, as in the case of LCD displays in cellular phones. It is also true that they are not the natural choice of light sources for analytical purposes;

however, they are everywhere and always inherently combined with substantial computing power, and their versatility and processing capabilities allow many of their weaknesses to be overcome.

The research group of Suslick, as well as others, have already demonstrated that polychromatic source, as flatbed scanners, can be used as light source for colorimetric assays [12]. In our studies, the choice of LCD screen for this purpose has been shown more flexibility, as has been demonstrated by D. Filippini and I. Lundstrom [2]. In fact LCD screens and flatbed scanners have got similar lamp, how it can seen in Figure 1.8, where it is shown a comparison of the emission spectra for these two kind of devices. But the fundamental difference between using a device rather another one as light source, it is the possibility of modulating the intensity of emission spectra of the LCD screen [13]. The flatbed scanner give out pseudo white light whereas the emission spectra of second device can be suitable programmed with an appropriate software. In this way we can modulate intensity of the three primary band of emission (Red, Green and Blue) as we wish.

Instead of exiting the target assay only by a white polychromatic light, we are able to use different colours in order to deeper investigate optical properties of our array. Therefore we generate a two-dimensional widows with different tonality of colour simply weighting the three primary colours.

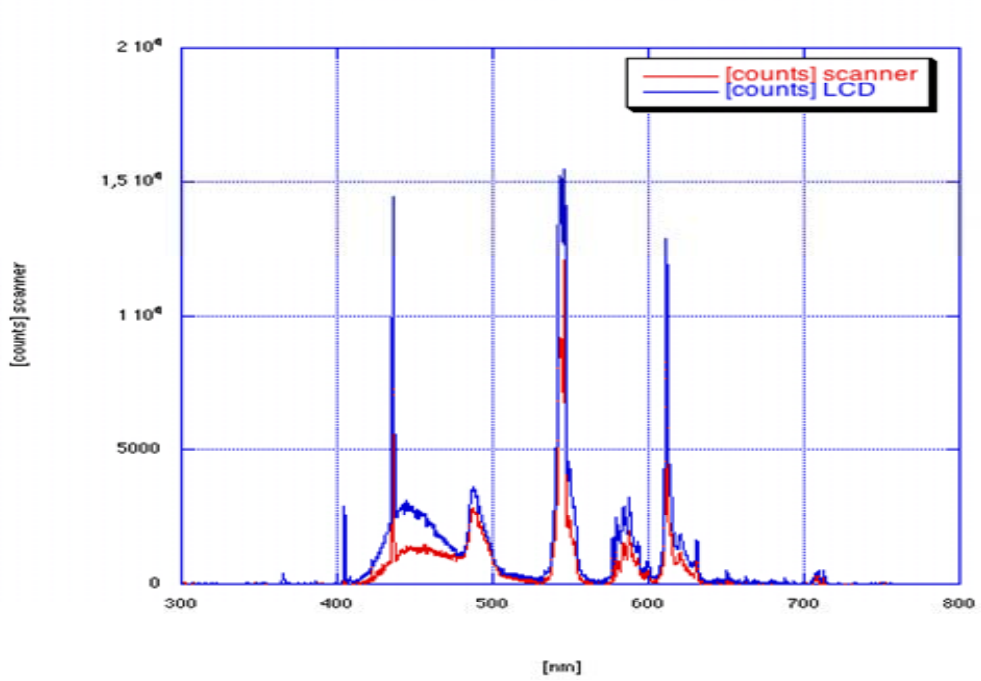

Figure 1.8: Scanner and LCD spectra emission comparison

1.2.2. Web Camera: 3 filters light detector

An increasing internet demand has allowed a multimedia devices evolution, like a web camera. Consequently a price reduction has introduced a huge number of suitable devices for our purpose. Therefore a web camera has become a familiar device with promising potentiality as instrumental for colorimetric assays [14].

The CCD (charge-coupled device) detector embedded, an invention originally intended for use as a digital memory, is the core of this kind of device. The basic building block for this detector is the MOS capacitor. It serves as a photon-sensing, storage and information-transferring element. A CCD is generally formed by an array of MOS capacitors in a two, three or four phase arrangement to the bus lines. Such as structure is capable of sensing a given light distribution by transforming incident photons into a pattern of discrete charges.

A lot of webcameras have enough pixel resolution and a video setting control that enable for colour recognition. In fact a web camera like a Logitech Quickcam PRO 4000, with a CCD

detector operating at a low resolution of 320 x 240 pixels, it is enough for being used as light detector in the CSPT platform. It is obvious that the control of the camera parameters varies from platform to platform. So the goal is to retain as much as possible of the full range of each colour channel (0–255 counts) for spectrally coincident illumination, and simultaneously to have zero counts for illuminating spectra outside each camera filter.

1.3. CSPT WORKING PRINCIPLE

As told above, the computer screen photo-assisted technique aims at evaluations of colorimetric assays [2] using only one instrumentation composed by regular computer sets and web cameras [15]. The availability and familiarity of such components are clear advantages, as are the versatility associated to the inherent computer power and the imaging capabilities supported by the web camera that enables the evaluation of assays with arbitrarily different formats.

In CSPT experiments, a part of the computer screen is used as a controlled light source displaying a colour sequence that illuminates the assay while the web camera records the image of the assay under the different illuminations. Further processing allows composing distinctive substance fingerprints from these measurements.

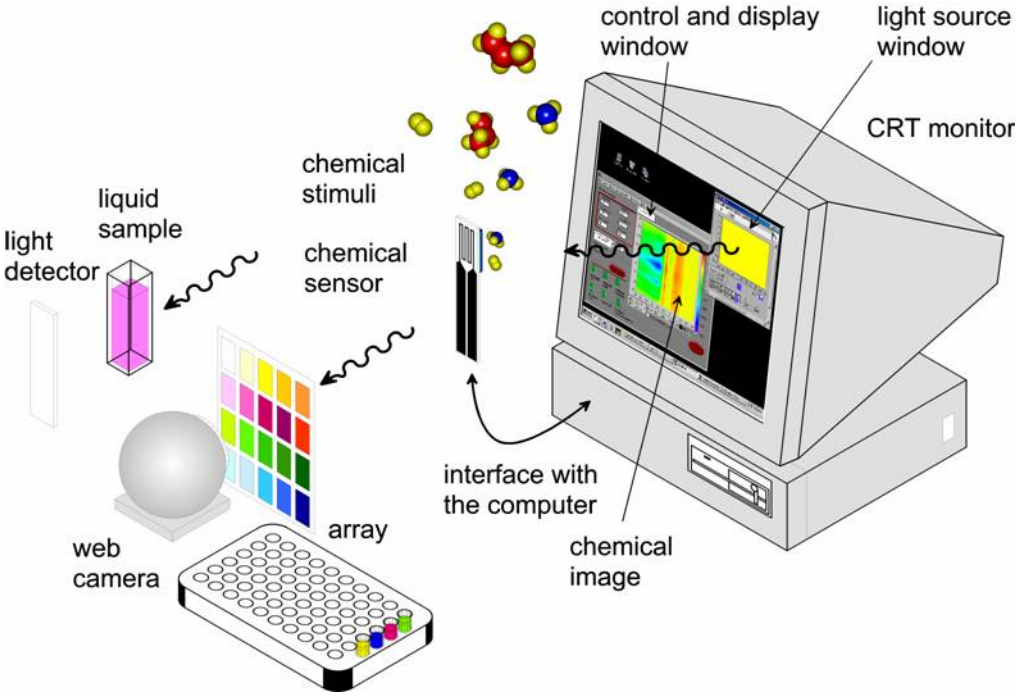

Figure 1.9: Schematic CSPT platform

Any colour, c(λ), displayed on the screen is represented by a linear combinations of the screen spectral radiances (R(λ), G(λ) and B(λ)) [10] as:

$$c_i(\lambda) = r_i R(\lambda) + g_i G(\lambda) + b_i B(\lambda) \qquad (1)$$

where the triplet of weights (r_i, g_i and b_i) specifies any particular color $c_i(\lambda)$ of an illuminating sequence *s* and λ is the wavelength, which in this thesis is limited to the interval [400, 700] nm.

True color screens can display up to 224 = 16.777.216 different colors defined by triplets (r_i, g_i, b_i) that can be represented as 3D points in a red, green and blue space. In the present study the color space is often represented by a 50 elements grid that retains its extremes and intermediate points.

Figure 1.10 displays this set of illuminating colors.

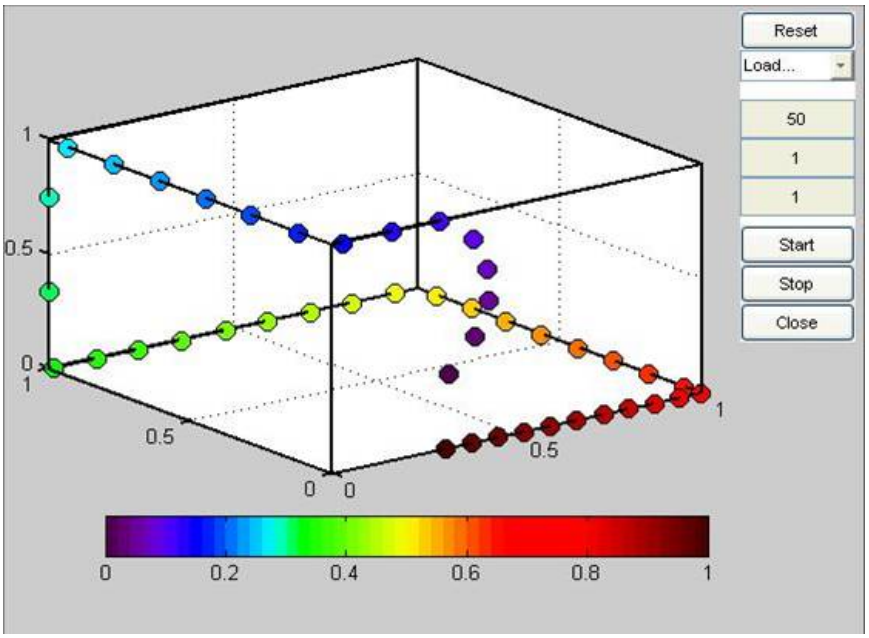

Figure 1.10: User interface of MatLab Program that controls Acquisition of video stream (measure acquisition) . There is showed a sequence of 50 colors covering the whole visible range, represented in the 3D RGB Space.

The primaries themselves are not monochromatic but a particular spectral distribution instead, how it can be seen in Figure 1.11.

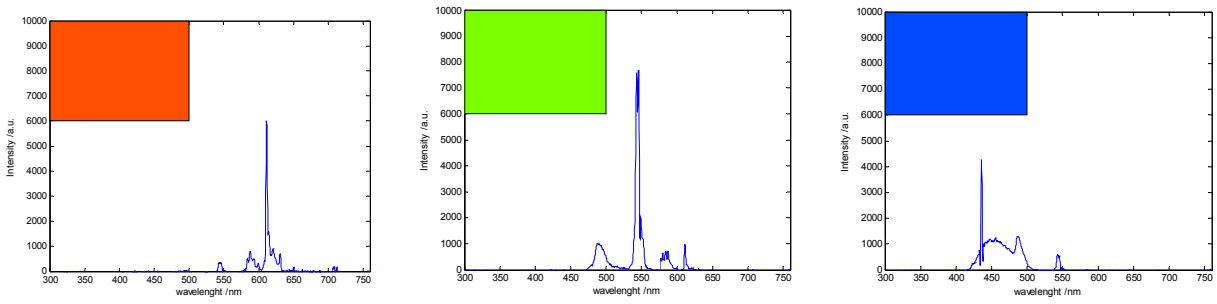

Figure 1.11: Spectra and relative color tonality of 3 primary colors (Red, Green Blue).

1.3.1. Programs description

All the processes, data acquisition, spectral fingerprints extraction and finally an appropriate multivariate data analysis, are managed by software.

A program written in MatLab® by us controls the illumination and camera acquisition composing as result of the measurement a video stream of the samples under different light colors. This can be done in different ways but in this case was carried out using specially designed software as described below.

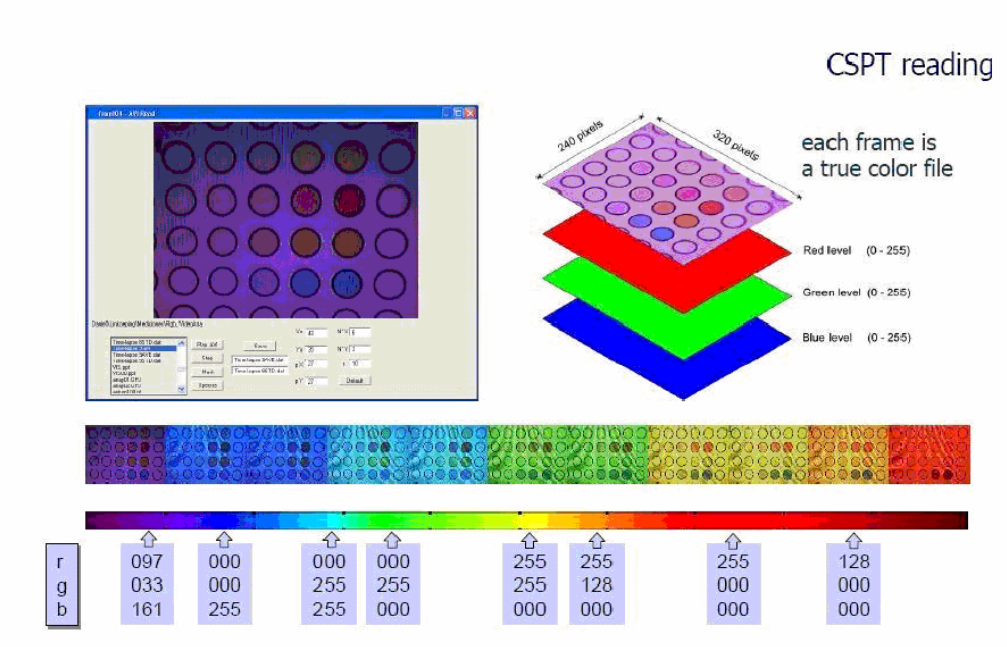

Figure 1.12: Screen colors through magnitude of intensities of three primaries in 256 levels. Electronically determined through the choice of the three levels (color indices, rgb)

Acquisition v1.0, developed in MatLab 7 R14 conceived as a simple interface for users. This program controlled camera settings, image acquisition, illuminating colors and the numeric masking and data extraction of the ROIs, whose coordinates were read from a configuration file or manually written.

The software produced a data array containing intensity values of the selected ROIs that were transferred for analysis to a standalone mathematic kernel written in MatLab 7 R14. This program performed calibration and control routines, extracting CSPT spectral fingerprints from the ROIs that were then used for classification and subsequent evaluation of the assay. Subsequent processing allows the composition of sample fingerprints and color classification; the details of this processing and classification routines are discussed after, in the next paragraph.

All these processing steps are transparent to the user in Acquisition, which only interacts with a graphic user interface that does not request a particular carefulness and displays the results of the evaluation. The illuminating sequence can be chosen from a lot of presents or created by the user. The illuminating sequence oftener used in this study was a optimized 50 color set chosen for providing a good sample classification in a short measurement time. The optimization colour sequence is composed of 50 different colors displayed at a rate of 1 color per second, then the total measuring time is accordingly these 50 seconds used for acquisition plus few seconds for processing depending on the computational power of the particular device, computer, cellular phone etc. It must be noted that the imaging capabilities of CSPT allows acquisition of all the ROIs at the same time independently of the number of ROIs by contrast with conventional reading that takes several more time for colorimetric test.

Each frame of the video stream is masked with a configured pattern of circles (sensitive ROIs: Figure 1.13), as previous told, that extracts the average value of all the pixels within each circle (the pixels number changes in each different kind of assay) for each channel of the web camera and for each frame of the stream.So, for M samples illuminated by N different colors and observed through the three camera channels, all the acquired information can be collected in an average transmitted or reflected light intensity tensor $I_{i,j,k}$ with:

$$i \in [1, N], j \in [1, M] \text{ and } k \in [1, 3]$$

In order to compensate from particular characteristics of the measuring platform and from random fluctuation of both LCD colour emission and Web camera RGB filters, a second set of regions is masked on the white regions between printouts. With similar procedures a reference tensor $I_{oi,j,k}$ is composed (background ROIs: Figure 1.13)

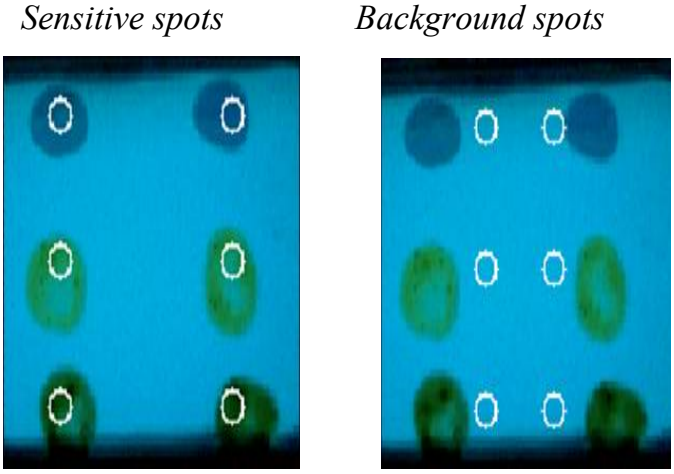

Figure 1.13: ROIs selections : Two different kinds of ROI; On the left ROIs of a sensitive layer array; On the right a possible choice of ROIs for background compensation of the near sensitive spots.

1.4. CSPT-SPECTRAL FEATURES: FINGERPRINTS EXTRACTION

For each color displayed on the screen, a composed spectral radiance is emitted and specifically modulated by the transmittance of the tested substance $T(\lambda)$. The emerging light passes through the camera filters ($F_R(\lambda)$, $F_G(\lambda)$ and $F_B(\lambda)$) exciting the detector, which has a defined spectral response $D(\lambda)$.

The transmittance corresponding to a substance j, is modelled as:

$$T_j(\lambda) = 1 - e^{-(\lambda - \lambda_j / \sigma)^2} \qquad (1.2)$$

where σ =50 nm and λ_j indicates the minimum transmittance of the substance j.

The measured intensities of every camera pixel, for every illuminating color i and substance j is then calculated as:

$$\begin{cases} I_{Ri,j} = \int_{\lambda} c_i(\lambda) \cdot T_j(\lambda) \cdot F_R(\lambda) \cdot D(\lambda) \cdot d\lambda \\ I_{Gi,j} = \int_{\lambda} c_i(\lambda) \cdot T_j(\lambda) \cdot F_G(\lambda) \cdot D(\lambda) \cdot d\lambda \\ I_{Bi,j} = \int_{\lambda} c_i(\lambda) \cdot T_j(\lambda) \cdot F_B(\lambda) \cdot D(\lambda) \cdot d\lambda \end{cases} \qquad (1.3)$$

The result of illuminating with a color sequence of N colors is to obtain an intensity profile from each channel of the web camera.

A common practice in CSPT experiments is to concatenate the intensity profiles of the camera channels forming a $3 \times N$ elements vector for every substance j.

$$\begin{cases} I_{[1,N],j} = I_{Ri,j} \\ I_{[N+1,2N],j} = I_{Gi,j} \\ I_{[2N+1,3N],j} = I_{Bi,j} \end{cases} \qquad (1.4)$$

Then the unfolding of the recorded information along the color channels of the web camera enables to generate distinctive substance features that retain key spectral information (spectral fingerprints), which are able to disentangle predominant emission from absorption features (Figure 1.14).

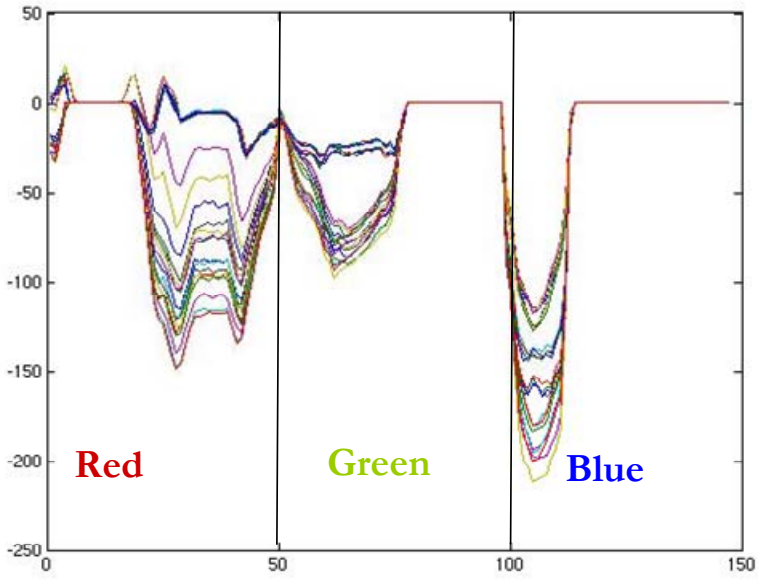

Figure 1.14: Overlap of fingerprints of the same substance in different conditions, obtained by Eq. 1.4, concatenating intensity profiles.

Then the measured space contains both the spectral signature of the substances and that of the particular CSPT assembly where the measurement is performed. In order to highlight the substance signature, the measured space is subtracted by the measured space without substance (a sort of background compensation). The resulting profiles are henceforth referred to as the CSPT fingerprints of the substances. This is not the only method to extract spectral fingerprints from substances, but of course it is quite intuitive and very interesting for our studies.

Therefore the CSPT measurement of any substance transmittance or reflectance transforms this illuminating space into a measured space distinctive of the substance. Each tested

substance produces an intensity signature according to Eq. 1.4. In theory the linear combination of three spectral radiances and the three overlapping filters of the web camera produce up to nine different spectral windows of analysis specifically modulated by a given tested substance, which means that more than three colors per substance are redundant [16] (Figure 1.15). Thus, the problem of classifying sets of *n* transmittances consist of maximizing the differences between these modulated windows of analysis [17] (evaluated by their areas according to Eq.1.3).

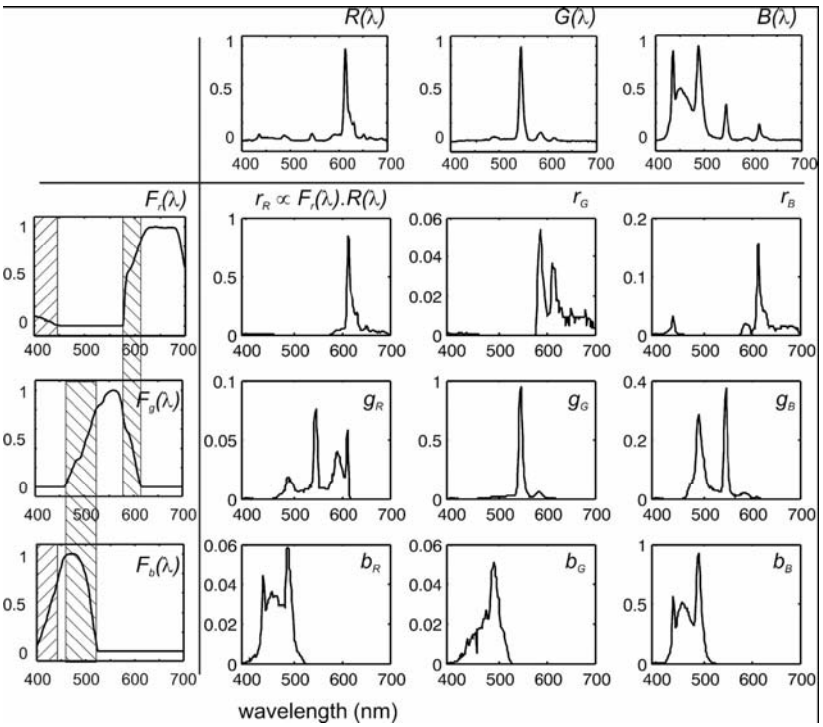

Figure 1.15: Nine spectral windows formed by combinations of a LCD screen spectral radiances and the web camera filters for a sample transmittance T(λ)=1 λ [390 nm,700 nm]. The hatched areas highlight the overlaps of the camera filters. Note the different amplitude of the windows.

By the way, it is interesting underline the two main methods used to extract information from CSPT measurements. In fact, as we will see in details in the next chapters, there is not a rule to find the best method how to do this, but this strongly depends by the kind of the assay we are measuring, by the sort of spectra which is detecting (reflectance or transmittance) and last but not least by the mode we are using the CSPT platform (e.g.

Spectroscopy mode or E-nose mode). Then it is really clear the way that these CSPT signals are composed has a main impact on the ability to distinguish the tested substances and consequently to evaluate the tests. So the CSPT fingerprints (a distinctive spectral signature of the substances) can be either difference or ratio fingerprints depending on how the spectral features of the used platform are compensated, as mentioned above.

Exploring convenient ways for feature extraction it is become clear that to compensate the spectral features of any particular platform in the fingerprints extraction we should involve two main possibilities. One alternative consists of disentangling the samples signatures from the platform features in order to evaluate a 'universal' substance fingerprint. More practical and robust, however, is to measure the samples together with calibrations (e.g. a set of possible assay outcomes) and comparing signatures obtained in a same instrument. To improve the attainable classifications the way of performing the experiments can be flexibly tuned when using CSPT platforms, for instance, adapting the illuminating sequence to a particular assay, customizing the camera settings or as in this case exploring particular processing strategies for different kinds of measurements. These strategies will be described in details in next chapters 3, 4, 5 where very different measurements were performed by CSPT.

1.4.1. RGB-Colour sequence optimization

We also investigated the optimization of illuminating sequences and the best possible performances of these optimum configurations for sets of substance transmittances systematically scanning the whole visible spectrum. The numerous possible combinations of substance sets and optimum configurations excluded the systematic experimental examination of the problem, which instead has been accomplished with the aid of a CSPT model. It is experimentally known that the performance of the CSPT evaluation, assessed as its ability to distinguish sets of colour substances, depends on the composition of the illuminating sequences and on the colours of the tested array of substances. As can be seen, by customizing the illumination is possible to maximize the ability of CSPT to distinguish substance transmittances that just differ from each other in a 10 nm shift.

Considering the CSPT fingerprints, other alternatives are feasible to enhance the substances classification, such as adapting the illuminating colors to maximize a particular target, nevertheless, for practical applications it is also important to minimize the illuminating sequence in order to keep the measurement time short.

In principle, the illuminating colors are just linear combinations of three screen spectral radiances, and only three colors should be enough to reconstruct any spectra in about 9 points (considering the unfolding in the three channels of the web camera), however, in practice the classification of sets of color samples depends on the choice of the illuminating colors, which are not necessarily the same for a different set of samples. The selection of an optimum illuminating sequence for several sets of color indicators is not trivial, and has been solved ad hoc, by means of longer sequences that despite the redundancy have better chances to compensate for the ignored optimum conditions. This approach can compensate several instrumental weaknesses, then the influence of the CSPT platform in the classification is minimized, making it more robust to random fluctuations in the instrument and allowing a simpler use. Even with a non-optimum illuminating sequence, in the this

thesis there will be showed an appropriate performance of the CSPT evaluation for the intended use.

1.4.2. Effect of fingerprints conformation

Introducing equation 1.2 in equation 1.3 and rearranging, we obtain:

$$\begin{cases} I_{Ri,j} = r_i \int_\lambda R_i(\lambda)\cdot T_j(\lambda)\cdot F_R(\lambda)\cdot D(\lambda)\cdot d\lambda + \\ g_i \int_\lambda G_i(\lambda)\cdot T_j(\lambda)\cdot F_R(\lambda)\cdot D(\lambda)\cdot d\lambda + b_i \int_\lambda B_i(\lambda)\cdot T_j(\lambda)\cdot F_R(\lambda)\cdot D(\lambda)\cdot d\lambda \\ I_{Gi,j} = r_i \int_\lambda R_i(\lambda)\cdot T_j(\lambda)\cdot F_G(\lambda)\cdot D(\lambda)\cdot d\lambda + \\ g_i \int_\lambda G_i(\lambda)\cdot T_j(\lambda)\cdot F_G(\lambda)\cdot D(\lambda)\cdot d\lambda + b_i \int_\lambda B_i(\lambda)\cdot T_j(\lambda)\cdot F_G(\lambda)\cdot D(\lambda)\cdot d\lambda \\ I_{Bi,j} = r_i \int_\lambda R_i(\lambda)\cdot T_j(\lambda)\cdot F_B(\lambda)\cdot D(\lambda)\cdot d\lambda + \\ g_i \int_\lambda G_i(\lambda)\cdot T_j(\lambda)\cdot F_B(\lambda)\cdot D(\lambda)\cdot d\lambda + b_i \int_\lambda B_i(\lambda)\cdot T_j(\lambda)\cdot F_B(\lambda)\cdot D(\lambda)\cdot d\lambda \end{cases} \quad (1.5)$$

Or briefly:

$$\begin{pmatrix} I_{Ri,j} \\ I_{Gi,j} \\ I_{Bi,j} \end{pmatrix} = \begin{pmatrix} r_R & r_G & r_B \\ g_R & g_G & g_B \\ b_R & b_G & b_B \end{pmatrix} x \begin{pmatrix} r_i \\ g_i \\ b_i \end{pmatrix} = S\,x \begin{pmatrix} r_i \\ g_i \\ b_i \end{pmatrix} \quad (1.6)$$

where the terms of the substance matrix S are functions of T(λ), and retain up to nine spectral windows of the substance transmittances, captured through these combinations of screen radiances and camera filters. The intensities measured in this way contain the spectral information that would allow spectral reconstruction, but also the spectral characteristics of the platform embedded in the signature. So far, two main approaches have been followed for highlighting the substance features: difference CSPT fingerprints and

ratio CSPT fingerprints depending on how a reference measurement for a sample with T(λ) = 1 is used. These two methods give different results such as more or less intuitive fingerprints, different performances with fluorescent substances or diverse classification.

1.4.2.1. Difference CSPT fingerprints

In this kind of fingerprint the spectral signature of the substance is highlighted by subtracting the spectral signature of the setup (T(λ) = 1).
Equation (1.7) and (1.8) describe this procedure:

$$\begin{pmatrix} \Delta I_{Ri,j} \\ \Delta I_{Gi,j} \\ \Delta I_{Bi,j} \end{pmatrix} = \begin{pmatrix} I_{Ri,j} - I^{0}{}_{Ri,j} \\ I_{Gi,j} - I^{0}{}_{Gi,j} \\ I_{Bi,j} - I^{0}{}_{Bi,j} \end{pmatrix} \begin{pmatrix} r_R - r_{\mathrm{R}}^0 & r_G - r_{\mathrm{G}}^0 & r_B - r_{\mathrm{B}}^0 \\ g_R - g_{\mathrm{R}}^0 & g_G - g_{\mathrm{G}}^0 & g_B - g_{\mathrm{B}}^0 \\ b_R - b_{\mathrm{R}}^0 & b_G - b_{\mathrm{G}}^0 & b_B - b_{\mathrm{B}}^0 \end{pmatrix} x \begin{pmatrix} r_i \\ g_i \\ b_i \end{pmatrix} = \Delta S \, x \begin{pmatrix} r_i \\ g_i \\ b_i \end{pmatrix} \quad (1.7)$$

and the elements of ΔS are differences in intensities (not in spectra), e.g.

$$\Delta S_{1,1} = \int_{\lambda} R_i(\lambda) \cdot T_j(\lambda) \cdot F_R(\lambda) \cdot D(\lambda) \cdot d\lambda - \int_{\lambda} R_i(\lambda) \cdot F_R(\lambda) \cdot D(\lambda) \cdot d\lambda = \int_{\lambda} R_i(\lambda) \cdot \left[T_j(\lambda) - 1\right] \cdot F_R(\lambda) \cdot D(\lambda) \cdot d\lambda \quad (1.8)$$

Naturally, the narrower the spectral window the better separation of the substance from the instrument spectral characteristics, however, these are given features in CSPT setups. The terms of ΔS [T(λ)] remain functions of the particular screen and camera characteristics used in the experiment. Although imperfect, the difference fingerprints require less illuminating colors for producing the same classification than the ratio CSPT fingerprints (as discussed later), and provide a clear distinction between predominant emission (in this case, positive values of ΔS) and absorption (negative values of ΔS).

1.4.2.2. Ratio CSPT fingerprints

The use of ratio fingerprints was the first processing approach in CSPT experiments, and defined several of the involved measuring and analysis procedures. It was based on stressing similarities with visible absorption spectroscopy and with the way that substance signatures such as the spectral transmittances are computed. In this kind of fingerprint the intensities from the three camera channels for a particular illumination i, are composed as:

$$I_i = r_i\,(r_R + g_R + b_R) + g_i\,(r_G + g_G + b_G) + b_i\,(r_B + g_B + b_B) \qquad (1.9)$$

in which case the three primary illuminating colors only provide three equations

$$\begin{pmatrix} I_1 \\ I_2 \\ I_3 \end{pmatrix} = \begin{pmatrix} \alpha & \beta & \gamma & 0 & 0 & 0 & 0 & 0 & 0 \\ 0 & 0 & 0 & \alpha & \beta & \gamma & 0 & 0 & 0 \\ \alpha & \beta & \gamma & 0 & 0 & 0 & 0 & 0 & 0 \end{pmatrix} x \begin{pmatrix} 1 \\ 0 \\ 0 \\ 0 \\ 1 \\ 0 \\ 0 \\ 0 \\ 1 \end{pmatrix} = \begin{pmatrix} \alpha \\ \beta \\ \gamma \end{pmatrix} \qquad (1.10)$$

with

$$\begin{cases} \alpha = r_R + g_R + b_R \\ \beta = r_G + g_G + b_G \\ \gamma = r_B + g_B + b_B \end{cases} \qquad (1.11)$$

Ratio CSPT fingerprints are finally computed similarly to spectral transmittances as:

$$\tau_i = \frac{I_i}{I_i^0} \tag{1.12}$$

where I_i^0 correspond to the measurement for T(λ) = 1, and for the primary illumination

$$\begin{pmatrix} \tau_1 \\ \tau_2 \\ \tau_3 \end{pmatrix} = \begin{pmatrix} \alpha' & \beta' & \gamma' & 0 & 0 & 0 & 0 & 0 & 0 \\ 0 & 0 & 0 & \alpha' & \beta' & \gamma' & 0 & 0 & 0 \\ \alpha' & \beta' & \gamma' & 0 & 0 & 0 & 0 & 0 & 0 \end{pmatrix} x \begin{pmatrix} 1 \\ 0 \\ 0 \\ 0 \\ 1 \\ 0 \\ 0 \\ 0 \\ 1 \end{pmatrix} = \begin{pmatrix} \alpha' \\ \beta' \\ \gamma' \end{pmatrix} \tag{1.13}$$

where now:

$$\begin{cases} \alpha' = \dfrac{r_R + g_R + b_R}{r_R^0 + g_R^0 + b_R^0} \\ \beta' = \dfrac{r_G + g_G + b_G}{r_G^0 + g_G^0 + b_G^0} \\ \gamma' = \dfrac{r_B + g_B + b_B}{r_B^0 + g_B^0 + b_B^0} \end{cases} \tag{1.14}$$

and for an illumination such as [1, 0, 0], we obtain:

$$\tau_1 = \frac{r_R + g_R + b_R}{r_R^0 + g_R^0 + b_R^0} \approx \frac{\int_\lambda R(\lambda) \cdot T_j(\lambda) \cdot F_R(\lambda) \cdot D(\lambda) \cdot d\lambda}{\int_\lambda R(\lambda) \cdot F_R(\lambda) \cdot D(\lambda) \cdot d\lambda} \tag{1.15}$$

1.5. MEASURING PLATFORM

The CSPT platform, as mentioned above, is very simple and casual assembled. In this thesis it was often composed by a laptop computer (a Toshiba Satellite SA60-198, with a 3.2 GHz clock Intel Pentium 4 processor) with a Philips LCD screen (operating at a resolution 1280 x 800 pixels with a color resolution of 32 bits, and at a refresh frequency of 60 Hz, keeping standard user settings of brightness, contrast and gamma) and a web camera (Logitech QuickCam Pro 4000, with a CCD detector operating at a low resolution of 320 6 240 pixels). The other camera settings were: brightness = 25%, gain = minimum, shutter speed = 1/30 s, saturation = 70%, gamma = 70%, white balance = outdoor or automatic. In this way, in the present thesis, the camera has been configured in the best possible way: the goal is to retain as much as possible of the full range of each colour channel (0–255 counts) for spectrally coincident illumination, and simultaneously to have zero counts for illuminating spectra outside each camera filter.

A sample holder was used to position the test arrays and also provided a light shield preventing external illumination. In this arrangement the samples which are contained in this removable holder light shield attached to the frame of the screen (schematically represented in Figure 1.16) are positioned at 90° respect to the screen and they are parallels to the plane of the camera.

The holder also provides a light shield preventing ambient illumination and support for the web camera which looks downwards focused on the samples. In this particular platform there is a mirror which is positioned at 45◦ respect to the screen and to the plane of the camera, used for reflecting the colours sequence.

So the web camera was fixed to one extreme of the holder, with its lens parallel to the surface of the samples and focused on them. The schemes of the holder and imaged areas are indicated in Figure 1.16. Since the only purpose of this accessory is to provide a fixed geometry for the measurements and to shield ambient light there are not demanding

constraints regarding materials, and aluminium, opaque plastic or even cardboard can be used.

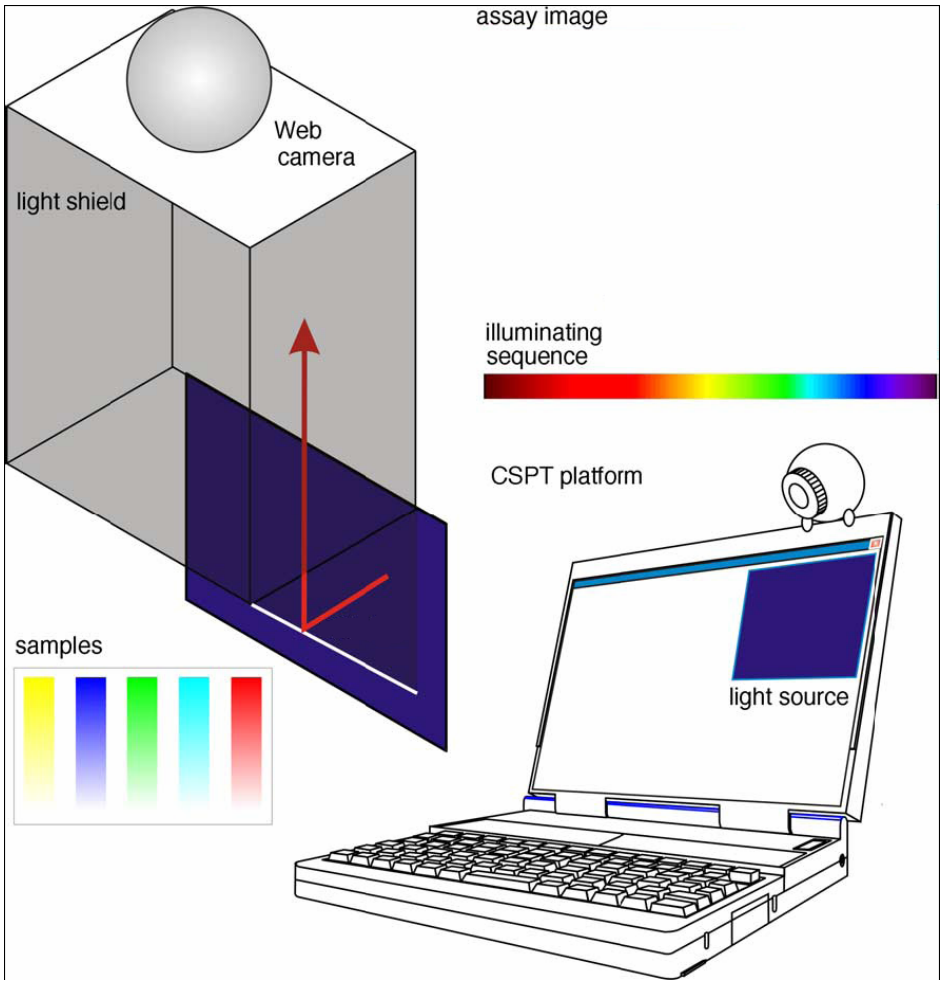

Figure 1.16: Scheme of a computer screen photo-assisted platform, showing the sample holder, light shield and frames of the resulting video stream. With white circles the areas masked for evaluation are indicated.

In the Figure 1.17 are shown a particular CSPT prototype made with cardboard, used in most of the measurements performed. How can be seen it is very simple.

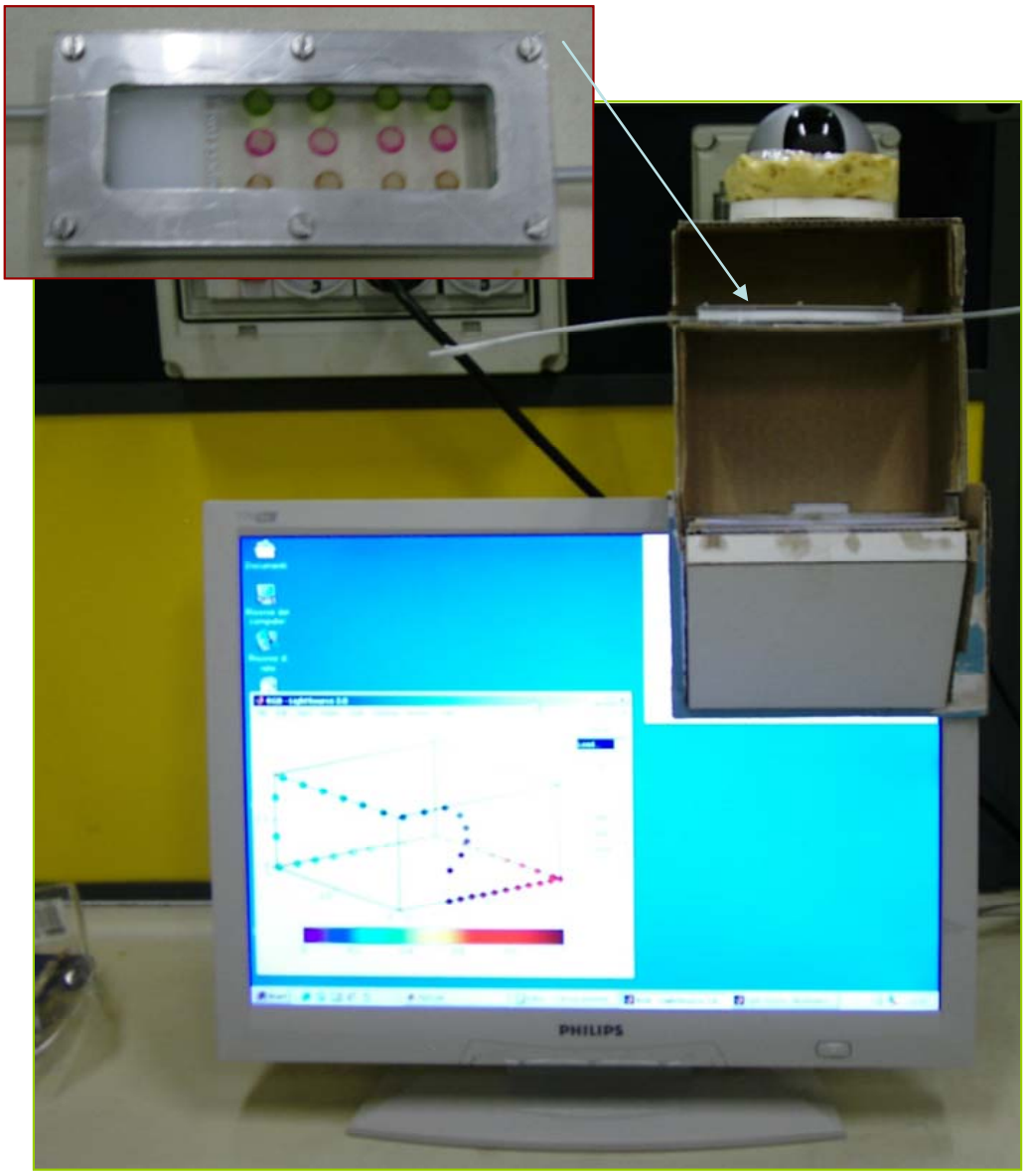

1)

Figure 1.17: A simple prototype of CSPT measurement setup, used in several trials in our laboratories

There is a lot of possible configurations that can be used, it mainly depends by that we want measured, thus the CSPT measurement not only acquires the signatures of the samples but also embeds the characteristics of the particular platform where it operates. Then in a typical experiment with CSPT we can try compensating this casual assembling of platform by using an appropriate spectral features extraction. The quality indices of measurements vary along the different determinations within certain limits, since the CSPT platforms are not necessarily designed for fulfilling analytical requirements such as stability. It is actually this

kind of aspect that the various measuring strategies aim to correct. In fact the number of possible combinations of screens and cameras is immense and makes the spectral characterization of each particular CSPT platform impossible. However, it is necessary to deal with these conditions since it is the possibility of building up a measuring platform from the casual assembly of ubiquitous devices that confers to CSPT its versatility and low cost. In the concept of CSPT it is implicit that potential users of this method already own computer sets or web cameras (the cost of the holder can be estimated as fraction of the cost of a standard web camera). In this context no other measuring approach with similar capabilities is available at such a global scale. These advantages of CSPT motivate the development of measuring strategies able to manage the assumed diversity of setups.

Although the spectral characterization of the platforms is impracticable, nonetheless, the spectral characteristics of the instrument become embedded in the CSPT fingerprints together with the spectral signatures of the target substances.

It is feasible to completely disentangle the spectral reflectance of the samples from the spectral characteristics of the platform when the latter are known, such as in the case of spectral reconstruction techniques, but this approach is not compatible with the purpose of CSPT. Therefore, even if the CSPT fingerprints differ from platform to platform, in theory it is still possible to compare (and classify) sample and reference signatures simultaneously measured in the same platform. This approach could minimize the influence of the platform in the measurements, but also eliminates additional calibration measurements, which makes the system more robust to instrumental instabilities and simpler for the end user. Since CSPT platforms are a casual assembly of components rather than a strictly defined instrument, the fingerprint constitution becomes vital to improve the robustness of the detection. Therefore these five features described above are strictly linked, and they must be assessed ad hoc for each application.

PLATFORM COMPENSATION: { 1 - embedded references or 2 - calibration set

FINGERPRINTS CONFORMATION: { 3 - Difference Fingerprints or 4 - Ratio Fingerprints

COLOURS CHOOSING: { 5 - Illuminating sequence optimization

Finally, is convenient to remark that computer sets and web cameras as showed above are not the only choice to conform CSPT platforms, but PDAs and mobile telephones increasingly incorporate all the components required to perform CSPT measurements, potentially enabling wireless mobile determinations.

1.6. TWO DIFFERENT MODALITIES: SPECTROSCOPY AND E-NOSE

As it has been already mentioned the CPST is enable to optical characterize arrays of coloured substances. Then it is possible using CSPT directly on substances that we want analyze whenever they have got a sharpened spectra, but we can also investigate substances that haven't got a absorption-emission spectra which cannot be immediately highlighted, such as gasses. These molecules can be detected by disposable arrays of sensing materials which respond with a variety of absorption and emission changes that can be well characterized by CSPT. These two mode of using CSPT can be respectively assimilated to a spectroscope and to an electronic nose.

In the first case we straight extract the optical features [18] of the substances arrays that we are illuminating by our colours sequence.

In the second one, to detect volatile molecules we can use an array of cross-sensitive chemical interactive materials that changes their optical spectra an therefore their CSPT fingerprints by absorbing molecules species. The goal is again to extract the right spectral fingerprints by an appropriate method. It could be different for every kind of measure that we are performing. In a further step, the suitable fingerprints features were analysed by using the same analysis techniques of multivariate e-nose data. These data analysis technique are referred in the Appendix. In the next chapters it will be described various kind of measurements by using CSPT in these two operating modes. In particular, we will describe the potentiality of CSPT e-nose mode in the Third Chapter, detecting of low concentrations of molecules such as CO, ETOH, NH_3, NO_x and triethylamine (TEA) [19] in nitrogen, and in the Fourth Chapter by detecting fish freshness with a similar gas sensor array of disposable CIMs (Chemical Interactive Materials). Various demonstrations of potentiality of CSPT-spectroscopy mode will be showed in the Fifth Chapter, where a lot of wine optical properties and bilirubin-hemoglobin concentration in a blood assay will be detected.

1.7. MODELLING CSPT OF COMPUTER SCREEN PHOTO-ASSISTED EXCITATION-EMISSION FINGERPRINTS

CSPT measures substance fingerprints that retain a combination of absorption and emission features. In this paragraph, that modeling [20] of such fingerprints is demonstrated for the case of three different substances composing a disposable gas sensing array, which will be described in details in the Third Chapter. The proposed model allows to reproduce the classification pattern of such sensing element upon exposure to NH_3, NOx, CO and triethylamine (TEA). The biplot analysis of these classification patterns also properly replicates the correlation between scores and CSPT signals. The concurrent classification of the considered spectral responses enables a closer identification of the origin of the CSPT responses. We demonstrate the modeling of CSPT fingerprints corresponding to fluorescent sensing substances and the classification patterns they produce. The model aims at reproducing main response features using representative but not specific spectral characteristics of the CSPT setup, which therefore can serve diverse assemblies. The array considered is a disposable gas sensing device composed by 6 dots (~1 mm in diameter each) of Zn-5,10,15,20-tetraphenylporphyrin (Zn-TPP), Fe-5,10,15,20-tetraphenylporphyrin chloride (Fe-TPPCl) and 2,3,17,18-tetraethyl-7,8,12,13-tetraamethyl-a,c biladiene dihydrobromide (BD) dispersed in a polyvinylchloride matrix and spotted on a glass slide (inset in Figure 1.18b). These substances change their absorption and emission characteristics upon exposure to target gases such as: NH_3, NOx, CO, triethylamine (TEA) and N_2, which is used as reference-. A fingerprint of the complete array is constructed by concatenating red, green and blue channel vectors of each ROI and subsequently by collecting the different ROI vectors in a single 900 elements vector.

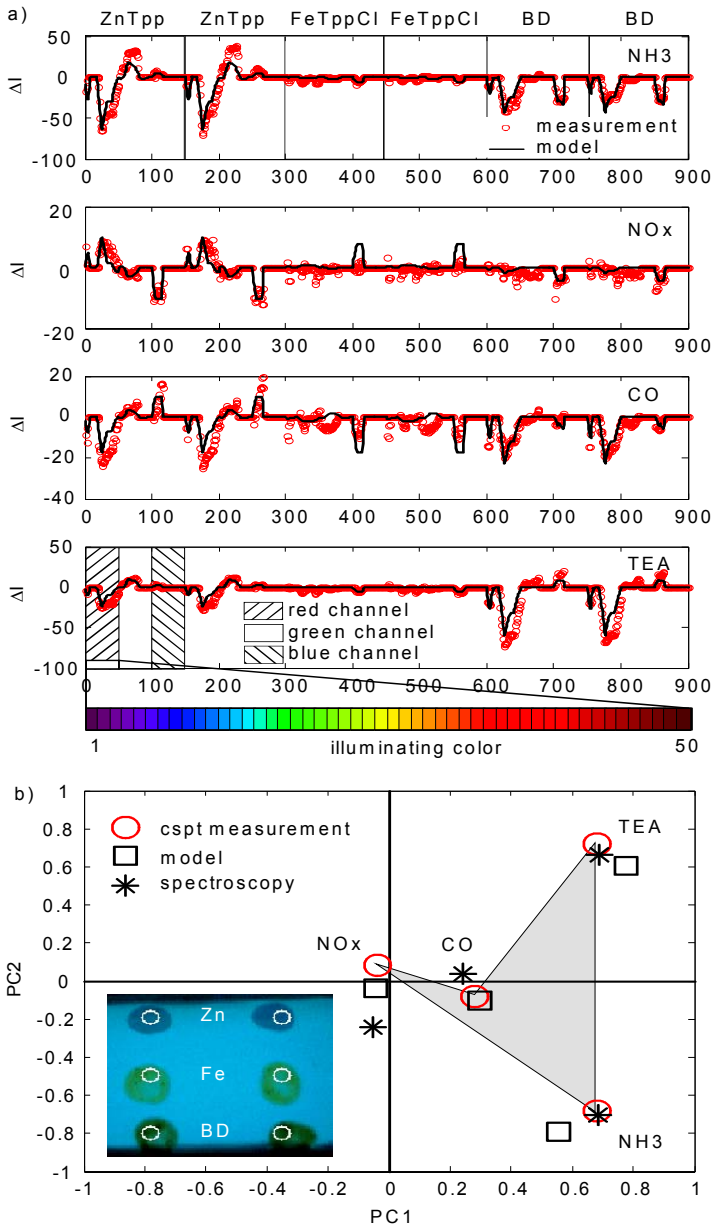

Figure 1.18: a) CSPT response fingerprints of a disposable gas sensing device depicted in the inset of Figure 1.18b, to NH_3, NOx, CO and TEA (10, 20, 500 and 1500 ppm respectively). The O correspond to the experimentally measured CSPT features of the array (see the text for details) and the solid lines to the model of the CSPT responses. The responses are individualized by the kind of porphyrin (ZnTpp, FeTppCL and BD respectively), the camera channels and the illuminating colors.
b) First two principal components of the measured CSPT fingerprints (O), the modeled CSTP fingerprints (□) and the spectral responses considered for the model (✳). The gray area is a guide to the eye indicating the classification pattern of the CSPT measurement. The inset is a color frame of the CSPT measurement and the white circles indicate the ROIs used to extract the fingerprints.

The fingerprints of the responses to different target gases are obtained by subtracting the signature corresponding to N_2.

Considering the spectral radiances of the red, green and blue screen primaries represented by $R(\lambda)$, $G(\lambda)$ and $B(\lambda)$, each color displayed on the screen can be written as:

$$c_i(\lambda) = \frac{r_i \cdot R(\lambda) + g_i \cdot G(\lambda) + b_i \cdot B(\lambda)}{3} \qquad (1.16)$$

where r_i, g_i and b_i are the triplet of weights that specify every screen color i. The radiances are in this work Gaussian functions centered at 455, 545 and 615 nm.

Given a fluorescent substance in a certain environment its spectral characteristic $S(\lambda)$, can be written as:

$$S_i(\lambda) = T(\lambda) + E_i(\lambda) \qquad (1.17)$$

where $T(\lambda)$ is the spectral transmittance of the substance and $E_i(\lambda)$ is the spectral emittance induced by the illuminating color i.

In order to account for the excitations provided by the polychromatic illuminations:

$$E_i(\lambda) = \alpha \cdot \frac{\beta(i)}{\hat{\beta}(i)} \cdot E(\lambda) \qquad (1.18)$$

where α represent the relative contribution of emission in the CSPT fingerprint, $\beta(i)$ modulates the amplitude of the emission spectra depending of the illuminating color and $E(\lambda)$ is the emission spectra corresponding to a monochromatic excitation at the wavelength of the maximum absorption.

$$\beta(i) = \int_{\lambda} c_i(\lambda) \cdot d\lambda \qquad (1.19)$$

The light emerging from the sample passes through the red, green and blue camera filters $F_R(\lambda)$, $F_G(\lambda)$ and $F_B(\lambda)$ and reach the detector represented by its spectral response $D(\lambda)$. Thus:

$$\begin{cases} I_R(i) = \eta \cdot \int_\lambda c_i(\lambda) \cdot S_i(\lambda) \cdot F_R(\lambda) \cdot D(\lambda) \cdot d\lambda \\ I_G(i) = \eta \cdot \int_\lambda c_i(\lambda) \cdot S_i(\lambda) \cdot F_G(\lambda) \cdot D(\lambda) \cdot d\lambda \\ I_B(i) = \eta \cdot \int_\lambda c_i(\lambda) \cdot S_i(\lambda) \cdot F_B(\lambda) \cdot D(\lambda) \cdot d\lambda \end{cases} \quad (1.20)$$

where η is an scale factor and together with α are fit for each substance and kept constant along the subsequent spectral responses. These modeled signals are assembled in the same way as the measured signals. The solid lines in Figure 1.18a correspond to the modelled responses and sufficiently reproduce the main features of the fingerprints.

It must be noticed that the purpose of the CSPT simulations is not to exactly match the measured signal, which would require the spectral characterization of the setup, but to reproduce the main features of the CSPT signatures that leads to its ability to distinguish the different target stimuli. The used model, rather than describing in detail the polychromatic excitation of a substance, aims at supporting the use of CSPT and its optimization by linking the CSPT signals with absorption-emission spectra obtained with standard spectrofluorometers.

Absorption and emission spectra in air have been measured by standard fluorescence spectroscopy as well as some of the responses, while the remaining ones are spectral responses compatible with the involved chemistry. ZnTpp has it absorption peak (~430 nm) well separated form the emission peak (~610 nm), which confers a good separation of excitation from emission that actually are recorded by separated channels of the camera. FeTppCl has not emission and BD is the most demanding situation since both excitation and

emission peaks (~530 and ~550 nm respectively) both are within the green camera channel, canceling the responses in this band, which was consequently zeroed in the modeled signals. Ultimately, the validation of the CSPT model is its ability to reproduce the classification patterns and their correlations with the signals. Principal component analysis is a multivariate method apt for the classification of complex signals, which allows to represent them by 2D or 3D points in a principal components (PCs) space that explain a substantial amount of the original information. Figure 1.18b collects the first two PCs of the CSPT fingerprints (○), the simulated CSPT fingerprints (□) and the spectral responses that motivated them (∗). In order to compare the classification performances all fingerprints have been normalized and the absorption-emission responses to each target gas concatenated in a single vector and re-sampled to 900 elements. Figure 1.18 shows a pretty similar pattern for all these alternatives, highlighting both: the correctness of the model and the good retention of absorption-emission spectra in the CSPT measurements.

To closely discern the correlation of PCs scores with the signals that originates them, a biplot of scores and loads is composed. In this kind of representation 100% correlated variables lies on a same direction, whereas orthogonal directions are not correlated. Thus, Figure 1.19a and b show that the detection of NH_3 is highly correlated with the response of ZnTpp and specially with CSPT features measured in the red channel of the web camera for yellowish and greenish illuminations (by contrast with the spectroscopy the illuminating colors in CSPT are polychromatic), whereas the detection of TEA is mainly explained by the response of BD observed in the red channel. Other parts of the fingerprints, such as the ZnTpp response observed in the blue channel are also correlated with NOx detection (Figure 1.19b). Beyond the detailed analysis of these figures, what is central for the purpose of this study is the similarity of the biplot produced by the modeled signals (Figure 1.19c and d), which correctly reproduce the main classification pattern and its correlations to the CSPT fingerprints.

Finally, the biplot of the spectral responses (Figure 1.19e and f) enables a deeper discrimination of the origin of the CSPT responses; since in this case absorption and emission responses are completely disentangled (in this case the illuminating colors

correspond to narrow band centered at the indicated wavelengths). Thus, the ZnTpp response correlated with the NH_3 detection can be clearly identified as a change in the emission spectra, alike the detection of TEA which is determined by the fluorescent response of BD, while different absorption responses correlate with these and other scores.

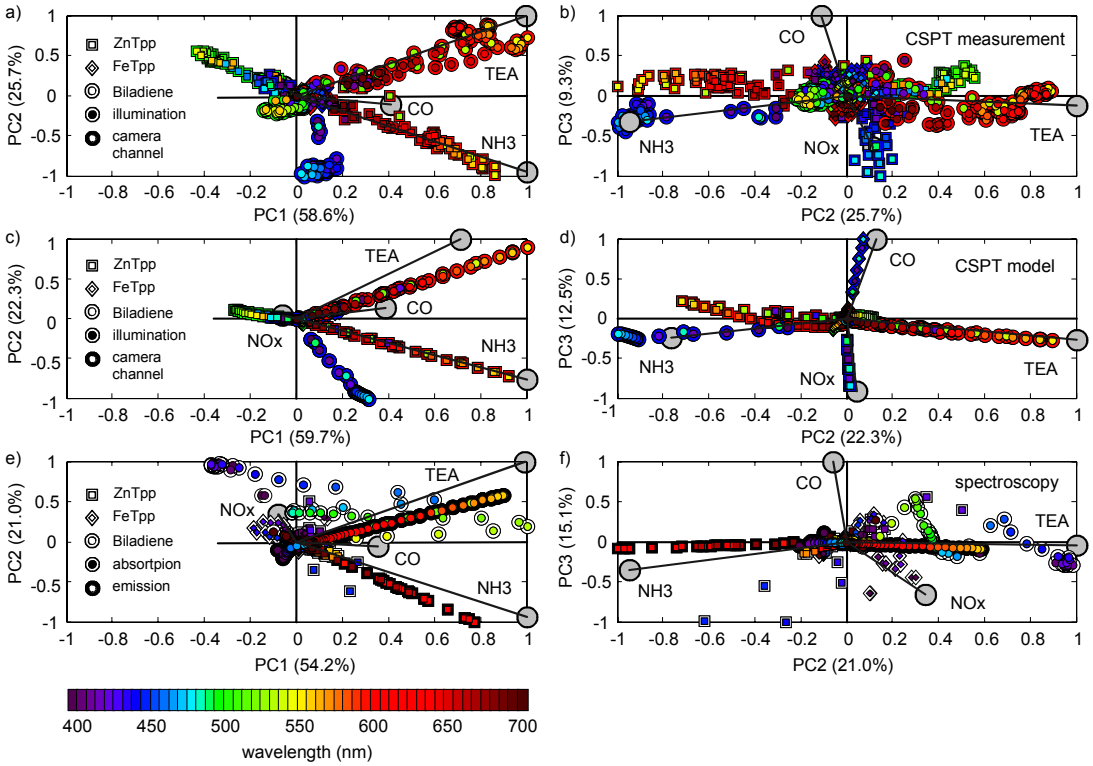

Figure 1.19: a) First and second PCs bilplot of the CSPT measured fingerprints, where the scores (gray ○) can be correlated with the substance responses of ZnTpp, FeTppCl, and BD (identified by □, ◇ and ○ respectively), the camera channels (color of external ring of the symbols) and the illuminating colors (color of the center of the symbols). The latter colors correspond to polychromatic light. b) Same as a) but for the 2nd and 3rd PCs. c) Same as a) but for modeled CSPT responses. d) Same as b) but for modeled CSPT responses. e) Same as a) but for the spectral responses considered for the CSPT simulation. In this case white externals rings correspond to absorption spectra and black rings to fluorescent responses. The colors in this case correspond to narrow band light at the indicated wavelengths. f) Same as e) but for the 2nd and 3rd PCs.

Despite of clear differences in the instrumentation, the present results show a good correlation with absorption and fluorescent responses measured by standard spectroscopy. Thus, beyond its natural attractive as an ubiquitous and affordable sensing platforms, CSPT also shows the possibility of rather sophisticated determinations based on the polychromatic interrogation of the excitation-emission matrix of target substances, an analytical capability not intuitively associated with such a simple setup.

Predicting a CSPT response from a given substance spectra enables to systematically chose optimum indicators from extensive libraries of spectra or to optimize the illuminating conditions giving the best possible classification form a given set of substances. Here this possibility has been extended to fluorescent indicators.

REFERENCES

[1] J. K. Albert, D. R. Walt, D. S. Gill, T. C. Pearce, Anal. Chem. 2001, 73, 2501.

[2] D. Filippini, S.P.S. Svensson, I. Lundstr¨om, Computer screen as a programmable light source for visible absorption characterization of (bio)chemical assays, Chem. Commun. 2 (2003) 240–241.

[3] "International Lighting Vocabulary", *CIE Publication No. 50,* 1987, CIE, Paris

[4] Newton, Isaac (1704). Optics.

[5] G. C. Brainard et al., J. Neurosci. 21, 6405 (2001). 11. D. M. Berson, F. A. Dunn, M. Takao, Science 295, 1070 (2002).

[6] S. Hattar, H.-W. Liao, M. Takao, D. M. Berson, K.-W. Yau, Science 295, 1065 (2002).

[7] Martin, R. Paul, Colour processing in the primate retina: recent progress, *Journal of Physiology*. 513 (3), 631-638, 1998.

[8] M. Richter, *Einfuhrung in die Farbenlehre*; Berlin: de Gruyter, 1980

[9] D. L. Mac Adam, *Color Measurements*; Heidelberg: Springer-Verlag, 1981

[10] G. Wyszecki, W. Stiles, Color Science: Concepts and Methods, Quantitative Data and Formulae, Wiley, New York, 1982.

[11] E. F. Schubert, J. K. Kim, Science 2005, 308, 1274. ---Solid State light source---

[12] N. A. Rakow, K. S. Suslick, Nature 2000, 406, 710.

[13] N. Birch, D. Stickle, Example of use of a desktop scanner for data acquisition in a colorimetric assay, Clin. Chim. Acta 333 (2003) 95–96.

[14] F. H. Imai and R. S. Berns, Spectral estimation using trichromatic digital cameras, in Proceedings of the International Symposium on Multispectral Imaging and Color Reproduction for Digital Archives, Chiba University, Chiba, Japan, 1999, pp. 42–49.

[15] Francisco Imai, Multi-spectral Image Acquisition and Spectral Reconstruction using a Trichromatic Digital Camera System associated with absorption filters, Munsell Color Science Laboratory Report 1998, http://www.cis.rit.edu/mcsl/research/reports.php#GibsonFairchild

[16] K. Nassau (Ed.), Color for Science, Art and Technology, Elsevier Science B.V, The Netherlands, 1998.

[17] J. Gibson, M. Fairchild, Colorimetric characterization of three computer displays (LCD and CRT), Munsell Color Science Laboratory Report, 2000, pp. 1–40.

[18] D. Filippini, I. Lundström, Spectroscopic information retained in screen photo-assisted techniques, Anal. Chim. Acta 512 (2004) 239–246.

[19] D. Filippini, A. Alimelli, C. Di Natale, R. Paolesse, A. D'Amico, I. Lundström; Chemical sensing with familiar devices, Angewandte Chemie Int. Ed. 45 (2006) 3800-3803

[20] D. Filippini, C. Di Natale, R. Paolesse, A. Alimelli, A. D'Amico, I. Lundström, "Modeling of computer screen photo-assisted excitation-emission fingerprints"-Applied Physics Letters, submitted

CHAPTER 2

Chemical-Interactive-Materials: Porphyrins, related Metal complexes and TetraPyrrolic Compounds

INTRODUCTION

The sensor performances in term of sensitivity, reproducibility and selectivity strictly depend on the properties of the sensing materials. For this reason a great effort has been made to develop sensing materials with improved properties [1]

From this point of view, the exploitation of organic compounds as sensing materials is particularly advantageous. The progress made in designing synthetic receptors [2] allows the orientation of the sensor selectivity towards different classes of compounds via modulation of weak interactions occurring between the sensing material and the analytes.

Among the different classes of receptors developed, porphyrins and metalloporphyrins represent one of the most promising, because of the richness of their properties, their stability and the development of the chemistry of these macrocycles that allow the possibility to modulate their properties by synthetic modifications or by changing the coordinated metal. In these applications porphyrins mimic their functions in biological systems, where they are able, for example, to reversibly bind oxygen. Because generally target analytes are also good ligands for metal ions, porphyrins represent a perfect match for the properties required to sensing materials.

For this reason researches in this area have experienced a significant growth in the last decade and porphyrin based chemical sensors are now going to be famous as much as those based on related phthalocyanines. Optical sensors are based on the variation of one optical property, such as absorption or luminescence, of the sensing material as a consequence of the interaction with the target analyte. Porphyrins have been called “pigment of life” and for these peculiar optical properties it is quite obvious that they have been considered as sensing materials for optical sensors. In this Chapter, we want to highlight their exploitation in optical sensors array based on, by showing in details their optical properties.

2.1. BIOLOGICAL ROLE OF PORPHYRINS IN NATURE

Porphyrins (Figure 2.1) and related tetrapyrrolic pigments occur widely in nature, to provide natural systems with brilliant colors and play very important roles in various biological processes.

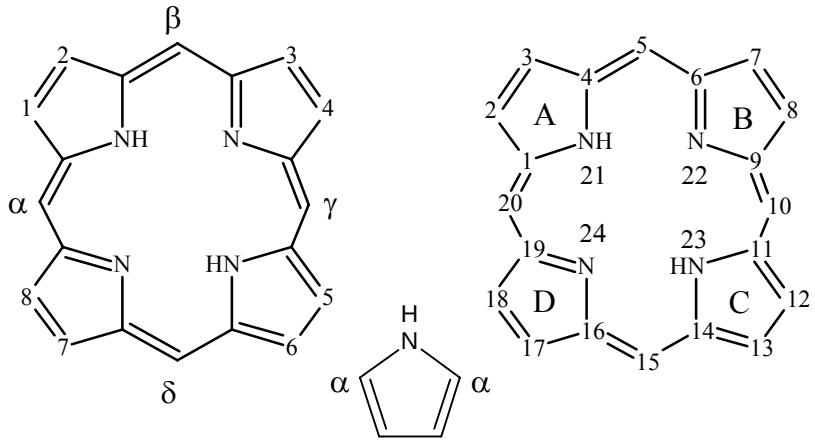

Figure 2.1: Structure and numeration of Porphyrin (IUPAC and Fisher)

Heme (Figure 2.2), the iron(II) protoporphyrin-IX complex, is the prosthetic group in hemoglobins and myoglobins responsible for oxygen transport in red blood cells, and oxygen storage in living tissues.

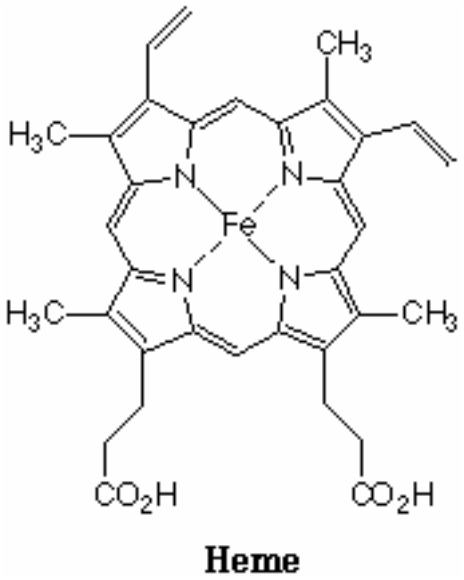

Figure 2.2: Heme (an iron-porphyrin) is the part of hemoglobin coordinating O_2 and CO.

Heme is also located in the enzyme peroxidase, which catalyzes the oxidation of substrates whit hydrogen peroxide. The related enzyme catalase, also containing heme, catalyzes the breakdown of hydrogen peroxide to water and oxygen. Other heme-containing proteins include the cytochromes, which serve as one-electron carriers in the electron transport chain. Reduction of a pyrrolic unit on the porphyrin ring leads to a class of porphyrin derivatives termed chlorines. Chlorophylls (e.g. chlorophyll-a), found abundantly in green plants, are classified in this category and play an essential role in the process of plant photosynthesis. Further saturation of another pyrrole unit on chlorins provides another type of porphyrin derivative termed bacteriochlorins, in which the saturated pyrrole units are diagonally opposite to each other. Bacteriochlorins (e.g. bacteriochlorophyll-a) are naturally occurring bacteriochlorins found in photosynthetic bacteria.

One of the vitamins, vitamin B_{12}, also contains a porphyrin-like unit called corrin, a reduced form of corrole. Porphyrins are also found in other systems such as the oxygen-carrying pigment chlorocruorin from *Sabella starte indica* [3] and in oil shales [4].

2.2. A BRIEF HISTORY OF PORPHYRIN CHEMISTRY

Thudichum [5] developed the first preparation of a porphyrin in 1867 by treatment of haemoglobin with concentrated acid. A few years later by a similar route, Hoppe-Seyler [6] obtained a purple substance which he called hematoporphyrin.

However, these procedures failed to provide a pure sample of porphyrin. Approximately 30 years later Nencki isolated [7] the first pure sample of porphyrin, preparing hematoporphyrin hydrochloride from isolated hemin. These initial studies marked the beginning of porphyrin chemistry, which now includes many disciplines of science and medicine and continues to flourish.

Porphyrins (Figure 2.1) possess a basic skeleton consisting of four pyrrole units linked by four methane bridges. This skeletal structure was first proposed by Küster [8] in 1912. However, it was suggested by both Fischer and Willstätter that such a large ring system would not be very stable; they proposed other structures containing smaller ring systems. The debate over the actual structure of a porphyrin continued until 1926 when Fischer successfully synthesized etioporphyrin-I by the first totally synthetic pathway [9]. Shortly thereafter Fischer completed the synthesis of octamethylporphyrin [10] by two distinctly different methods. These preparations led to the acceptance of the structure initially proposed by Küster as the basic structure of porphyrins.

2.3. PROPERTIES AND CHARACTERISTICS OF PORPHYRINS

All porphyrins are derived from the cyclic porphyrin (Figure 2.1) formula, $C_{20}H_{14}N_4$, consisting of four pyrrole units connected by four methane (*meso*) carbons. The porphyrin macrocycle is an aromatic system containing 22π electrons of which 18 are involved in any one delocalization pathway. Porphyrins obey Hückel's rule of aromaticity (4n+2π electrons, where n=4). The aromatic character of porphyrins is also evident in their NMR spectra. HNMR spectroscopy of porphyrins shows that the N-H protons appear at δ = ~ -5 ppm (upfield from TMS), indicative of NHs located in an anisotropic aromatic shielding cone [11]. Whereas the methine protons appear at ~ 10 ppm, a δ-value indicating a highly deshielding environment resulting from the aromatic ring current. All visible absorption spectra of porphyrins display the following characteristic spectra (Figure 2.3):

***B* band**: An exceedingly intense band (referred to as the "Soret" band [12]) appears between 380 and 420 nm. It is the origin *B* (0,0) of the second excited singlet state and has molar extinction generally from 2 to 4 x 10^5 M^{-1} cm^{-1}. This is characteristic of a highly conjugated porphyrin macrocycle. Better – resolved spectra sometimes show another band ~ 1250 cm^{-1} to the blue; it is attributed to addition of one mode of vibrational excitation and is denoted *B*(1,0).

***Q* bands**: There are several weaker absorptions at longer wavelengths between 500 and 700 nm: four visible bands are seen (sometimes called "satellite" bands). The lower-energy band (sometimes called α) is the electronic origin $Q_{x,y}(0,0)$ of the lowest–energy excited singlet state. The higher-energy band (sometimes called β) includes one mode of vibrational excitation and is denoted $Q_{x,y}(1,0)$; it is actually a merging of several different vibrations. It was originally identified as a vibration on the basis of the relative constant energy gap between $Q_{x,y}$ (1,0) and $Q_{x,y}$ (0,0). The $Q_{x,y}$ (1,0) band has molar extinction coefficient in a narrow range between 1.2 and 2 x 10^4 M^{-1} cm^{-1}, in fact they are not allow by selection rules.

All these bands are interpreted as (π,π*) in origin. The nomenclature *Q*, *B*, was originally given by Platt [13]; *B* implies a strongly allowed excited state and *Q* a quasi-allowed one. The basic porphyrin ring, as shown in Figure 2.1, provides the electronic "heart" of a porphyrin. The ring is structured with a basic fourfold symmetry, including four nitrogen atoms directed toward the center. This electronic "heart" is responsible for porphyrin-type optical spectra, which are then perturbed to a greater or lesser extent by various chemical modifications to the basic structure. Variations of the peripheral substituents on the porphyrin ring often cause minor changes in the intensity and wavelength of these absorptions. Protonation of two inner imine nitrogen atoms or insertion a metal into the porphyrin cavity also changes the visible absorption spectra. These absorptions can often be very helpful in elucidating certain structural features on a porphyrin. X-ray structural determinations of both metalloporphyrins and free-base porphyrins have basically shown the core porphyrin to be planar, a fundamental requirement for perfect aromaticity [14].

Measurements of heats of combustion and thermodynamics also indicate the existence of aromatic stabilization energy [15].

The porphyrin ring is very stable on both concentrated acid and base, and the macrocycle can act both as an acid and a base. Strong bases such as alkoxides remove the two central protons (Pk_a ~16) on the inner nitrogen atoms of a porphyrin to form a dianion. However, trifluoroacetic acid easily protonates the two free pyrrolenine nitrogen atoms (pK_b ~9) to form a dication.

Porphyrins also undergo a number of chemical reactions typical of aromatic compounds. For example, electrophillic substitution reaction such as nitration, halogenation, acetylation, and formylation are often performed on porphyrins. Only the *meso* carbons and the β-pyrrolic carbons participate in these reactions. The α-pyrrolic carbons rarely take part in any kind of reaction.

Porphyrins are also capable of being metallated and demetallated. Almost every metal in the periodic chart has been inserted into the porphyrin macrocycle but most typically are: Fe, Zn, Cu, and Ni, which can be inserted into the porphyrin cavity by using simple metal salts [16]. Demetallation can usually be achieved by treatment with acids of various strengths.

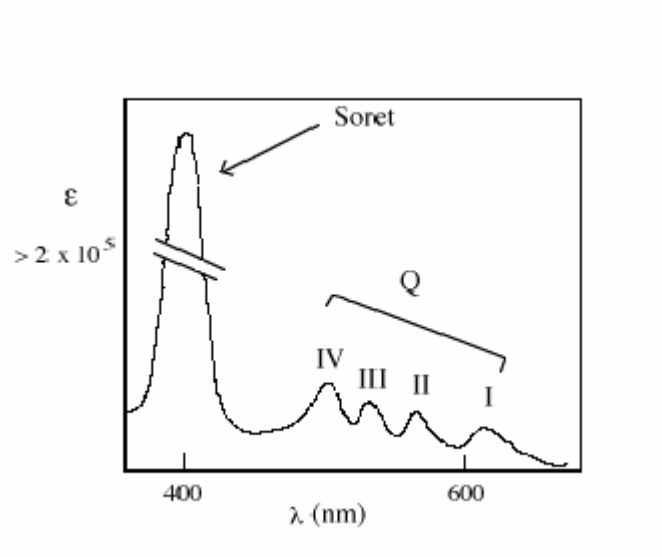

Figure 2.3: Typical UV-Visible absorption Spectrum of a Porphyrin

2.4. PHOTOPHYSICAL FEATURES OF METALLOPORPHYRINS

The purpose of this Section is to present the facts on the optical absorption and emission spectra of porphyrins and the current theory by which these facts are understood. The leading optical phenomena are ground state absorption and excited state emission. It is with these two phenomena, as observed in porphyrins and related molecules in liquid or glassy solutions, and the electronic interpretation of these phenomena that this Section will be concerned. The porphyrins capability to lose of two inner imine allows a large number of metal insertion into the porphyrin cavity that changes the visible absorption spectra. So the absorption spectra of metalloporphyrins are diverse and complex. Any discussion of porphyrin photochemistry profits from an understanding of the electronic transitions responsible for the observed spectra. Then we introduce a general categorization of metalloporphyrin photochemistry, a classification based on absorption and emission spectra.

2.4.1. Absorption Spectra

2.4.1.1. "Normal"

Normal spectra (Figure 2.4b) are observed for metalloporphyrins with metals from groups 1 to 5 with oxidation states of I to V, respectively, and for other d^0 or d^{10} metals. These type of spectra have one intense absorbance (the Soret band) between 320 and 450 nm and one or two absorbance (Q bands) between 450 and 700 nm. Mesosubstituted porphyrins often show a merging of the lower energy bands. Free base porphyrins also have normal spectra, although they have a four-banded spectrum between 450 and 700 nm because of their lesser symmetry.

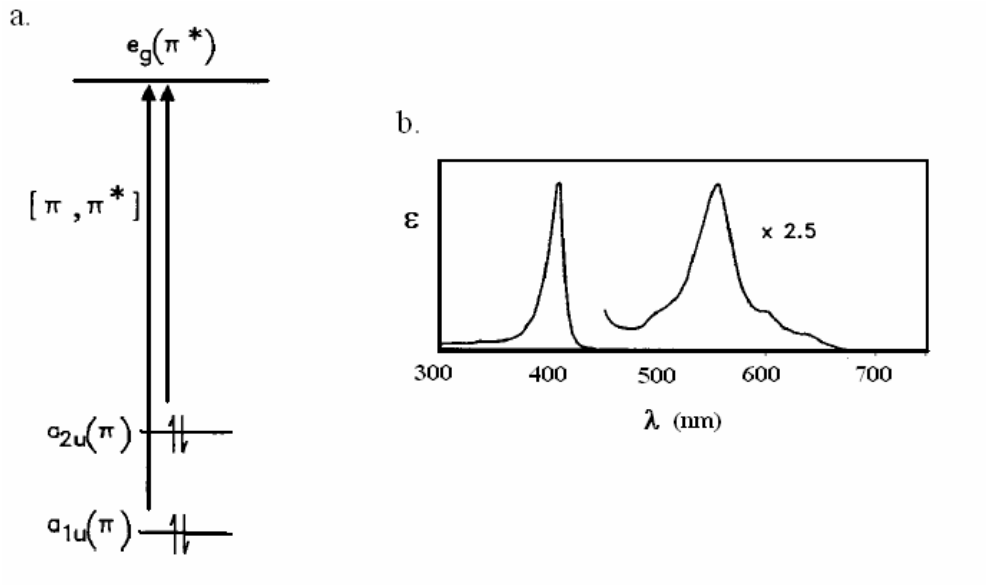

Figure 2.4:Metallo-porphyrins with Normal spectra. a) Porphyrin Orbitals. b) Absorption spectra.

In fact this increase in the number of bands is attributed to lowering of the D_{4h} symmetry of the metalloporphyrin to D_{2h} by protonation of two pyrrole nitrogens in the metal-free porphyrin. In Gouterman's four orbitals model [17], the four orbitals are porphyrin π and π* orbitals; the two HOMO (highest occupied molecular orbital) of a_{1u} and a_{2u} symmetry, and the two LUMO (lowest unoccupied molecular orbital) of e_g symmetry. The two major absorbance arise from coupling of the two transitions between the HOMO's and LUMO's ($\pi \rightarrow \pi^*$) (Figure 2.4a). The Q bands are the result of the transition dipoles nearly cancelling each other out, therefore resulting in a weaker absorbance. The higher energy Soret transition results from a linear combination of the two transitions with reinforcing transition dipoles and is therefore very intense. Some shifts in the positions of the bands as a function of metal occur due to weak interaction of the metal with the a_{2u} and e_g orbitals.

2.4.1.2. "Hypso"

This spectra type look very much like the Normal spectra except that the Q-band is blue shifted to wavelengths of less than 570 nm (Figure 2.5b).

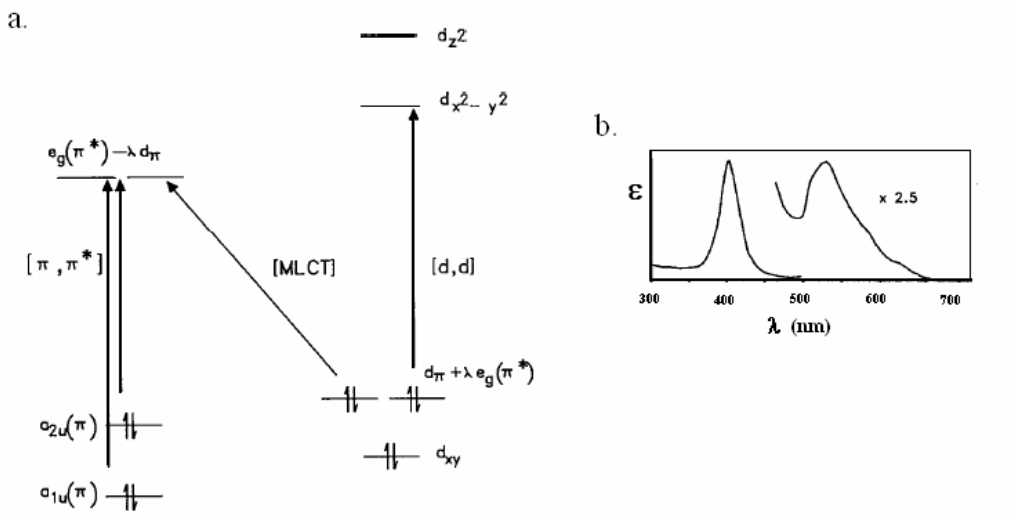

Figure 2.5: Metallo-porphyrins with Hupso spectra. a) Porphyrin and Metal Orbitals. b) Absorption spectra.

The Hypso spectrum is found with transition metal complexes with electron counts of d^6 to d^9 and therefore filled $e_g(d_\pi)$ orbitals. Common examples are Pd(II), Pt(II), Rh(II), and Ni(II). The blue shift in the Q-band is explained by mixing of the e_g LUMO of the porphyrin ring with the filled $e_g(d_\pi)$ metal orbitals. Figure 2.5a shows this interaction, which pushes the porphyrin LUMO to higher, thus increasing the π-π* energy gap of the porphyrin. The overlap is greatest for 4d and 5d metals, which show the largest blue-shifts (hypsochromic shift). Within a given row of transition metals, the energy of the d_π electrons decreases with increasing electron count. Thus, as the number of d-electrons increase, the energy gap between the porphyrin LUMO and the metal increases, and the orbital mixing decreases. For the late first-row transition metal ions, the spectra become less blue shifted as the d-electron count increases from Fe(II), Co(II), Ni(II), Cu(II) to Zn(II).

2.4.1.3. "Hyper"

The Hyper spectra, both p-type and d-type**,** show additional absorbance compared to the Normal and Hypso varieties. These additional bands are generally to the blue of the Q-band and are of moderate intensity (Figure 2.6b and Figure 2.6d).

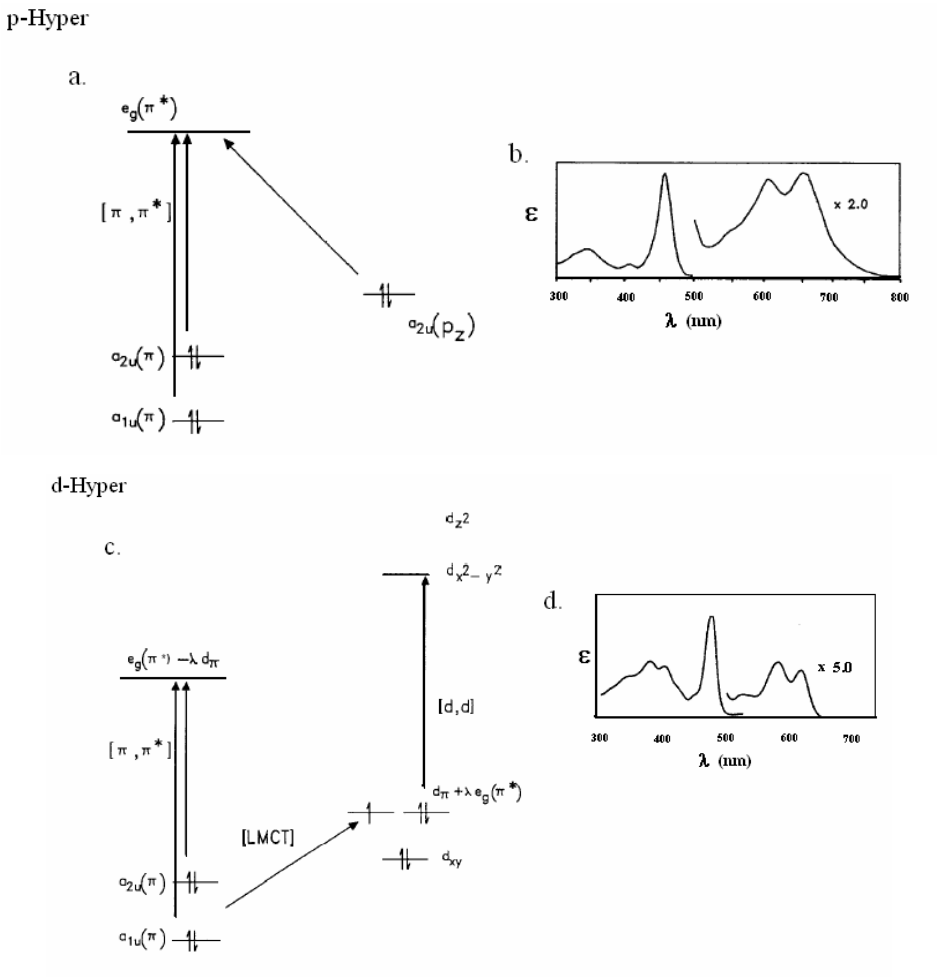

Figure 2.6: Metallo-porphyrins with p-Huper and d-Hyper spectra.

Main group elements in low oxidation state (e.g., Sn(II), Pb(II), P(III), As(III)) give p-type Hyper spectra. In this case the extra bands are due to metal to ligand charge transfer. The

charge transfer originates in the metal p_z orbital of a_{2u} symmetry (Fig. 2.5a): $n_{pz}(metal) \rightarrow e_g(\pi^*)$ (porphyrin).

The porphyrin complexes that exhibit d-type *hyper* spectra are found with d^1 through d^6 metals that have vacancies in the $e_g(d_\pi)$. These vacancies make a porphyrin ligand to metal charge transfer transition possible(Figure 2.6c).

2.4.2. Emission Spectra

Emission spectra of porphyrins and related metal derivatives can be described by a energy level diagram, like Jablonski one, that is applicable for description of emission from most aromatic molecules with singlet ground states.

Excitation from the ground state S_0 to any singlet exited state S_x leads to very fast radiationless decay to the lowest excited singlet S_1 in times ~ 10^{-12} -10^{-13} sec.

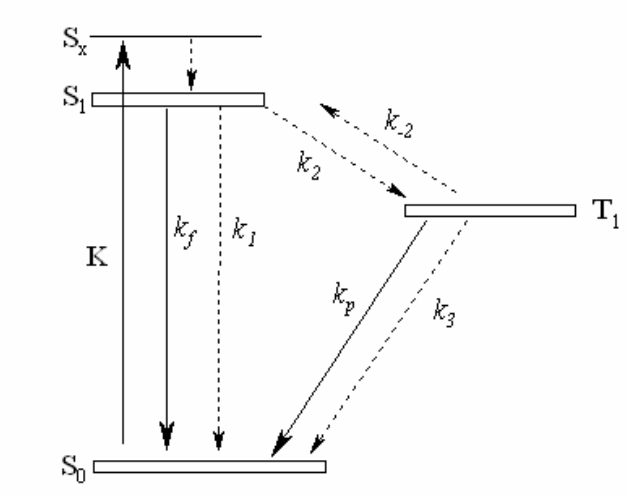

Figure 2.7: Decay scheme for singlet and triplet relaxation. The radiation processes are shown as straight lines; radiationless processes are shown by wavy lines.

From S_1 the molecule can emit fluorescence [18] radiation $S_1 \rightarrow S_0$ with rate k_f, can radiationlessly decay $S_1 \rightsquigarrow S_0$ with rate k_1, or can internally convert to the lowest triplet $S_1 \rightsquigarrow$

T_1 with rate k_2. (We here use straight arrows to denote radiative transitions and wavy arrows to denote radiationless transitions.) S_1 decays over times between $10^{-12}$and 10^{-7} sec, after which, if the system is still excited, it exists in the lowest triplet T_1. From T_1 the molecule can emit phosphorescence radiation $T_1 \rightarrow S_0$ with rate k_p, can radiationless decay $T_1 \rightsquigarrow S_0$ whit rate k_3, or can be reexcited to the first excited singlet $T_1 \rightarrow S_1$ whit rate k_{-2}. Such repopulation of S_1 can lead to delayed fluorescence. It requires an input of energy to T_1, which can occur in one of two ways: thermal repopulation (*E*-type delayed fluorescence) or triplet-triplet collisions (*P*-type delayed fluorescence).

It can be shown that thermal delayed fluorescence will decay with the same lifetime as the triplet state. However since triplet-triplet collisions are a bimolecular process, delayed fluorescence from this mechanism decays with a lifetime of half that of the triplet state.

The observables of emission consist of spectra, lifetimes, and quantum yields for fluorescence (ϕ_f) and phosphorescence (ϕ_p). Delayed fluorescence spectra are identical to that of fluorescence, but have different lifetimes and quantum yields. By quantum yield we refer to the ratio of photons in to photons out.

Equations for the excitation process can be set up. Using the rate constants in Figure 2.6 and assuming k_{-2} is thermal in origin, rather than bimolecular we obtain

$$\frac{dS_0}{dt} = -KS_0 + (k_f + k_1)S_1 + (k_p + k_3)T_1$$

$$\frac{dS_1}{dt} = KS_0 - (k_f + k_1 + k_2)S_1 + k_{-2}T_1$$

$$\frac{dT_1}{dt} = k_2 S_1 - (k_p + k_3 + k_{-2})T_1$$

Where k is the rate of photon excitation. Under steady state illumination the quantum yields of fluorescent and phosphorescent photons are

$$\phi_f = \frac{(k_p + k_3 + k_{-2})k_f}{(k_f + k_1 + k_2)(k_p + k_3) + k_{-2}(k_f + k_1)}$$

$$\phi_p = \frac{k_2 k_p}{(k_f + k_1 + k_2)(k_p + k_3) + k_{-2}(k_f + k_1)}$$

Generally, all fluorescence spectra essentially display two peaks, Q(0,0) and Q(0,1), as shown in Figure 2.8. They are specular images of Q(0,0) and Q(1,0), absorption peaks; often other weak peaks can be observed: Q(2,0)-absorption, Q(0,2)-emission. Instead, the phosphorescence consists in a high band T(0,0) and other ones of variable intensity T(0,1).

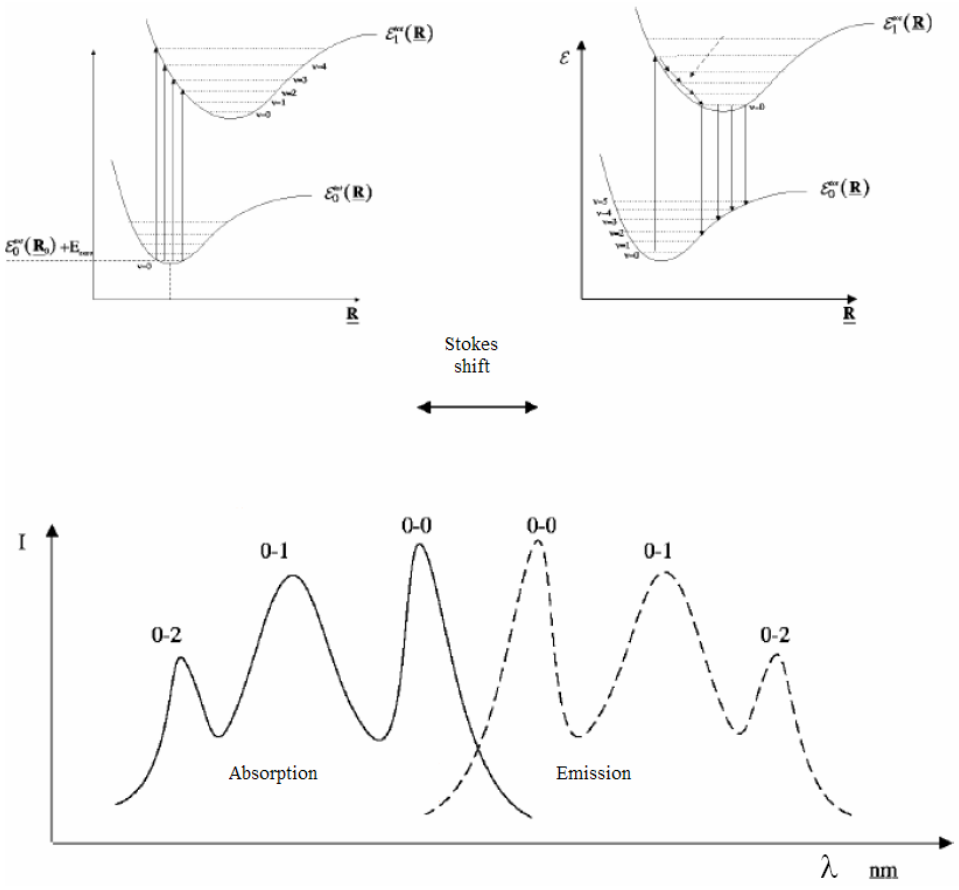

Figure 2.8: Absorption and Emission Spectra.

2.4.3. Optical Classification of Metalloporphyrins

Metallo-porphyhrins can be classified as “regular”, “irregular” and “pseudo-normal”, it depends on kind of their optical phenomena.

2.4.3.1. Regular porhyrins

A **regular porphyrin** is one whose optical absorption and emission spectra are determined essentially by the π electrons of the porphyrin ring, with only minor perturbation from the electrons of the central substituent. This is a theoretical definition. Empirically we define *regular* porphyrins as those with *normal* absorption and *fluorescent* (k_f^{-1}~60 ns) emission spectra. The optical spectra of regular porphyrins are attributed entirely to π→π* transitions of the ring, with the central metal contributing only small electronic or spin orbit perturbations. The electronic perturbations are responsible for the small observed differences among the absorption spectra, while the spin orbit perturbations cause the large variations in ϕ_f, ϕ_p and τ_p(phosphorescence decay rates).

2.4.3.2. Irregular phorphyrins

Instead **irregular** metalloporphyrins differ from the regular in emission properties and in most cases in absorption also. They present the unusual absorption types as Hypso and Hyper. In addition to fluorescence emission, we can distinguish three other emission types: phosphorescence, luminescence, radiationless decay.

Phosphorescent metalloporphyrins show no more than weak prompt (as opposed to delayed) fluorescence, that is, $\phi_f < 10^{-3}$, and in many cases no fluorescence at all is observed. Phosphorescence yields are variable over the entire range from $10^{-4} < \phi_f < 1$. Phosphorescence lifetimes are short, with $\tau_p < 3$ ms.

Luminescent porphyrins contain paramagnetic metals. The emission cannot really be characterized as fluorescence or phosphorescence because the molecular states are not singlet and triplets. The emission yields are above 10^{-4}, and the emission parameters often show strong temperature dependence.

Radiationless porphyrins show at most very week emission, that is, total emission yields are under 10^{-4}. In many cases no emission at all has been documented. It should be noted that, since k_f<60 ns, quantum yields in this range mean that the excited state lives only from 6 ps to 60 fs, and any prompt emission may be from unvibrationally relaxed excited states.

2.4.3.3. Pseudonormal Porphyrins

It the end, **pseudonormal** metalloporphyrins show normal absorption spectra but are not fluorescent, and present luminescence. All contain either partly filled *d* or partly filled *f* shells. These porphyrins are coordinate to paramagnetic metal, and all the lanthanides with partly filled *f* shells appear to be pseudonormal.

Table 2.1 provides a matrix of the three absorption and four emission types and has one last piece of nomenclature.

Emission type \ Absorption type	Normal	Hypso	Hyper	Definition
Fluorescent	Regular	—	—	$\Phi_f > 10^{-3}$, $\tau_p > 1$ msec, $\Phi_{em} > 10^{-3}$
Phosphorescent	—	Irregular	Irregular	$\Phi_f < 10^{-3}$, $\tau_p < 3$ msec, $\Phi_p > 10^{-4}$
Luminescent	Irregular / Pseudonormal	Irregular	Irregular	Paramagnetic metal, $\Phi_{em} > 10^{-4}$
Radiationless	Irregular / Pseudonormal	Irregular	Irregular	$\Phi_{em} < 10^{-4}$
Definition	For $\lambda > 320$ nm, only (π, π^*) bands, *Q*, *B*, *N*. $\lambda(Q) > 570$ nm[c]	For $\lambda > 320$ nm, only (π, π^*) bands, *Q*, *B*, *N*. $\lambda(Q) < 570$ nm[c]	For $\lambda > 320$ nm, relatively intense absorption bands not (π, π^*) in origin	

1)

Table 2.1:Electronic Absorption an Emission Taxonomy

2.5. 1,19-DIUNSUBSTITUTED A,C-BILADIENES

Open-chain tetrapyrroles are a class of compounds directly correlated with their cyclized counterparts such as porphyrins and related macrocycles, although their chemistry has been studied far less extensively. These compounds can be considered as the synthetic analogs of natural bile pigments, such as bilirubin and biliverdin. However, while in nature bile pigments are generally produced from the catabolism of heme [19], in tetrapyrrole synthetic chemistry these compounds have been used as precursors of the porphyrin ring [20]. Furthermore, different macrocycles can be obtained from the cyclization of a,c-biladienes depending upon both the reaction conditions and the substituents present at their 1,19-positions [[21]]. Corroles have experienced renewed interest over the last few years because of unique properties that make this macrocycle of interest for exploitation in catalysis and sensor applications [22]. The first preparation of corrole was reported by Johnson and Kay in the mid- 1960s and it was carried out by the photochemical cyclization.

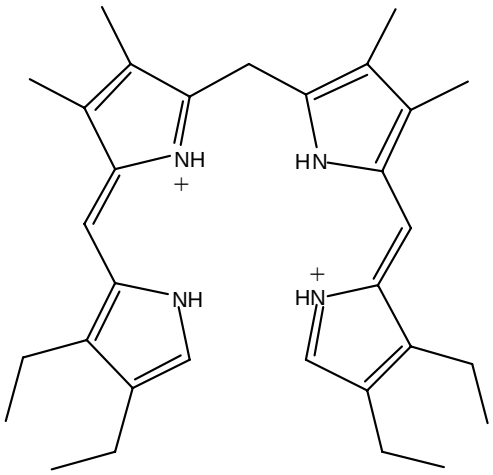

Figure 2.9: Biladiene Structure.

2.6. EXPLOITED CIMS SPECTRA

For our purposes many different porphyrins and some open-chain tetrapyrroles have been investigated. In fact, as reported above, absorption and emission spectra, furthermore interesting optical phenomena (as fluorescence quenching), are strictly related to porphyrin type (see Table 2.1). Furthermore selectivity, sensitivity reproducibility, reversibility, stability etc. depend on particular material that has been chosen. In this way it is clear that an important step to design an sensorial system, matter in hand an optical device, is the choice of right CIMs, that must have suitable optical properties. For these reasons we exploit biladiene and metalloporphyrins with different central-metals, which confer to these CIMs very different absorption-emission spectra and then various colors. In this Thesis we investigate a very versatile colorimetric sensor array that exploits different type of CIMs. In particular we have successfully used (5,10,15,20-tetraphenylporphyrin)zinc ([Zn(tpp)]), (5,10,15,20-tetraphenylporphyrin chloride)iron ([Fe(tppCl)]), 2,3,17,18-tetraethyl-7,8,12,13-tetraamethyl-a,c-biladiene dihydrobromide (BD), Mn(tpp), Co(tpp), etc. because their optical-cross sensitivity properties to the classes of volatile compounds that have been measured.

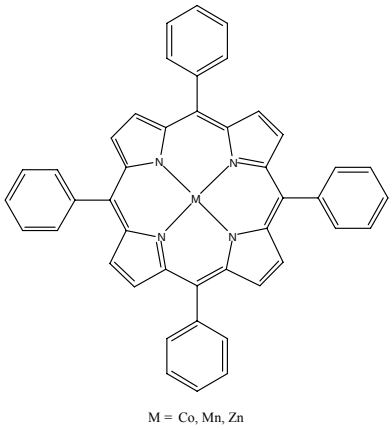

Figure 2.10: Structure of a tetraphenylporphyrin.

The optical features showed by these CIMs make these molecules particularly appealing for optical sensing purposes. As has been shown in previous paragraphs the absorption and luminescence properties derive from the aromatic character of these materials and are related to electronic transitions within their π-aromatic system. In this case the coordination of ligands at the axial positions can strongly influence the electronic structure and consequently the electronic spectra. Furthermore, in solid state porphyrins another important feature that must be take into account is the presence of π - π interactions between macrocycles: the consequence of these aggregation phenomena in the absorption spectra is broad, splitting and shifts of the bands with respect to the solution spectra [23]. Interactions with volatile organic compounds (VOCs) can induce a decrease of these interactions, leading to additional modifications of the spectra. All these spectra changes are proven to be interesting and useful for applications of these CIMs in optical sensors. Several examples have been reported in the literature concerning the exploitation of porphyrins in optical devices [24], then these materials have been proven to show, in solid state phase, a broad selectivity in order to cope with the much large number of compounds. For choosing the right CIMs, have been made a lot of measurements by spectrometer. From these preliminary experiments results sometimes a significant variation in absorption/emission spectra upon exposure of different analytes, for example, amines (Figure 2.11), or sometimes only subtle modification of the spectrum (Figure 2.12), but enough for their exploitation by CSPT.

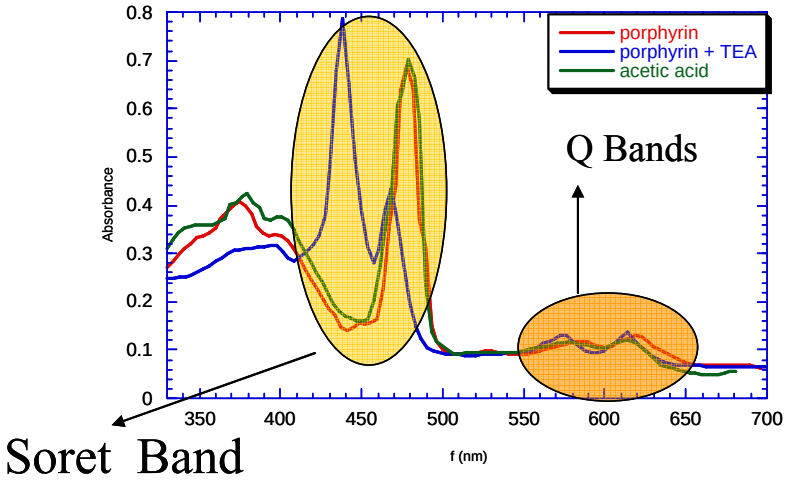

Figure 2.11: Examples of changes in absorption spectrum of porphyrins after exposure with TEA and acetic acid.

For these reasons metalloporphyrins, related Metal complexes and TetraPyrrolic Compounds have been chosen in the CSPT measurements like sensing materials.

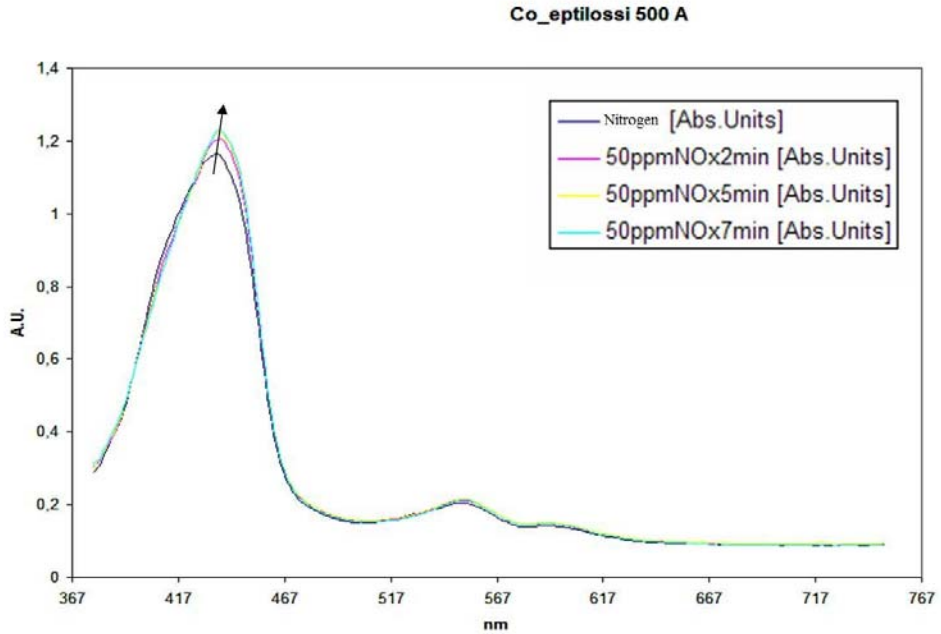

Figure 2.12: Absorbance spectrum changes of a 500 A thickness film of porphyrin upon exposure different concentration of NOx.

REFERENCES

[1] J. W. Grate, Chem. Rev. 100, 2627 (2000).

[2] a) J.-M. Lehn, *Supramolecular Chemistry*, Wiley-VCH, Wienheim, (1995); b) J. L. Atwood, J.-M. Lehn, *Comprehensive Supramolecular Chemistry*, Pergamon Press, Oxford, 1996.

[3] R. Lemberg, J.Falk, *Biochem.J.*, 1951, 49,674.

[4] D:T: Lash, *Energy & Fuels*, 1993, 7, 166.

[5] J.L.W. Thudichum, *Report Med.Off.Privy Council*, 1867*, Appendix 7-10,* 152

[6] M. Nencki, N. Sieber, *Arch. Exptl. Path. Pharmakol.,* 1884, 18, 401.

[7] M. Nencki, J. Z. Zaleski, *Z. Physiol. Chem.*, 1901, 34, 997.

[8] W. Kuster, *Z. Physiol. Chem.*, 1912, 82, 463.

[9] H. Fisher, J. Klarer, *Liebigs Ann. Chem.*, 1926, 440, 181.

[10] H. Fisher, B. Wallach, *Liebigs Ann. Chem.*, 1926, 468, 98.

[11] D. C. Becker, B. R. Bradley, C. J. Watson, *J. Am. Chem. Soc.*, 1961, 83, 3743

[12] J. L. Soret, *Compt. Rend.*, 1883, 97, 1267.

[13] J.R.Plat, in "*Radiation Biology*" (A. Hollaender, ed.), Vol III, Chapter 2. McGraw-Hill, New York, 1956.

[14] J. L. Hoard, in *Porphyrins and Netalloporphyrins*; Smith, K. M., Ed.; Elsevier: Amsterdam, 1975; pp. 317.

[15] A. Stern, G. Klebs, *Ann. Chem.*, 1932, 500, 91.

[16] J. W. Buchler, in *Porphyrins and Netalloporphyrins*; Smith, K. M., Ed.; Elsevier: Amsterdam, 1975; pp. 157-231.

[17] Gouterman M., The *Porphyrins,* Dolphin D., Ed., Vol. III, p. 1, Academic, N. Y., 1978.

[18] Joseph R. Lakowicz, *Principles of Fluorescence Spectroscopy*, Plenum Press, New York and London.

[19] a) Falk H. *The Chemistry of Linear Oligopyrroles and Bile Pigments*; Springer Verlag: Wien, 1989. b) O. Carra P. *In Porphyrins and Metalloporphyrins*, Smith KM. (Ed.) Elsevier: Amsterdam, 1975; pp 123-155. c) Schmid R and Mc Donagh AF. In *The Porphyrins*, Vol. 6, Dolphin D. (Ed.) Academic Press: New York, 1979; p 257. d) Kadish KM, Guilard R and Smith KM, Eds. *The Porphyrin Handbook*; Academic Press: San Diego, 2003; Vol. 13.

[20] Smith KM. In The Porphyrin Handbook, Vol.1, Kadish KM, Smith KM, Guilard R. (Eds.) Academic Press: San Diego, 2000; pp 1-43.

[21] R. Paolesse, A. Froiio, S. Nardis, M. Mastroianni, M. Russo, D. J. Nurcob and Kevin M. Smith, Novel aspects of the chemistry of 1,19-diunsubstituted a,cbiladienes, Journal of Porphyrins and Phthalocyanines, 2003; 7: 585-592, Published at http://www.u-bourgogne.fr/jpp/

[22] Di Natale C, Paolesse R, Macagnano A, Mantini A, Goletti C and D'Amico A. *Sens. Actuators, B* 1998; B52: 162-168.

[23] G.A. Schick, I.C. Schreiman, R.W. Wagner, J.S. Lindsey, D.F. Bocian, J. Am. Chem. Soc. 111_1989.1344.

[24] J. Spadavecchia, R. Rella, P. Siciliano, M.G. Manera, A. Alimelli, R. Paolesse, C. Di Natale, A. D'Amico, Optochemical vapor detection using spin coated thin film of ZnTPP, Sensors and Actuators B 115 (2006) 12–16.

CHAPTER 3

CSPT-Enose mode based Chemical Sensor Array

INTRODUCTION

GAS SENSOR ARRAY

According to the International Union of Pure and Applied Chemistry (IUPAC) nomenclature, '*a chemical sensor* is a device that transforms chemical information, ranging from the concentration of a specific sample component to total composition analysis, into an analytically useful signal'. Then a gas sensor array is an appropriate chemical sensor matrix that enables detection of volatile compounds; it is something like an artificial olfactory system if it is a non selective and enough sensitive sensor array capable to respond to mixture of gas. In few words, electronic nose can be considered "an instrument, which comprises an array of electronic chemical sensors with partial specificity and an appropriate pattern-recognition system, capable of recognising simple or complex odours" [1]. An alternative way to define the electronic nose, is to consider the subject of its investigation: complex samples characterized by the simultaneous presence of many compounds. The "quality" of these samples are sometimes not related to few specific compounds but rather to the global composition. According to this philosophy the odor could be described not by a sum of its individual components but by some abstract representation, a sort of *chemical image*, a virtual fingerprint. A strategy to measure these samples is to use instruments sensitive to the globality of the compounds. An electronic nose is an array of individual sensors different one each other but globally selective according to the principle that each sensor senses more compounds and each compound is sensed by more sensors.

The concept of using sensor array for chemical analysis offers advantages over individual sensors concerning sensitivity to a wider range of analytes, improved selectivity and the capability for recognition of both single and complex analytes.

There are three main steps designing artificial olfactory systems: the sensing material, which must 'catch' the odorant molecules; the transducer, which transform the chemical

information in a physical one; and the basic device, which translate this physical quantity variation in an electronic signal. The chemical recognition translates information from the chemical domain, into a physical output signal with a defined sensitivity. The electrical signal is the starting point of the measurand properties extraction and elaboration.

In analogy with natural olfaction an array of non-specific, cross-sensitive sensors is utilized together with a CSPT platform and a suitable data processing method in order to detect molecules such as amines, NO_x and CO. This possible exploitation of CSPT (running in electronic nose modality) such as a Gas Sensors Array will be presented in this Chapter.

3.1. PHOTOPHYSICAL FEATURES OF METALLOPORPHYRINS

Brief description of sorption phenomena

Considering the different interactions taking place in the binding processes between odorant molecules an CIMs, we can observe two main types of solid gas interaction:

- Physisorption
- Chemisorption

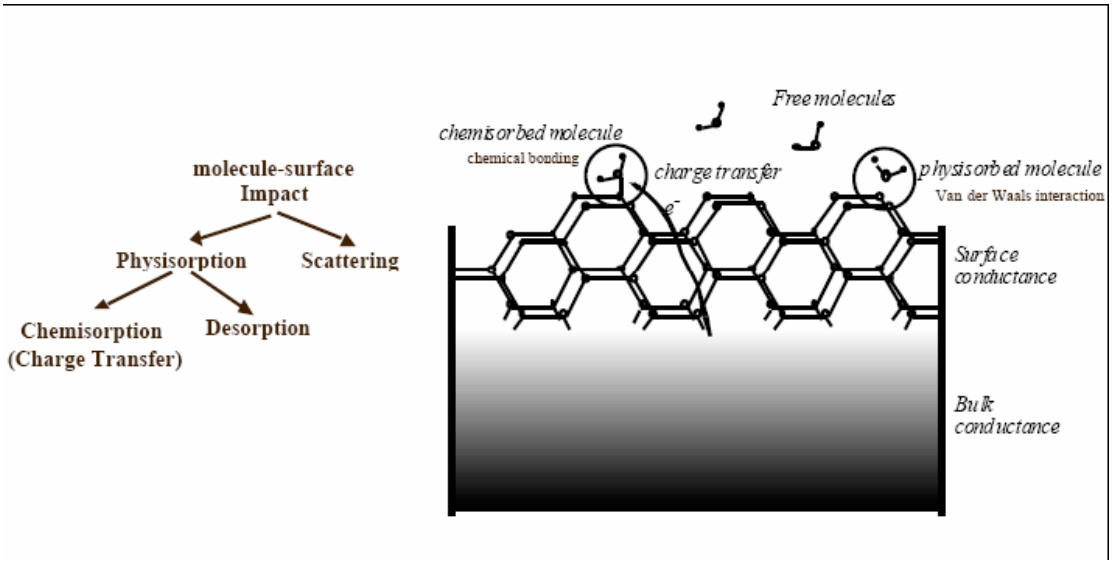

Figure 3.1: Schematic representation of sorption phenomena

The contribution of each of the above mentioned mechanisms depends on the nature of receptors centers, thickness of the sensitive layer and film structure. The forces involved in Chemisorption are the valence forces involved in the formation of chemical compounds. The forces involved in Physisorption are intermolecular forces, with not significant change in the electronic orbital patterns of the species involved. Between Chemisorption and Physisorption a not absolutely definite distinction can be made because of the relevance of intermediate cases; for instance adsorption involving strong hydrogen bonds or weak charge transfer. There are a number of factors which determine the strength and specificity of

intramolecular interaction, such as molecular size and symmetry; polarizabilty of the molecular skeleton; substituents type, number and polarity; degree of freedom of individual molecular components; hydrophilic-hydrophobic properties of interacting components. Usually, the higher is the interaction specificity, the stronger is the interaction. But for sensor applications reversibility of the sorption process is a must. In these processes the adsorbed molecule is held on the solid surface by the forces of predominantly electrostatic nature. These are Van Der Waals, Hydrogen, donor-acceptor interactions. The Van Der Waals forces are a special kind of weak non-valence interactions. The dispersion force is the most general example of these type of interactions. The main features of these interactions is that they are not oriented somewhere. The polar molecules demonstrate interaction not only through the dispersion forces but also by means of dipole and induction forces of electrostatic origin. Hydrogen bonding, another type of intermolecular interaction characteristic of the reversible adsorption processes, presents an energy much more over Van Der Waals one. It determine a stronger interaction of higher specificity. A weak donor-acceptor bonding also can be a reason for physical adsorption.

An understanding of the sorption and selectivity is important to design such sensors, this choice, anyway, depending not only on the CIM but also on the target analyte. Indeed the goal is finding suitable materials that change some of their physical property, in our case optical properties. Furthermore tailoring the physical and chemical properties of sensitive materials used in the sensors can control the selectivity and sensitivity of each sensor.

3.2. PORPHYRINS AS CHEMICAL INTERACTIVE MATERIAL

One of the main steps for designing a gas sensor array is the choice of Chemical Interactive Materials (CIMs). In fact, these materials are strictly connected with particular transducer, because the choice of the CIM keeps the definition of the transduction mechanism. In our case, as has been detailed described in the Second Chapter, Porphyrins and related macrocycles are able to change their optical properties becoming suitable for Computer Screen Photo-assisted Transduction Technique.

In the last decade the capability of these molecules to bind guest molecules in gaseous and liquid phases has been exploited to fabricate chemical sensors [2]. In particular, sensors based on porphyrins behaved quite well in artificial olfaction systems [3] where it is required a control of selectivity properties in terms of orienting the sensitivity towards certain classes of molecules maintaining a large selectivity. From this point of view metalloporphyrins are the widest family of metallo-organic compounds ensuring a large spectra of coordination and other weaker binding processes.

Metalloporphyrins are a natural choice for the detection of ligating vapors because of their open coordination sites. The rich combination of metal ions, ring, and peripheral compounds provides a large number of possibility to assemble sensors. In order to assemble sensors is necessary to transduce some physical variation of molecular properties changing upon the interaction with the analyte (as can be seen in previous paragraph).

In the past metalloporphyrins have been only used coupled with quartz microbalances nonetheless, porphyrins are very well known for their optical properties whose importance can be understood from Nature. Indeed, the difference in color between artherious and venous blood is due to the color shift underwent by the porphyrins that in one case carry oxygen (artherious blood is red) and in the other carry carbon dioxide (venous is blood is blue). In particular, the coordination of a CO molecule at a free ligand site of a metalloporhyrin results in a modification of the optical spectrum. Optical transduction of

porphyrins sensing effects have been proposed measuring either the spectra or the integral of the transmitted light [4].

3.3. DETECTION OF VOLATILE COMPOUNDS

In this Section will be demonstrated the analytical capabilities of CSPT for detecting and recognizing different molecules with an inexpensive (and eventually disposable) optical-sensing interface. By using semitransparent spots of porphyrins as sensors we show that is possible to detect detailed and partially disentangled absorption and emission responses resulting from molecules such as amines, CO, and NO_x. The current system is also representative of other sensing approaches that use arrays of fluorescent indicators, and highlights the possibility of analyzing complex response patterns with available means. We demonstrate a disposable array of sensing substances that responds with a variety of absorption and emission changes that can be characterized by CSPT. The ability of the system to generate and analyze complex response patterns enables sophisticated determinations using an available and globally disseminated infrastructure (for example, computer sets). Here such a molecular system is chosen because of its rich variety of spectral responses that are used to test the method and to exemplify its possibilities for evaluating fluorescence-labeled assays in general.

3.3.1 Experiment details and Measurements setup

Thus it has been made experiments on spots of thin layers of (5,10,15,20-tetraphenylporphyrin)zinc ([Zn(tpp)]), (5,10,15,20-tetraphenylporphyrin chloride)iron ([Fe(tppCl)]), and 2,3,17,18-tetraethyl-7,8,12,13-tetraamethyl-a,c-biladiene dihydrobromide (BD) dispersed in a polyvinylchloride (PVC) matrix and spotted in duplicate on a glass slide (inset in Figure 3.2).

Metalloporphyrins and BD were prepared according to a literature method [5]. The array was prepared by deposition of drops of PVC membrane solutions (1 wt% of porphyrin, PVC/bis(2-ethylhexyl)sebacate (1:2) polymeric matrix) in tetrahydrofuran onto glass slides [6]

Evaporation of the solvent led to the formation of a PVC/porphyrin membrane. Two spots of each porphyrin were made as illustrated in the inset of Figure 3.2 to test the reproducibility of the method. The glass slide with the printed sensing array was introduced into a gas cell (Figure 3.2) with glass walls, where it was exposed to controlled concentrations of different gases with the aid of an automatic gasmixing system.

The sensing array was exposed to low concentrations of molecules such as NH_3, NO_x, CO, ETOH and triethylamine (TEA) in nitrogen [7]. The measuring procedure used is standard to CSPT experiments [8] and involves a regular LCD screen (Philips 170S4) used as a light source and a Logitech Quickcam pro 4000 operating at a resolution of 320 x 240 pixels used as the image detector. A sample holder such as that described in The First Chapter provides a controlled geometry for the measurements, and shields the experiments from ambient illumination.

Software written by us in Matlab commands the measurement procedure (illuminating sequence and video acquisition) and extracts the information (CSPT fingerprints) from manually selected ROIs (white circles in the inset Figure 3.2).

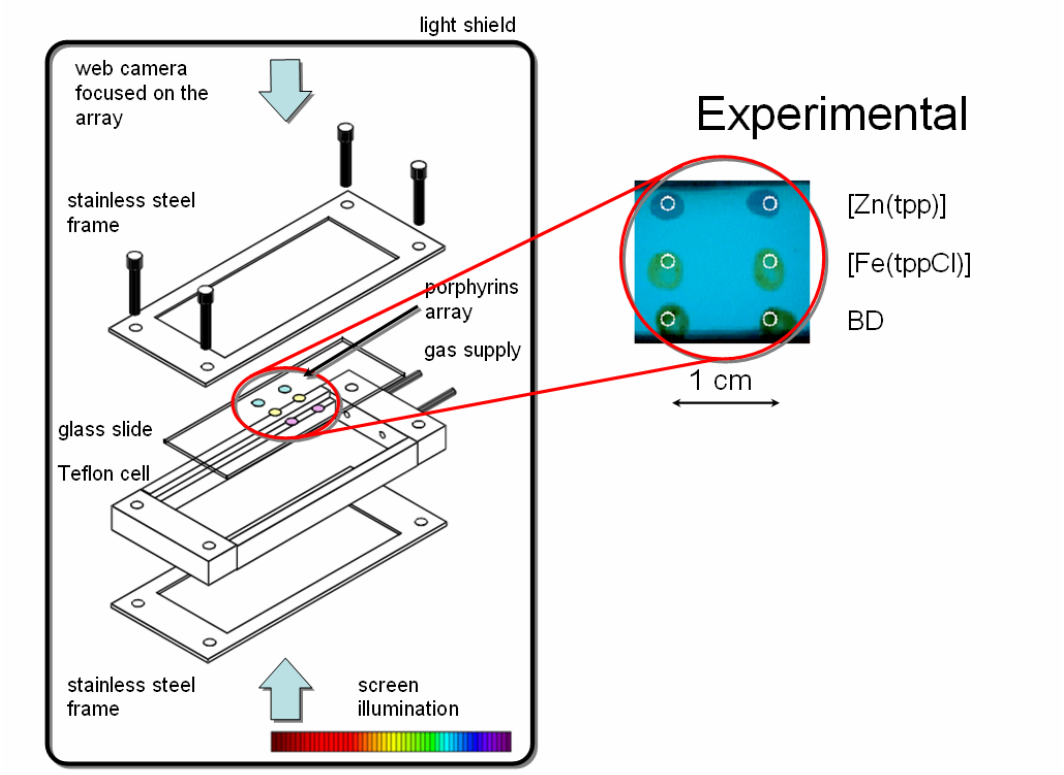

Figure 3.2: Measurements Cell Details.

3.3.2 Spectral-Fingerprints extraction

During this CSPT measurement web camera captures the image of the array under an illuminating sequence of a rainbow of 50 colors provided by the LCD screen. From this video stream regions of interest (ROI) are selected (the white circles in Figure 3.2) and used to compose substance fingerprints. The changes in the intensity (average of all the pixels in each ROI) recorded in the channels of the web camera with respect to the intensities recorded in pure nitrogen are shown in Figure 3.3a. Signals from the red, green, and blue channel are concatenated in this order, and the fingerprints of all the spots are composed in a single fingerprint of the array (Figure 3.3a). An CSPT-fingerprint of 1500 ppm of triethylamine (TEA) are showed in Figure 3.3a. The data correspond to absorption/emission changes of the indicator spots upon exposure to TEA observed as intensity changes in the

red, green, and blue channels of the web camera for different screen illuminations. These results were obtained from exposure, at room temperature, of the array to 1500 ppm of TEA in N_2 with the signal of N_2 subtracted.

In fact in almost all chemical sensors the measurement of sensor reaction exposed to gas is calculated subtracting (in some cases dividing) the response to the response to a blank exposure (typically nitrogen). This strategy for chemical sensors measurement has been applied to the CSPT transduced chemical sensors. Then each Fingerprints has been calculated as Difference-Fingerprints: ($Response_{gas}$-$Response_{nitrogen}$). Moreover replica of the same molecular films have a common behaviour (Figure 3.3a)

Each spot becomes represented by 50 values in the red channel, 50 values in the green channel, and 50 values in the blue channel. The units on the y axis are in "intensity level changes" of the web camera signal (that is, between -255 to +255)). The numbers on the x axis identify illuminating colors for the three camera channels and for the six imaged spots. All 900 points were obtained during one single run of the illuminating sequence of 50 colors (about 50 s per measurement). The inset of Figure 3.3a shows an image of the array at one given color frame ("blue") on the computer screen. The circles, as mentioned above, illustrate "the Regions of Interest" (ROIs) used to calculate the average intensity of the light reaching the web camera through the indicator spots. In this figure are also shown the illuminating sequence used (colors 1–50) as well as the concatenation of the camera channels to construct the fingerprints of a particular spot.

The intensity measured, for example, in the red channel of the web camera, for an illuminating color i defined by the triplet (r_i, g_i, b_i) is given by Equation (3.1):

$$I_{Ri,j} = \int_{\lambda} \left[r_i R(\lambda) + g_i G(\lambda) + b_i B(\lambda) \right] \cdot S(\lambda, i) \cdot F_R(\lambda) \cdot D(\lambda) \cdot d\lambda \qquad (3.1)$$

The spectral radiances of the screen primary colors (R(λ), G(λ), and B(λ)) are polychromatic sources illuminating the tested substance, and represented by S(λ, *i*), which accounts for the substance transmittance T(λ) and emission (E(λ,*i*) spectra weighted by the spectral

composition of the illumination. The red, green, and blue filters of the web camera and the spectral response of the detector are represented by $F_R(\lambda)$,$F_G(\lambda)$, $F_B(\lambda)$, and $D(\lambda)$, respectively. Equation (3.1) summarizes the way that CSPT perceives the excitation emission characteristics of the tested substances when illuminated by the polychromatic light provided by the screen. Figure 3.3b collates the response features from different concentrations of target stimuli.

The different features of the results in Figure 3.3b are understood from the corresponding absorption and emission changes of the different porphyrins resulting from the target molecules, and are related to shifts in the absorption and emission peaks, as well as changes in the peak sizes and widths.

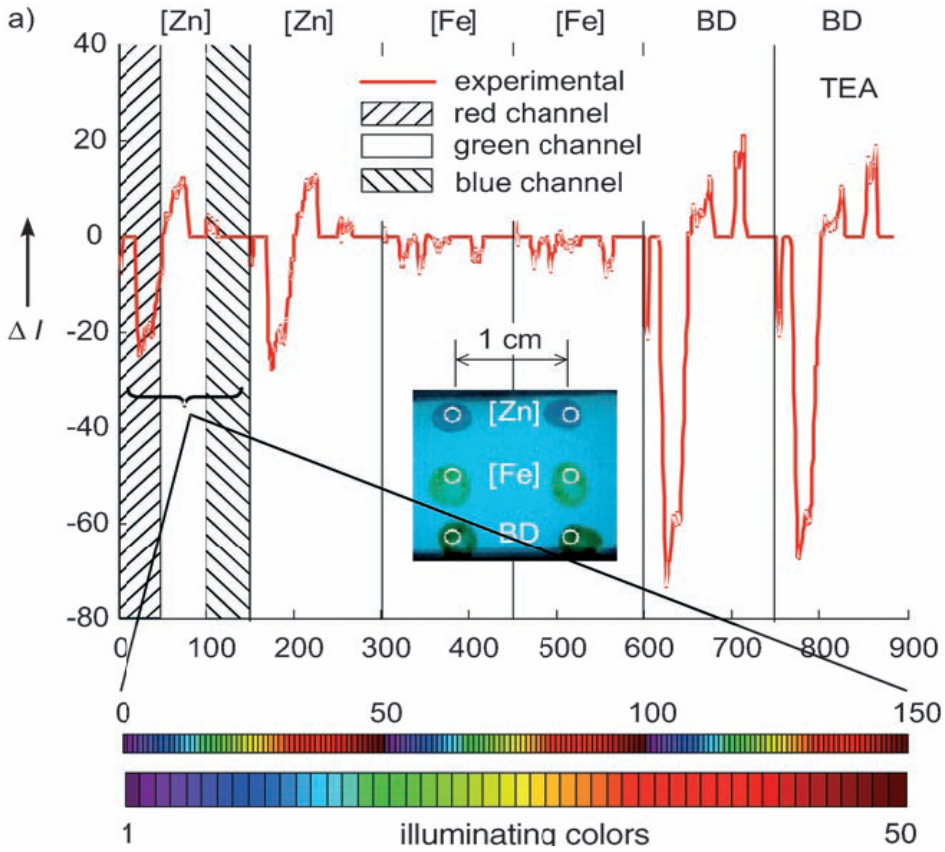

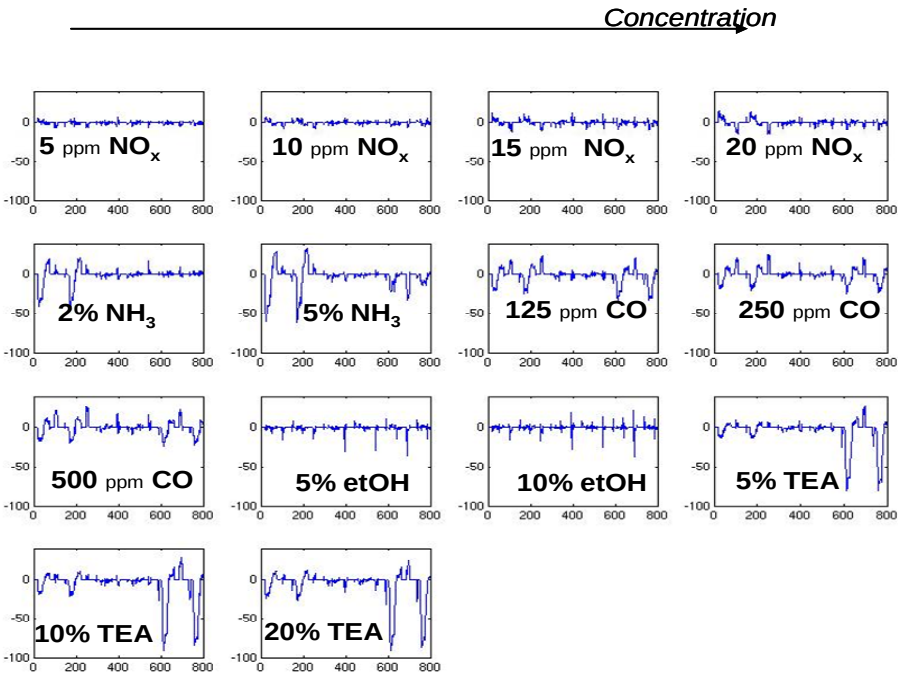

Figure 3.3: a:) CSPT-Fingerprint of 1500 ppm of triethylamine (TEA). [Zn]=[Zn(tpp)], [Fe]=[Fe(tppCl)], BD=biladiene; b) CSPT-Fingerprints of a number of molecules at different concentrations obtained with the array of porphyrin spots. Sensitive films were exposed to: NO_x: 5, 10, 15, 20 ppm, NH_3: 2%, 5%, CO: 125, 250, 500 ppm, Ethanol: 5%, 10%, Triethylamine: 5%, 10%, 20%. Before each gas sequence, sensitive films were "washed" in N_2. For each sequence, the response has been calculated subtracting the response to gas from the response to the first N_2. Data were analyzed by Principal Component Analysis.

3.3.3 Principal Component Analysis of Spectral-Fingerprints

The ability of CSPT as a method for practical evaluations depends on how well the fingerprints in Figure 3.3b distinguish different molecules. A simple and efficient way to summarize and compare information in complex signals is to apply Principal Component Analysis (PCA, details in Appendix) to the fingerprints.

Figure 3.4a shows the first two principal components of the whole set of fingerprints which explain about 92% of the original information. This plot shows the classification of the considered molecules for the different tested concentrations. The Score Plot with some Raw Data representations in Figure 3.4b address the correlation of the classification with the source of the CSPT signals. In these graphics, scores that are 100% correlated with a measuring condition lie in the same direction, while perpendicularly oriented elements are

not correlated. Thus, possible is to identify the CSPT measuring conditions that determine the ability of the CSPT fingerprints to distinguish the different target stimuli. For example, NH_3 detection is mainly correlated with the [Zn- (tpp)] response observed in the red channel (Figure 3.4b), which identifies changes in the emission, whereas the blue channel recognizes CO. Similarly, the detection of TEA is correlated with the quenching of the BD fluorescence. From Figure 3.4 it is also possible to identify a subset of optimum illuminating conditions that could produce a similar result with a shorter color sequence, an important aspect for implementing fast measurements or determination based on mobile phones instead of computer sets.

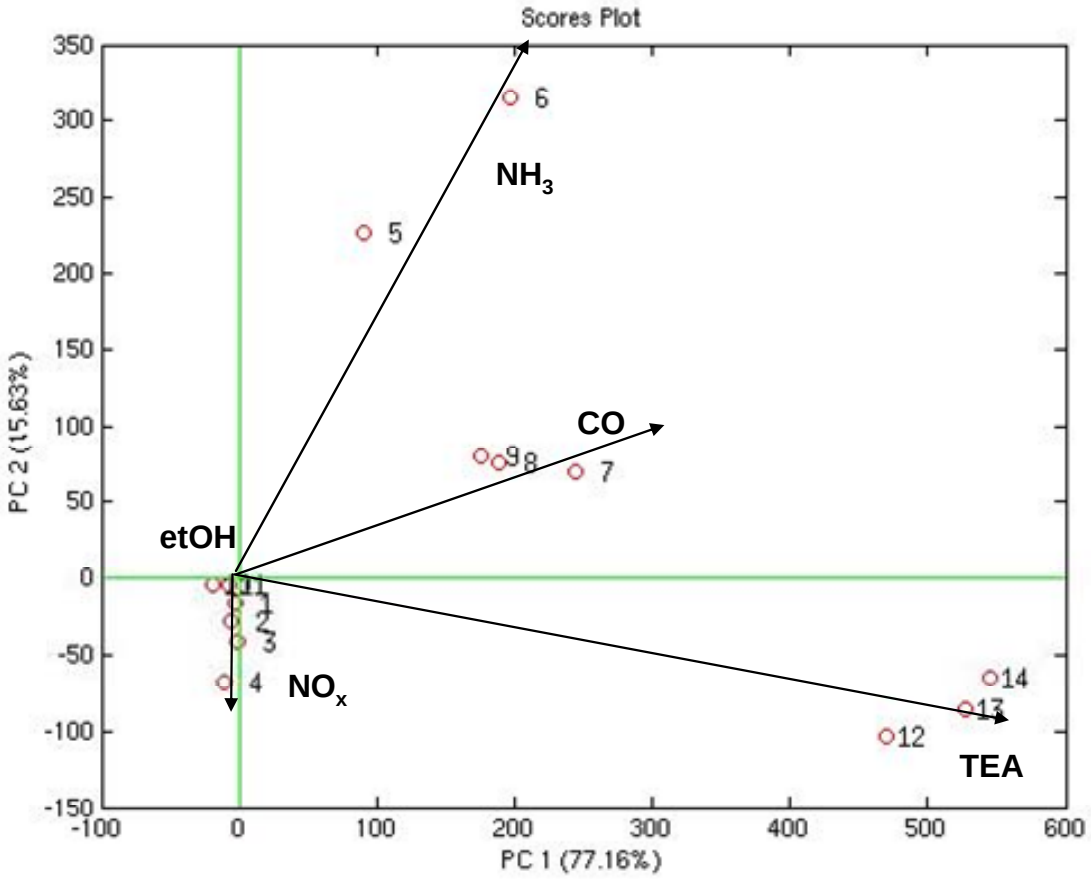

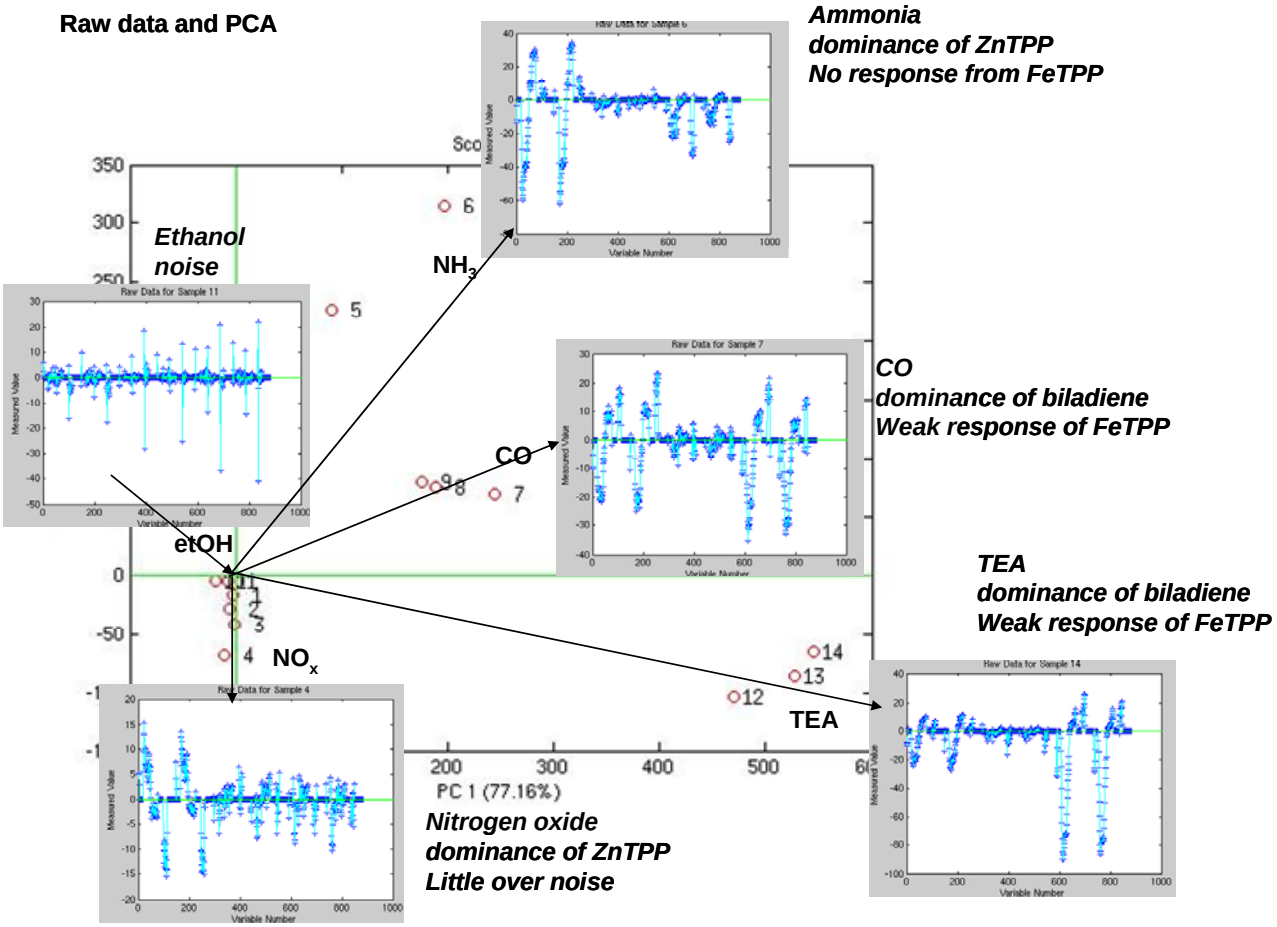

Figure 3.4: a) Score Plot of the first two Principal components of the results in Figure 3.3b. The intensities in the three channels were made into a data set consisting of 900 points for each measurement and evaluated by standard PCA. The scores plot shows the classification properties of CSPT. The arrows indicate the evolution of the points in the score plot for increasing concentration of the target gases.
b) Some Raw Data of PCA analysis. Comments: Not sensitive to ETOH, ETOH cluster coincides with the zero. Sensitive (with different intensities to the other gases). Different directions means different contribution of porphyrins -> good orthogonality.

3.3.4 Analysis of the Chemical Responses

In this measurements we selected Zn– and Fe–metal complexes of tpp and a linear tetrapyrrole (BD). In the case of metalloporphyrins, the coordination of the analytes to the metal center is the expected sensing mechanism; aggregation of macrocycles or other matrix effects are ruled out by the dispersion of the porphyrins into the PVC membrane. We selected Zn and Fe complexes because they are representatives of two broad classes of

porphyrins according to Gouterman's classification: [Zn(tpp)] represents a "regular" porphyrin, while [Fe(tppCl)] is a typical "irregular" porphyrin [9].

As an important consequence for CSPT applications, [Zn- (tpp)] produces fluorescence emission, while [Fe(tppCl)] is a radiationless substance.

In the case of [Zn(tpp)], coordination at the metal center generally induces a red-shift of both the absorbance and emission bands, together with a significant quenching of the fluorescent emission [10] (which is observed as a negative peak in the red channels for a blue illumination, see for example Figure 3.3a). All these features are well represented in the CSPT results by positive and/or negative peaks arising from predominant absorption and/or emission responses, respectively.

In the case of [Fe(tppCl)], the "irregular" absorbance optical spectrum gave less evident changes in the CSPT responses and this feature, together with the lack of emission, results in smaller responses (Figure 3.3b).

A completely different sensing mechanism should be considered with BD; the linear tetrapyrrole is stable as a dication and its interaction with bases induces significant changes in the molecular structure and consequently in the optical spectra. Loss of a proton leads to the formation of the 22,24-a,b,c-dihydrobilatriene hydrobromide and the loss of a further proton to the corresponding free base, with color changes from red to yellow-orange to green. In solution the formation of the BD free base leads to the formation of corrole by a ring-closure reaction [11].

In the CSPT measurements we observed an unexpected reversibility of the BD layers upon interaction with TEA or NH_3. Concurrent spectral analysis of a model system suggests that the cyclization reaction does not occur so rapidly in the PVC membranes. From the CSPT results a significant variation in fluorescence after interaction, for example, with amines, even stronger than those obtained with [Zn(tpp)], was expected and corroborated by emission/absorption spectroscopy.

3.4. FISH FRESHNESS DETECTION

In the last years a large number of different measurement methodologies were applied to measure the freshness of fishes. Among them the connection between freshness and headspace composition has been considered by gas chromatographic analysis and from the last two decades by a number of sensors and biosensors aimed at measuring some characteristic indicator (usually amines). More recently also the so-called artificial olfaction systems gathering together many non specific sensors have shown a certain capability to transduce the global composition of the fish headspace capturing the differences between fresh and spoiled products. One of the main objectives related to the introduction of sensor systems with respect to the analytical methods is the claimed possibility to distribute the freshness control since sensors are expected to be “portable” and “simple”. In spite of these objectives, until now sensor systems did not result in any tool that may be broadly distributed.

Then we have exploited a chemical sensor array where the optical features of layers of chemicals, sensitive to volatile compounds typical of spoilage processes in fish, are interrogated by CSPT.

A current regulation of the European Community (1996) establishes the principles, mainly based on sensory analysis and chemical and microbiological tests, to control and certify the quality warranty in the seafood field [12], However, the quality attributes include a series of parameters related to safety, nutritional quality, availability, freshness and edibility [13], which may be affected mainly by handling, processing and storage procedures from the catch to the consumers. Physical, chemical, biochemical and microbiological changes occurring post-mortem in fishes, result in a progressive loss of food characteristics in terms of taste and general concept of quality. Both the passed time and the storage temperature of fish are key factors for the final quality of the product. Fish spoilage depends, in fact, mostly on temperature, which controls to a large extent the bacterial and the autolytic breakdown. Moreover, the rate of spoilage depends on several factors such as the kind of

fish species, the sanitary conditions on board, and the amount of food in the guts. Fish freshness is the most required property from the consumers because of its strong relationship to the taste. A number of sensorial inspection procedures have been introduced to point out the state of freshness. These procedures involve the use of sight (to evaluate the skin appearance and the colour and the global aspect of eyes), tactile (to test the flesh firmness and elasticity) and olfaction (to smell the gill odour). However, trained panels are generally expensive, time consuming, and not always available along the different steps of the fishery chain. Consequently, to satisfy the need for quality measurements in the fish industry, instrumental methods are needed.

Several instrumental techniques are available to measure physical, chemical and biological parameters of fishes such as spectrophotometers, texture meters, image analysers, colorimeters, devices to test surface electrical properties and electronic noses. An excellent introduction to instrumental methods for fish freshness determination is found in ref. 14. There the determination of the overall freshness was shown to be viable for a complete instrumental quality evaluation [15].

3.4.1 Fish Headspace and Chemical Sensors

The composition of fish headspace is a source of information about its freshness. Previous investigations evidenced that the headspace composition is a result of the balance between the “fresh fish” odour and the microbial spoilage produced compounds [16]. The most important chemicals involved in the fresh fish odour are long-chain alcohols and carbonyls, bromophenols and N-cyclic compounds. Their concentration and the presence of other compounds are rather typical of each species. On the other side, microbial spoilage produces short-chain alcohols and carbonyls, amines, sulphur compounds, aromatic, N-cyclic, and acid compounds. The concentrations of these chemicals are directly correlated to the degree of spoilage. Among these compounds amines are considered as the typical markers for fish freshness detection. Standard analytical methods for volatile amines and

also sensors for some specific amines have been used to inspect fish freshness. Nevertheless, amines become instrumentally appreciable only when spoilage processes take place. Minor contributions to the fish headspace come from contamination of the environment (e.g. petroleum in sea), from fish processing and finally from products of lipid oxidation [17].

The large number of compounds whose concentrations are only partially correlated make this application particularly appealing for sensor arrays of partially selective chemical sensors. Such sensor arrangement consists in the application of a number of sensors characterized by a broad sensitivity towards those species that are relevant for a certain application. When properly analyzed by pattern recognition methods, the data produced by a sensor array can classify samples according to some of their global features. In case of fishes typically according to the freshness, or more precisely according to the balance between fresh and spoilage produced compounds. The similarities between arrays of chemical sensors and natural olfaction was argued in the mid of eighties [18] and therefore this kind of sensor system was nicknamed as electronic nose. In the last twenty-five years electronic noses were demonstrated making use of almost all the available gas sensor technologies [19]. The aptitude of some of these electronic noses to capture the changes in fish headspace and to correlate these changes with the freshness was demonstrated in several applications using different kinds of chemical sensors such as: metal oxide semiconductors [20], quartz microbalances [21], electrochemical sensors [22] among the others. Although known for several years [23], the colorimetric detection of fish freshness received recently a great interest. In particular, the importance of amines induced to consider their reducing role and then the possibility to detect them with functional layers sensitive to pH. Paquit et al. recently demonstrated the feasibility of this approach using as sensitive layer a film of a sodium salt (bromocresol green) [24]. This salt exhibits a rather large change in colour also appreciable by eye. Nonetheless, this method is rather limited by the fact that only amines are considered (limiting the detection not to freshness but rather to spoilage) and furthermore visual determinations have limited performances and may greatly vary between individuals.

Chemical sensing based on optically sensitive layers is a captivating strategy due to the strong influence of target chemicals on the absorption and fluorescence spectra of chosen indicators. Nonetheless, the chemical practice of this approach is badly balanced by the transducer counterpart. Indeed, traditional optical instrumentations of high quality are usually bulky and expensive. On the other hand CSPT has demonstrated its utility to study optical changes in biological samples [25] to characterize fruits according to hyperspectral imaging [26], and to classify chemicals [7]. This last application demonstrated the possibility to use CSPT as a transducer in electronic nose applications. Previous optics-based electronic noses are based either on absorbance [27, 28, 29] or on fluorescence [30, 31] while CSPT arrangement gives the possibility to evaluate both the effects.

3.4.2 Description of two Experiments type

In this Section the application of an array of metalloporphyrins and similar compounds to the measure of fish freshness will be illustrated. The experiments described provide simple examples of the potentials of the technology; they were aimed at measuring the occurrence of spoilage in ice-stored thawed fish and in fresh anchovies. CSPT measurements were complemented by gas-chromatographic analysis to consider the evolution of the headspace content.

Experimental tests of fish freshness may be biased by the fact that headspace evolution with time is to some extent correlated with the drift of sensors. Then, in order to have a randomized measurement sequence it is necessary to work with different batches of fishes. Since spoilage processes and the related headspace compositions depend on the initial conditions of fish the use of different batches can introduce an apparent non-linearity in the relationship between sensor signals and storage time [32]. Considering that the main scope of this measurements is to demonstrate the feasibility of a novel sensor technology based on the change in optical properties of some colour indicators measured with computer

peripherals, has been chosen to measure the occurrence of spoilage in a couple of basic experiments.

The first was concerned with thawed fish fillets. Thawing fillets at different time, offered the possibility to measure in one session fillets stored at 0°C for different times in a random sequence.

In the second experiment the evolution of a rapidly changing fish like anchovies is considered, measuring in a short time interval the headspace of anchovies stored at the constant temperature of 20°C in order to reproduce a room temperature storage.

3.4.2.1 Samples

Commercial frozen fillets of dusky grouper (*Epinephelus marginatus*) were bought over the counter. Each package contained 16 fillets of about 70g each. The package was preserved at -18°C and each day four fillets were thawed and kept on an ice-bed at 0°C until the measurement session. Eventually, at the measurement session samples stored for 1, 2, 3, and 4 days were available with four samples for each storage day.

For the real time spoilage experiment, a batch of anchovies was purchased. About 40 fishes were eviscerated and beheaded, the fillets were kept at the controlled temperature of 20°C, properly ventilated and measured each 15 minutes with the optical sensor array. The experiment lasted about eight hours when spoilage became evidently perceivable by human senses. The scope of this experiment was to assess the spoilage when fish is not refrigerated. Nonetheless, in order to avoid uncontrolled changes in spoilage rate the temperature was kept constant.

3.4.2.2 Instrumentations

Thawed and fresh fish headspace were analyzed with GC/MS (Shimadzu QP 2010) and a CSPT based sensor array.

In both experiments the GC was used in the splitless mode with an injection temperature maintained at about 280 °C. The GC was equipped with an EQUITY-5 Fused Silica Capillary Column 30m x 0.25mm x 0.25 μm film thickness from Supelco. The flow control mode was fixed to 27 sccm, with a column pressure of 11.6 k/Pa and a total flow of 5.2 sccm. The temperature of the column was held at 40°C for the first 4 min, then temperature was increased with rated of 2°C/min until the temperature of 200 °C was reached and maintained constant for 2 min. A final temperature ramp was then applied with a growing rate of 60°C/min to reach the temperature of 300°C. The final temperature was kept constant for 2 min.

The mass spectrometer was set with the ion source temperature and interface temperature kept fixed at 250 °C while the detector voltage was set at 0.70 kV in absolute mode; the operating time interval was between 4.30 min and 85.67 min in scan acquisition mode. The scan speed was 833 scan/sec with a mass range from 50 m/z to 450 m/z.

Conjectural compound identifications were performed comparing the mass fragmentation pattern with the NIST 147 library embedded in the GCMS solution analysis software from Shimadzu Co.

In the basic arrangement of CSPT, shown in Figure 3.5, transparent measurement cell was placed in the optical path between a computer screen and a web cam.

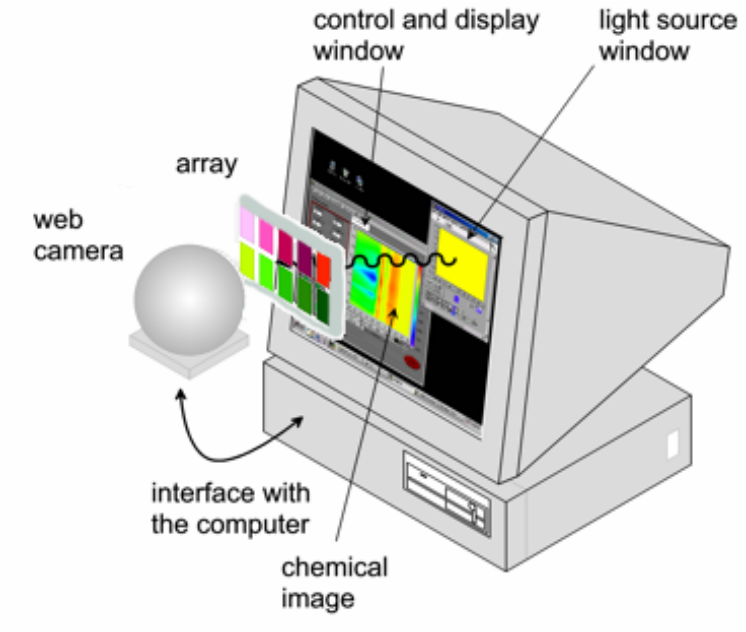

Figure 3.5: Schematic arrangement of the CSPT platform. A window in the computer screen is programmed to display colours and a web cam is placed in front of the screen in correspondence to the illuminating window. A transparent measurement cell with the sensitive layers is placed in the optical path between screen and web cam. Everything is properly shielded from ambient light and kept mechanically rigid.

As sensitive layers, three metalloporphyrins based on tetraphenylporphyrins and differentiated by the presence of iron, zinc, and manganese were used (FeTPP. ZnTPP, and MnTPP). Porphyrins were dissolved in a polymeric matrix and spotted on one of the internal glass surfaces of the cell. Figure 3.6 shows a schematic of the measurement cell and the appearance of the spots inside the cell.

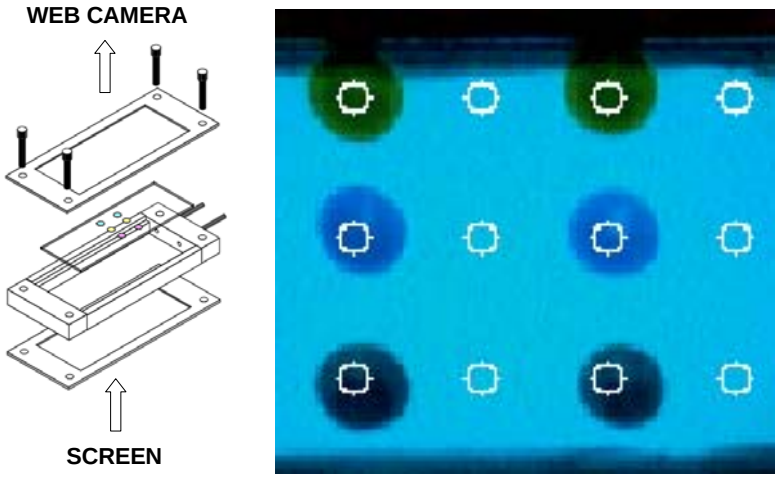

Figure 3.6: Schematic of the measurement cell consisting of two glass slides and proper spacers and provided with in- and outlets for gases (left hand image).Web cam image of the measurement cell with the sensing layers taken with a bluish illumination. In order from the top: MnTPP, ZnTPP, and FeTPP spots are visible each; porphyrin is spotted twice. In the picture the region of interest (ROI) for each sensitive layer and the corresponding background are also shown. The RGB values of the pixels inside each ROI are averaged and after subtraction of the background contribute to form the CSPT fingeprint.

Also in these two experiments type a rainbow of 50 has been used as illuminating sequence, and from video stream of CPTS measure two regions of interests (ROI) for each sensing layer are selected (the white circles in figure 3.6). One ROI is centered on the indicator spot and the other on a region close to the particular spot. RGB values of the pixel enclosed by a ROI are averaged, and a fingerprint for each sensitive layer of each substance is then calculated subtracting the RGB sequence of the two ROIs. The background subtraction is necessary to take into account the non uniformity of computer screen produced webcam images. The fingerprints of all the spots are composed in a single fingerprint of the array. Porphyrin layers were duplicated and the average fingerprint for each porphyrin was considered.

The measuring setup involved a regular LCD screen (Philips 170S4) used as a light source and a Logitech Quickcam pro 4000 operating at a resolution of 320x240 pixels used as image detector. The measurement cell was properly shielded from ambient illumination and placed in a suitable holder keeping the geometrical arrangement small.

Software written in Matlab controlled the illuminating sequence, the video acquisition, and

extracted the information (CSPT fingerprints) from manually selected ROIs (white circles in Figure 3.6). Fingerprints were then treated as spectral data and analyzed using multivariate techniques.

3.4.2.3 Procedures

In each experiment, part of the samples was also analyzed with Gas Chromatography-Mass Spectrometry (GC-MS) for reference. In the first experiment, one sample per storage time was measured while anchovies headspace were measured with the GC 3 hours, 4,50 hours, and 6 hours after the start of the experiment.

For each measurement 5 g of fillet was placed in a 22 ml glass vial and immediately sealed with screw top hole caps with teflon septum. The vials were kept in a water bath at 30°C for 30 min. Headspace was sampled by a SPME Fiber Assembly 75 μm Carboxen – PDMS for Manual Holder by Supelco. The SPME fiber was kept in contact with the headspace for 5 min and then immediately inserted in the GC injector for thermal desorption [33].

For CSPT measurements fish fillets were taken from the ice bed, closed in a sealed bottle, and held at room temperature for 10 minutes to allow the formation of a stable headspace. The headspace was then recirculated into the measurement cell by a peristaltic pump. Between two successive measurements the cell was flushed by a flow of ambient air. The difference between fingerprints taken during the exposure to fish headspace and to the reference air were taken as the measurement result and were successively analyzed to identify the storage time.

3.4.3 Results and Discussion

The first experiment was aimed at recognizing different storage times of thawed fillets kept at 0°C from 1 to 4 days. Figure 3.7 shows the chromatograms of the headspaces of one sample per each storage day. As expected the abundance of the headspace grows with the storage days, mass spectrometer identification of compounds indicate that most of the compounds are amines of different origin but nonetheless indicators of a progressive microbial activity in the organic tissue.

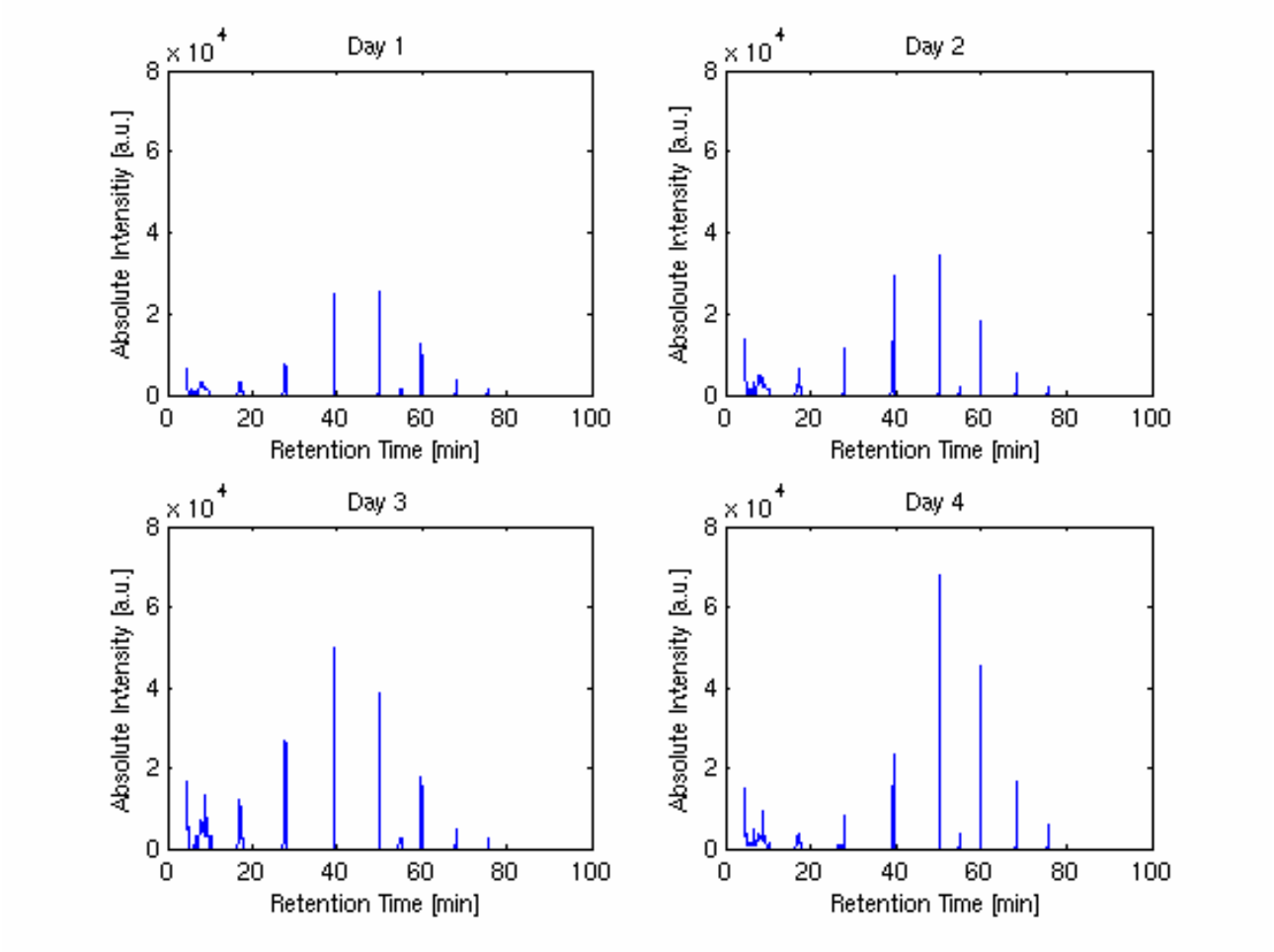

Figure 3.7. Complete chromatograms of fillets stored for different days.

A simple evidence of the progress of the microbial activity can be obtained considering that the integral of the gas-chromatogram increases with the storage time with an approximately linear behaviour with a slope of $1.13*10^6$ absolute abundance per day.

CSPT fingerprints were calculated following the procedure described in the previous section. In Figure 3.8 the mean CSPT fingerprints for each storage day are shown. Qualitatively the spectra in Figure 3.8 are very similar to the progressive increase of compounds abundancy found in gas-chromatograms this results in a progressive build-up of the sensor signals.

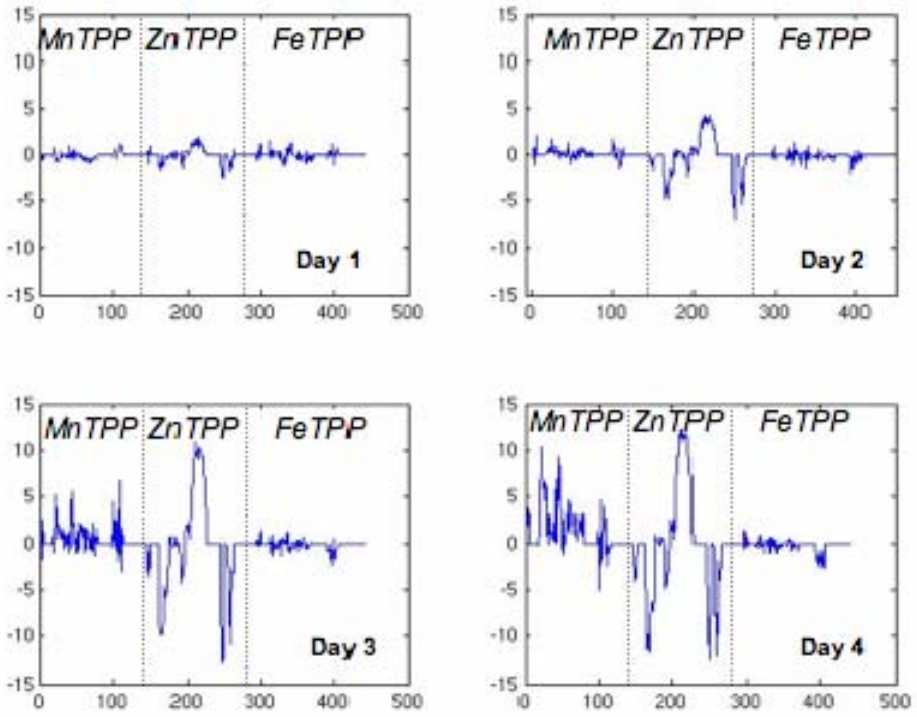

Figure 3.8: Mean CSPT fingerprints for 4 storage days.

Previous applications of metalloporphyrins based chemical sensors demonstrated that different porphyrin films show a different sensitivity towards the molecular families present in the fish headspace [34]. In particular, the nature of the central metal determines a large part of the sensitivity of the sensor. This behaviour can be qualitatively explained considering the Hard-Soft Acid-Base (HSAB) principle. This states that hard acids exhibit

preference for hard bases and soft acids prefer to bind soft bases. Since zinc, manganese, and iron are ordered in this sequence, according to their degree of hardness their affinity to bind nitrogen-donating sites follows the same order [35, 36]. The three metalloporphyrins used in this experiment may then be ordered according to their reactivity in the following sequence : ZnTPP, MnTPP, and FeTPP.

A synthetic representation of the discrimination performance of the four storage times may be obtained analyzing the data with a multivariate technique such as Principal Component Analysis (PCA). Nonetheless, PCA provides a representation of a multivariate dataset projecting the data onto a small dimensional space (usually a plane) selected among all the possible oriented planes as that where the data span the maximum variance [37]. PCA is particularly useful to explore the data in order to study if data clusters to form classes. On the other hand, when classes are known *a-priori* the optimal representation is that, where the classes are separated as much as possible. This last method may be called discriminant analysis and can be solved with a manifold of different algorithms. Among them particularly interesting is the partial least squares discriminant analysis (PLS-DA) that is a particular way of use of PLS, an algorithm originally developed for quantitative regression [38]. One of the drawbacks of the application of multivariate techniques is the relationship between the number of variables and the number of samples. In general, an increase in the number of variables reduces the reliability of multivariate techniques based on covariance matrix estimation (such as PCA). This problem is particularly present in the analysis of spectra and then also on CSPT fingerprints. Nonetheless to this regard it has been demonstrated that when the number of variables exceeds the number of samples and when the variables are highly correlated with each other, another typical characteristics of spectral data and then CSPT, PLS-DA was found more reliable than linear discriminant analysis [39].

A PLS-DA model aimed at classifying the four classes corresponding to the storage days was built. The model was properly cross-validated by the leave-one-out technique. Figure 3.9 shows the multivariate CSPT fingerprints projected onto the plane defined by the first two latent variables of the PLS-DA model.

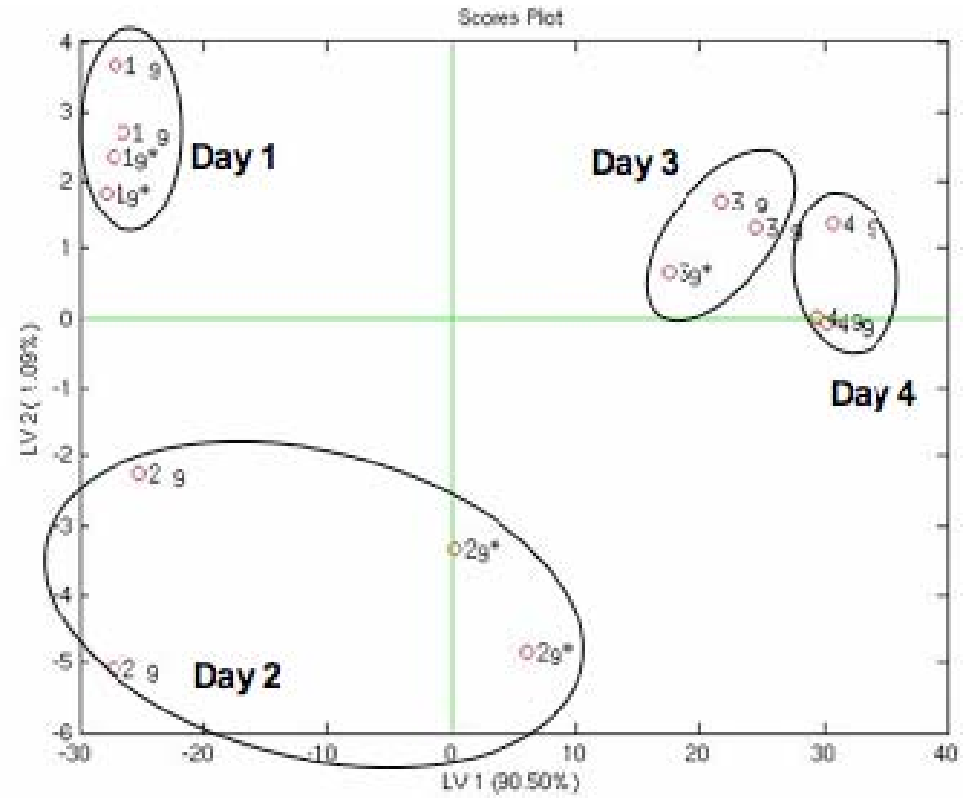

Figure 3.9: Plot of the first two latent variables of the PLS-DA model aimed at classifying the four different storage days. About 92% of the total variance of the data is expained in this plot.

While, as shown the headspace enrichment is proportional with the storage days, the class separation, in Figure 3.9, tends to decrease with storage time. This saturation effect is most likely due to the saturation of the sensing layers that are characterized by limited amount of adsorption sites leading to Langmuir like adsorption isotherms . Another conclusion that can be obtained from Figure 3.9 relates to the fact that the classes do not lie along a straight line. This behaviour indicates that classes differ not only for the increased total abundance of the chemicals in the headspace but that the concentration increase is not the same for all the compounds. Such a conjecture is also supported by the chromatograms of Figure 3.9 where the chromatograms differ both in the relative changes of the magnitudes of the peaks and in their number.

The second experiment was concerned with the monitoring of the spoilage process in anchovies kept at the controlled temperature of 20°C. Anchovies are small fishes with a rather accelerated rate of spoilage with respect to more massive species. The headspace of anchovy fillets of was sampled each 15 minutes and measured with the CSPT based sensor array. As a reference, the headspace was also measured with GC-MS at three times occurring 180, 270, and 360 minutes after the start of the experiment. As expected the global composition of the headspace was found less abundant with respect to the fillets freshness experiment previously discussed. The headspace build-up is rather evident with many compounds changing their abundance with time. Furthermore, not all of the compounds change their concentration with the same rate. As an example of the observed evolution of concentration, Figure 3.10 shows a portion of the gas-chromatogram with retention time in the range 14 – 15.2 min. In this region two peaks are found, The Mass Spectroscopy fragmentation spectra of the peaks were tentatively identified as N-tetramethylene (peak a) and methylamine (peak b), according to the NIST147 mass fragmentation database.

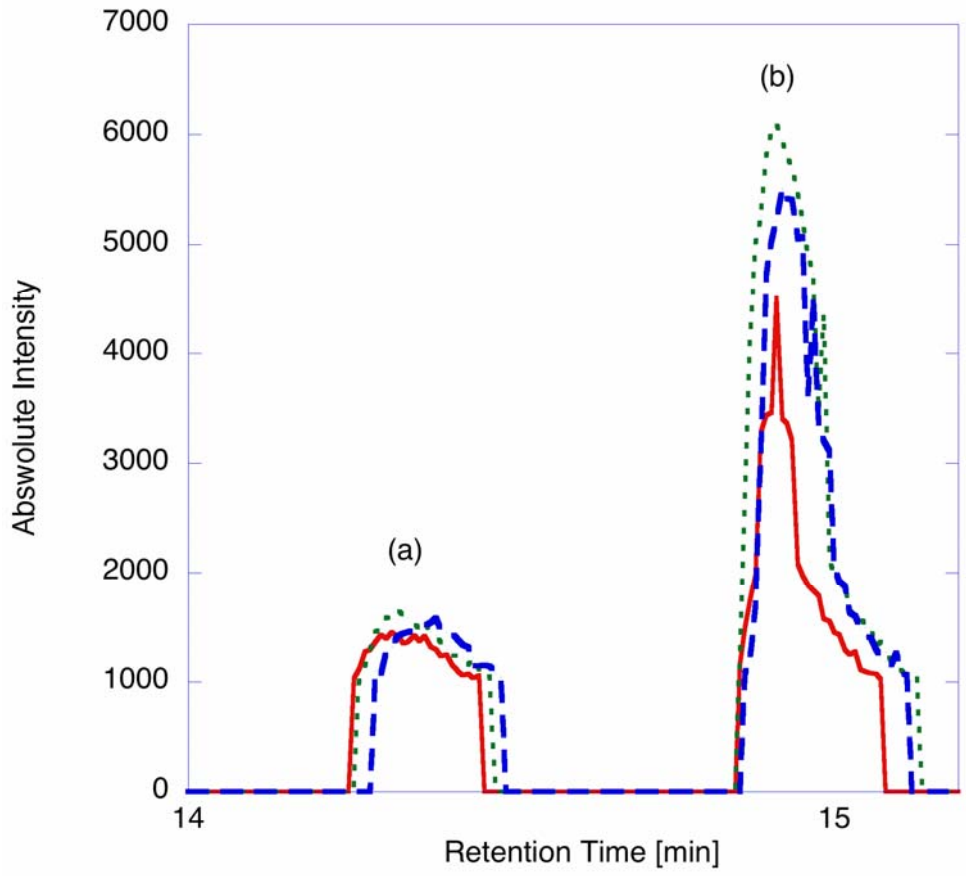

Figure 3.10: Portion of the chromatograms of anchovy fillets around the peaks of compounds tentatively identified as N-tetramethylene (a) and methylamine (b). Chromatograms are related to the headspace sampled at 180 min (continuous line), 270min (dashed line), and 360 min (dotted line).

A comparison of the peaks recorded at 180, 270, and 360 minutes after the start of the experiment shows different time evolution of the two compounds: peak a remains almost constant and peak b steadily grows evidencing that, at these time scales, the headspace changes not only in term of quantity but that a significant distortion of the chemical pattern of the headspace also takes place.

In Figure 3.11 the CSPT fingerprints recorded each 15 minutes are shown. The fingerprints have been calculated as the difference with the CSPT fingerprint taken at the beginning of the experiment.

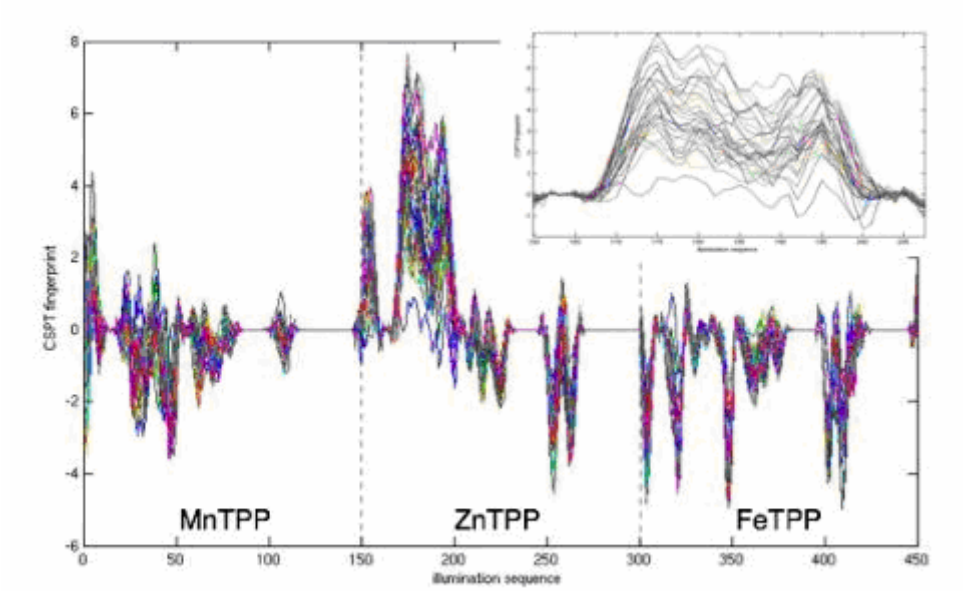

Figure 3.11: CSPT fingerprints of the headspace of anchovies taken from 0 min to 460 min after the experiment start. In the inset, the large band in the red channel of ZnTPP is shown where the change of CSPT signal with time is most evident.

As the headspace is less abundant the magnitude of the CSPT signal is less with respect to that found in the fillets experiment. Nonetheless, also in this second experiment, ZnTPP is characterized by the largest sensitivity towards the compounds evolving during the spoilage of anchovies flesh. In the inset of Figure 3.11, the evolution of the large band of ZnTPP in the red channel is shown. A rough idea about the growth of the CSPT signal can be achieved considering the plot of Figure 3.12 where the integral of the ZnTPP band in the red channel versus the experiment time is shown.

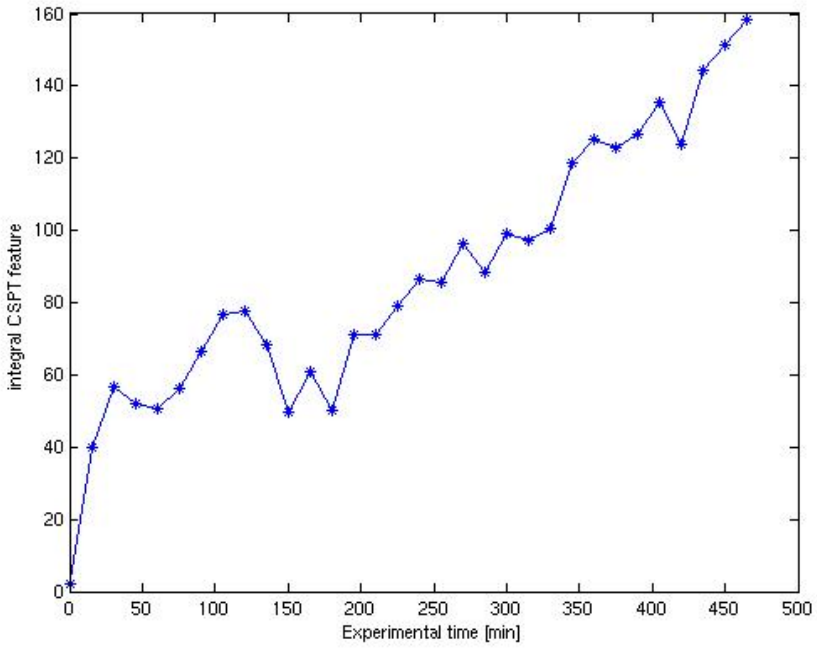

Figure 3.12: Integral of the band in red channel of ZnTPP versus the experiment time.

Although well correlated with the time, the curve suggests some non linear behaviour in the first part, of course, the integral of a wide band is characterized by a limited reliability because many contemporaneous sources of variation of the optical properties are averaged. For a better investigation of the CSPT signals the multivariate analysis can be utilized. Differently from the previous experiment, in this case rather than a classification a regression aimed at quantifying the experimental time seems the most appropriate choice. Therefore a PLS regression model aimed at quantifying the experimental time, namely the time of storage of anchovies at 20°C, was built. The model was cross-validated with leave-one-out algorithm, the minimum root mean square error of prediction was about 30 minutes and it was obtained with 8 latent variables. It is worth to note that the error includes the uncertainty of the CSPT measurement and also the fact that very likely the evolution of fish headspace is more complex that a simple linear law.

Figure 3.13 shows the score plot of the first two latent variables. It is rather interesting to note that the behaviour of Figure 3.12 finds some correspondence in the PLS score plot where data shows two different regions.

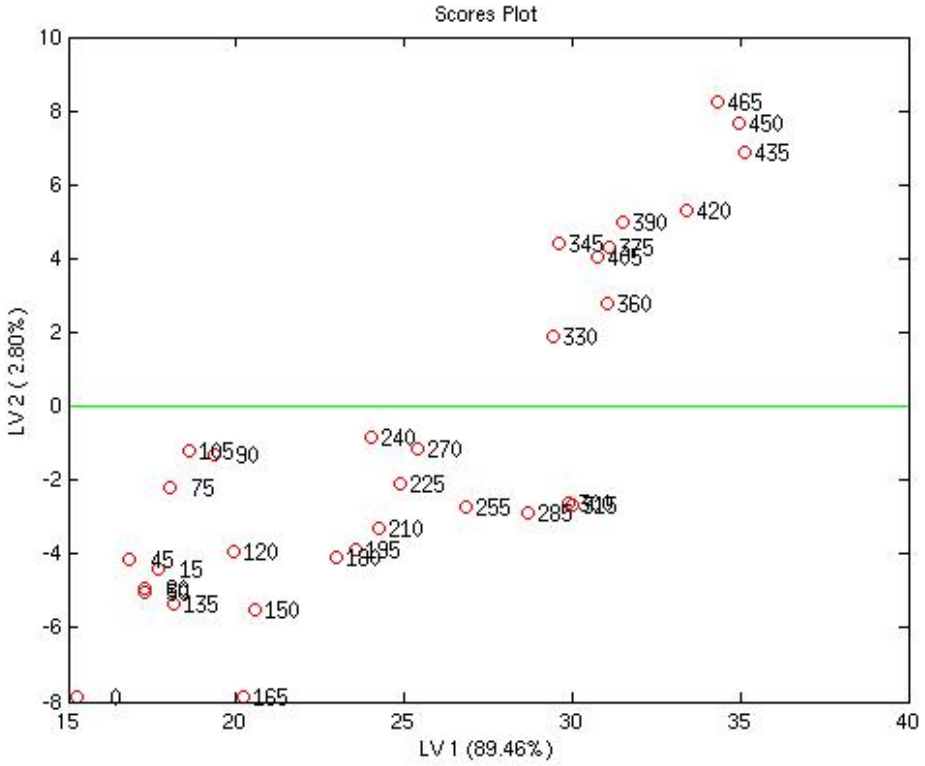

Figure 3.13: Plot of the first two latent variables of the PLS model aimed at the regression of the experiment time in the anchovies experiment. About 91% of the total variance of the data is explained in the plot. Data are labelled as "minutes" from the start of the experiment.

Data in Figure 3.12 are aligned along the diagonal of the plot; however, in the last portion of data, after 330 minutes, the alignment becomes more evident suggesting that concentration increase becomes more important than the chemical pattern distortion, which on the other hand, is more evident in the first portion of data. A proper support to this conclusion can be obtained with an extensive identification of the compounds found in fish headspace.

Therefore in both cases, the array provided sufficient sensitivity to recognize the different steps of the spoilage process. The great value of the results presented is that they can, in principle be obtained with any equipment endowed with a programmable colour screen and a camera, devices nowadays largely diffused being included in a very large number of notebooks, PDAs, and cellular phones. The diffusion of analytical capabilities everywhere and at any step of the food chain is expected to have a great impact on the general control of

the quality of food. Furthermore, it is supposed to have also a great social impact providing consumers with objective tools to test freshness of food and then to judge the market value of products. The array presented here has been formed by sensitive layers known for their reactivity towards the chemicals relevant in the chosen situations. A more accurate selection of sensitive layers would provide a better performing array and in general a manifold of compounds are available whose optical properties (absorbance and fluorescence) change according to the quantity and the quality of the molecules to which they are exposed, giving the possibility to extend the findings illustrated in this Chapter to other applications.

REFERENCES

[1] J.W. Gardner , P. N Bartlett. 'A Brief History of Electronic Noses'. *Sensors and Actuators B.*, 18, 211–220 (1993)

[2] R. Paolesse, F. Mandoj, C. Di Natale Porphyrins based chemical sensors, in Nalwa (ed.) *Encyclopedia of nonoscience,* APS, 2003

[3] A. D'Amico, C. Di Natale, R. Paolesse, A. Macagnano, Metalloporphyrins as basic material for volatile sensitive sensors. *Sensors and Actuators B* 65 pp 209-215, 2000

[4] C. Di Natale, R. Paolesse, D.. Salimbeni, A. Macagnano, A. Mantini, A. D'Amico; Optoelectronic nose based on absorbance variations in porphyrin films, *Proc. Of the 5" International Symposium on Olfation and Electronics Nose,* Baltimore, MD, USA, 30 Sept. 1998

[5] C. Behringer, B. Lehmann; J.-P. Haug, K. Seiler, W.E. Morf, K. Hartmann, W. Simon; Anal. Chim. Acta 1990; 233; 41-47

[6] U. Schaller; E. Bakker; E. Pretsch; Carrier mechanism of acidic ionophores in solvent polymeric membrane ion-selective electrodes; Anal. Chem. 1995; 67; 3123-3132

[7] D. Filippini, A. Alimelli, C. Di Natale, R. Paolesse, A. D'Amico, I. Lundström; Chemical sensing with familiar devices, Angewandte Chemie Int. Ed. 45 (2006) 3800-3803

[8] D. Filippini, S. Svensson, I. Lundström; Computer screen as a programmable light source for visible absorption characterization of (bio)chemical assays, Chemical Communications (2003) 240-241

[9] M. Gouterman in The Porphyrins, Vol. III (Ed.: D. Dolphin), Academic Press, New York, 1979, p. 1.

[10] a) D. G. Whitten, I. G. Lopp, P. D. Wildes, J. Am. Chem. Soc. 1968, 90, 7196; b) M. Nappa, J. S. Valentine, J. Am. Chem. Soc. 1978, 100, 5075.

[11] R. Paolesse in The Porphyrin Handbook, Vol. 2 (Eds.: K. M. Kadish, K. M. Smith, R. Guilard), Academic Press, San Diego, 2000, p. 201.

[12] European Community, Council regulation (EC) No. 2406/96 of 26 November laying down common marketing standards for certain fishery products, Off. J. Eu. Commun., L334/1–14, 23/12/96.

[13] H.A. Bremner, Toward practical definitions of quality for food science, Crit. Rev. Food Sci. Nutr. 40 (2000) 83–90.

[14] Methods to Determine the Freshness of Fish in Research and Industry, International Institute of Refrigeration, Paris, France, 1997.

[15] G. Olafsdottir, P. Nesvadba, C. Di Natale, M. Careche, J. Oehlenschlager, S.V. Tryggvadottir, R. Schubring, M. Kroeger, K. Heia, M. Esaiassen, A. Macagnano, B. Jorgensen, Multisensor for fish quality determination, Trends Food Sci. Technol. 15 (2004) 86–93.

[16] D. Josephson, R. Lindsay, G. Olafsdottir, Measurement of volatile aroma consituents as a means for following sensory deterioration of fresh fish and fishery products; in D. Kramer, L. Liston (eds), Seafood quality determination symposium, 10-14 Nov 1986, Elsevier (Amsterdam, Netherlands) 1986

[17] Ólafsdóttir G, and Fleurence J. Evaluation of fish freshness using volatile compounds-Classification of volatile compounds in fish, in Methods to Determine the Freshness of Fish in Research and Industry, Proceedings of the Final meeting of the Concerted Action "Evaluation of Fish Freshness" AIR3 CT94 2283. Nantes Nov 12-14, 1997. International Institute of Refrigeration, 55-69.

[18] K. Persaud, G. Dodds, Analysis of discrimination mechanisms in the mammalian olfactory system using a model nose. Nature 299 (1982) 352–355

[19] T. Nagle, S. Schiffmann, J. Gardner, T. Pearce (editors), Handbook of Machine Olfaction, J. Wiley and sons. Weinheim, Germany, 2003

[20] Schweizer-Berberich M., Vahinger S, Göpel W. Characterization of food freshness with sensor array, Sensors and Actuators B, 18 (1994) 282-290.

[21] C. Di Natale, J.A.J. Brunink, F. Bungaro, F. Davide, A. D'Amico, R. Paolesse, T. Boschi, M. Faccio, G. Ferri; Recognition of fish storage time by a metalloporphyrins coated QMB sensor array, Measurement Science and Technology 7 (1996) 1103-1114

[22] G. Olafsdottir, E. Martinsdottir, E.H. Johnson, Rapid gas sensor measurements to predict the freshness of capelin, J. Agric. Food Chemistry 45 (1997) 2654-2659

[23] H. Tozawa, K. Enokihara, K. Amano, Proposed modification of dyer's method for trimethylamine determination in cod fish, Fish Inspection and Quality Control (1971) 187–190.

[24] A. Pacquit, K.T. Lau, H. McLaughlin, J. Frisby, B. Quilty, D. Diamond; Development of a volatile amine sensor for the monitoring of fish spoilage, Talanta 69 (2006) 515-520

[25] A. Suska, D. Filippini, T. Andersson, I. Lundström, Generation of biochemical response patterns of different substances using a whole cell assay with multiple signaling pathways Biosensors Bioelectronics 21 (2005) 727-734

[26] C. Di Natale, D. Filippini, G. Pennazza, M. Santonico, R. Paolesse, A. Bellincontro, F. Mencarelli, A. D'Amico, I. Lundstrom; Sorting of apricots with computer screen photoassisted spectral reflectance analysis and electronic nose, Sensors and Actuators B in press

[27] C. Di Natale, D. Salimbeni, R. Paolesse, A. Macagnano, A. D'Amico; Porphyrins-based opto-electronic nose for the volatile compounds detection, Sensors and Actuators B 65 (2000) 220-226

[28] K. Suslick, N. Rakow, A. Sen; Colorimetric sensors array for molecular recognition, Tetrahedron 60 (2004) 11133-11138

[29] C. Di Natale, A.G. Mignani, R. Paolesse, A. Macagnano, A. Mencaglia, A. D'Amico; Array of opto-chemical sensors based on fiber optic spectroscopy, IEEE Sensors Journal 5 (2005) 1165-1174

[30] T. A. Dickinson, J. White, J. S. Kauer, and D. R. Walt, “A chemical detecting system based on a cross-reactive optical sensor array,” Nature, 382 (1996) 697–700

[31] S. M. Drew, D. E. Janzen, C. E. Buss, D. I. MacEwan, K. M. Dublin, K. R. Mann, “An electronic nose transducer array of vapoluminescent platinum(II) double salt,” J. Amer. Chem. Soc., 123 (2001) 8414–8415

[32] Di Natale C, Olafsdottir G, Einarsson S, Martinelli E, Paolesse R, D’Amico A. Comparison and integration of different electronic noses for freshness evaluation of cod-fish fillets. Sensors and Actuators B 77 (2001) 572-578.

[33] M. Mansur, A. Bhadra, H. Takamura, T. Matoba; Volatile flavor compounds of some sea fish and prawn species, Fisheries science 69 (2003) 864-866

[34] J.A.J . Brunink, C. Di Natale, F. Bungaro, F. Davide, A. D’Amico, R. Paolesse, T. Boschi, M. Faccio, G. Ferri, “The application of metalloporphyrins as coating material for QMB Based chemical sensor” Analytica Chimica Acta 325 (1996) 53-64

[35] R.G. Pearson, Hard and soft acids and bases, Journal American Chemical Society 85 (1963) 3533

[36] R.Pearson, Acids and bases, Science 151 (1966) 172-177

[37] R. Johnson, D. Wichern, Applied Multivariate Statistical Analysis, Pearson Education, Prentice Hall, New Jersey, 2002.

[38] S. Wold, M. Sjöström, L.Erikskson; PLS-regression: a basic tool of chemometrics, Chemometrics and Intelligent Laboratory Systems 58 (2001) 109-130

[39] J. Prats-Montalban, A. Ferrer, J. Malo, J. Gorbeña, A comparison of different discrimination analysis techniques in a steel industry welding process, Chemometrics and Intelligent Laboratory Systems 80 (2006) 109-119

CHAPTER 4

CSPT-Spectroscopy mode: Wine Optical Properties detection, and Bilirubin analysis

INTRODUCTION

The growing necessity of quality control requires an expansion of the analytical capabilities of the whole society. The number of analysis for the determination of levels of a manifold of compounds is steadily increasing to increase the safety and to improve the quality of life. A typical field where a diffused analytical control is required is that related to food and beverages.

In general medical tests are certainly another aspect that has growing interest by the society. The possibility of making non invasive monitoring, home tests, early diagnosis, "semicontinuous" health checks, internet based evaluations etc., gives very much importance to the development of new sensors and instrumentation for primary health care and home based medical tests and diagnosis, with de-centralized tests but centralized evaluation. One interesting question is find dedicated solutions for each parameter of interest and the use of a general platform for all parameters.

CSPT-spectroscopy mode more than a specialized instrument, is a general (and highly available) platform instead, which tunes its functionality depending on the particular assays it evaluates certainly becoming an attractive candidate for these very different kind of applications.

4.1. WINE OPTICAL PROPERTIES

To monitor the freshness and safety of foodstuff is of fundamental importance and well disciplinated by regulaments and laws in the majority of countries. But, beside the safety a great importance is rising in the certification of food quality in terms of enhanced and typicized taste and smell and in terms of quantification of chemical species, naturally occurring in food and known for their benifical effects on human health.

Among these compounds a great attention is devoted towards antioxidant molecules such as polyphenols. The presence of these compounds adds a great value to many food stuff that

are suggested to be included in the diet. A particular case of the importance of such compounds in the general consideration of foods is offered by red wine. Indeed, in spite of the may unhealthy effects of wine in human body (e.g. the physical and psychical effects of ethanol) a moderate consumption of red wine is often recommended because the benefits of polyphenols outweighs, in normal subjects, the negative effects of alcohol.

Beside their outstanding effects on human physiology, polyphenols are characterized by typical optical properties on which the color of many vegetables are based.

In particular, in the case of red wine the content of total polyphenols and antocyans in particular determine the color of the beverage. Polyphenols in wine are known for their contribution to the sensorial properties of wine such as colour and astringency[1].

The color of red wine is mainly due to grape-derived antocyanins, a minor contribution is given by other pigmented molecules formed during fermentation and ageing.

The measure of total polyphenols and antocyanins is considered of great importance to determine the quality of red wines. High performance methods are based on liquid chromatography, while standard routine analysis in enology laboratories are based on the use of specific reagents changing the color of wine, the evaluation of concentration is obtained measuring the absorbance between 400 to 700 nm.

A rough estimation of these compounds can be obtained through a number of optical attributes that have been introduced along the years. Indeed several studies of red wine color indices show high correlations between several of them. So the best, and most used, colorimetric control of wines in the cellar can be made using Intensity of Colorand Sudraud's index, Tint (or Tonality) and Glories' index.

The measurements of optic density, absorbance, is widely used to determine wine color and total phenolic compounds concentration. The optic density is noted as OD, OD_{420} (Yellow), OD_{520} (Red), OD_{620} (Blue) to indicate the optic density at the indicated wavelengths.

The spectrum of red wines has a maximum at 520 nm, due to anthocyanins and their flavylium combinations, and a minimum in the region of 420 nm. Color Intensity, and Hue, as defined by Sudraud (1958), only take into account the contribution of red and yellow to overall colour. These two values are perfectly suitable for studying wines with some age,

but do not always cover the relatively deep colours of young wines. The blue component, attributed to the quinoid forms of free and combined anthocyanins, must be take into account in assessing these colors. Data obtained by means of optical density measurements at 420, 520 and 620 nm on a 1 mm optical path may be used to interpret various aspects of color [2].

Color Intensity represents the amount of color. It varies a great deal from one wine and grape variety to another (0.3 – 1.8). Wine color Intensity is defined as sum of the optical densities at 1 mm thickness, it is expressed as:

$$Intensity = OD_{420} + OD_{520} + OD_{620} \quad (4.1)$$

or is sometimes expressed in a more simple form: $OD_{420}+OD_{520}$.

The Hue indicates the development of a color towards orange. Young wines have a value on the order of 0.5-0.7 which increases throughout aging, reaching an upper limit around 1.2-1.3. It is defined as:

$$Tonality = \frac{OD_{(420nm)}}{OD_{(520nm)}} \quad (4.2)$$

It is also possible evaluate the Color Composition of red wines, simply calculating the contribution (expressed as a percentage) of each of the three components in the overall color (Color Intensity).

The brilliance of red wines is linked to the shape of the spectrum. When wine is bright red, the maximum at 520 nm is narrow and well defined. On the other hand, it is flattened and relatively broad when wines is deep re or brick red. This characteristic may be show by the Glories' index:

$$dA\% = (OD_{520} - \frac{OD_{420} + OD_{620}}{2}) \frac{1}{OD_{520}} 100 \quad (4.3)$$

The results are between 40 and 60 for a young wine. The higher the value, the more dominant the red color of the wine.

Other two indices can be defined to evaluate the color of red wines: Luminosity (dY%) and Purity (or Saturation, P%) of color, but they are someway correlated with the previous ones. The Luminosity represents the amount of “black”, instead Purity take in account the amount of “white”, being inverse proportional to white color in red wine. So if the Saturation is closed to zero it means the color of wine is gray. So these couple of indices represent the vividness of color. Then, henceforth will be take in account these five indices for our investigation, much more representatives than others.

Furthermore, it is very interesting to assess the role played by various pigments involved in the color of a wine. Direct optical measurement of polyphenols in wine was demonstrated by measuring absorbance spectra in visible and most of all in near infrared region up to 2.5 μm [3] by using different reagents [4]. Nonetheless, all these techniques are time consuming and costly and necessitate of laboratory instrumentation usually not available in enological plants.

In addition to absorbance, colour properties of antocyanins, and polyphenols in general, are due to fluorescence which contribute to enhance the red colour of wine.

The properties of fluorescence are actually exploited for detection and identification of polyphenols in HPLC columns analysis [5].

Wine fluorescence is rarely considered, as an example, Figure 4.1 shows the absorbance spectrum of a typical red wine with a medium content of antocyans and polyphenols. Figure 4.2a shows the emission spectrum of the same wine induced by excitations at 450 nm and 520 nm. A strong emission is observed exciting the sample at 450 nm, Figure 4.2b shows the excitation spectra at 450 nm corresponding to the emission of Figure 4.2a.

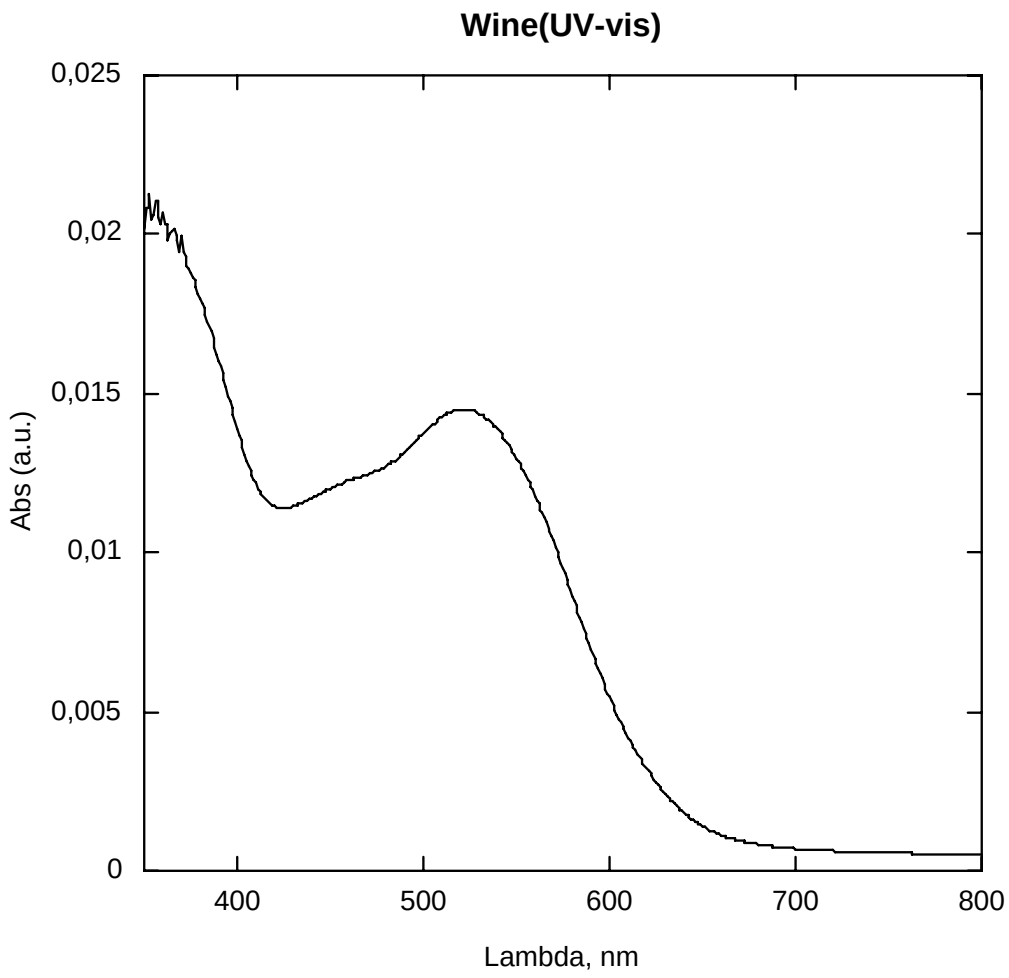

Figure 4.1: UV-vis Absorbance Spectra of a typical red wine.

The measure of fluorescence for analytical purposes is rather limited by the relative complexity and cost of the opto-electronic setup although the miniaturization efforts have reduced the complexity and the cost of such instrumentations, the application of optical methods, although encouraging, has been hindered by the relative high cost of the instrumentation.

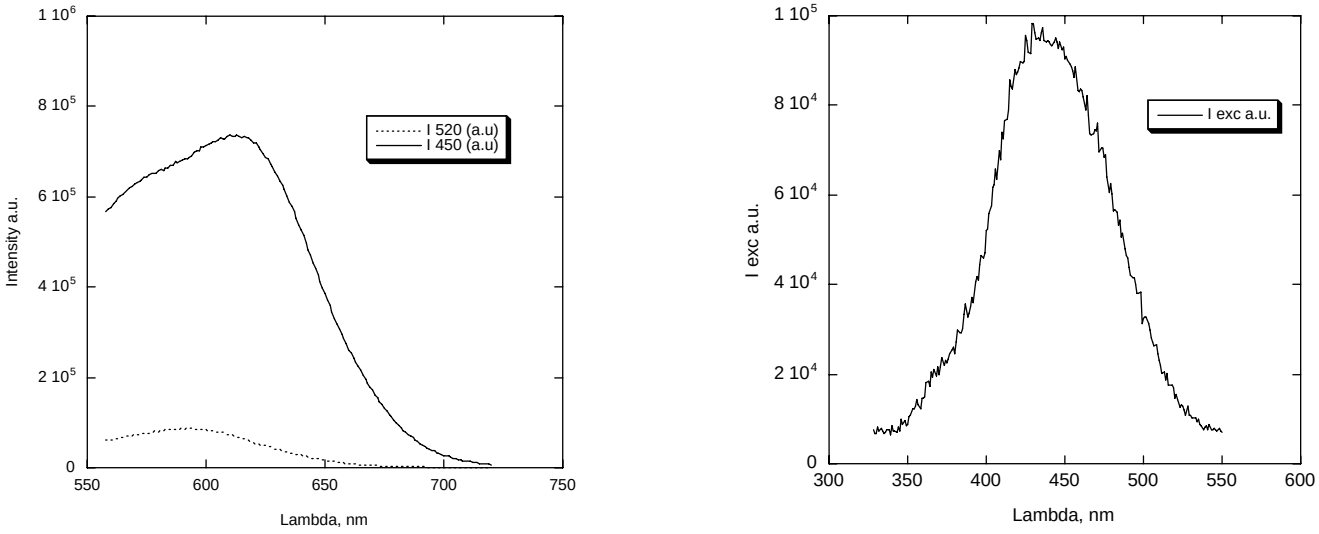

Figure 4.2: a) Emission spectra for excitation at two different wavelengths (520 and 450 nm); b) Absorbance spectra focussed at 450 nm.

In spite of the high cost of optical instruments, CSPT could then in principle be used to detect both general parameters related to the absorbance spectra such as Intensity and Tonality of colour, and more specifically the amount of emission light that can be correlated to the content of total polyphenols and, in particular, total antocyans.

4.2. MEASUREMENTS DETAILS

The test was performed on a set of Italian wines covering a wide range in colour and polyphenols content. The CSPT evaluations were calibrated using as a reference method the standard analytical procedures [4].

4.2.1 Wine samples

Ten samples of different denomination were selected for the experiment. The selection was driven in order to calibrate the method at wide intervals of analytical parameters.
Wines were commercial products bottled in cork stopped 0.75 l *bourgognon* bottles. Seven wines were from 2005 vintage and three from 2003 vintage (see Table 4.1). Experiments were performed at the Laboratories of Agriculture Ministry in Velletri (Roma).
Each bottle was opened 10 minutes before the analysis, bottle content was splitted in four parts: one for the CSPT measurement and the others for the standard analytical measurements. Analytical parameters were colour indicators, total polyphenols and antocyanins.

Aglianico	2003
Rosato Aglianico	2005
Cesanese Comune	2005
Montepulciano	2005
Cabernet Sauvignon	2005
Nerobuono di Cori	2005
Refosco	2005
Syram	2003
Petit Verdot	2003
Teroldego	2005

Table 4.1: List of wines with relative vintage, used during measurements

4.2.2 CSPT arrangement

Wine samples were placed in transparent vials with 5 mm of internal diameter. Vials were fixed to a sample holder keeping them in between the optical path connecting a computer screen and a webcam. Up to six wine samples were simultaneously measured. Screen, webcam, and sample holder was placed in a suitable support properly shielded from ambient light and keeping tight the geometrical arrangement [6].

The experimental setup used for the experiments here described involves a regular LCD screen (Philips 170S4), used as a light source, a Logitech Quickcam pro 4000 operating at a resolution of 320x240 pixels, used as image detector, and a Toshiba SA60-198 laptop.

In Figure 4.3 the spectra of the three primary colours emitted by the used LCD screen are shown. It is rather interesting to remark that the blue colour has its maximum emission around 450 nm where the excitation of wine fluorescence occurs.

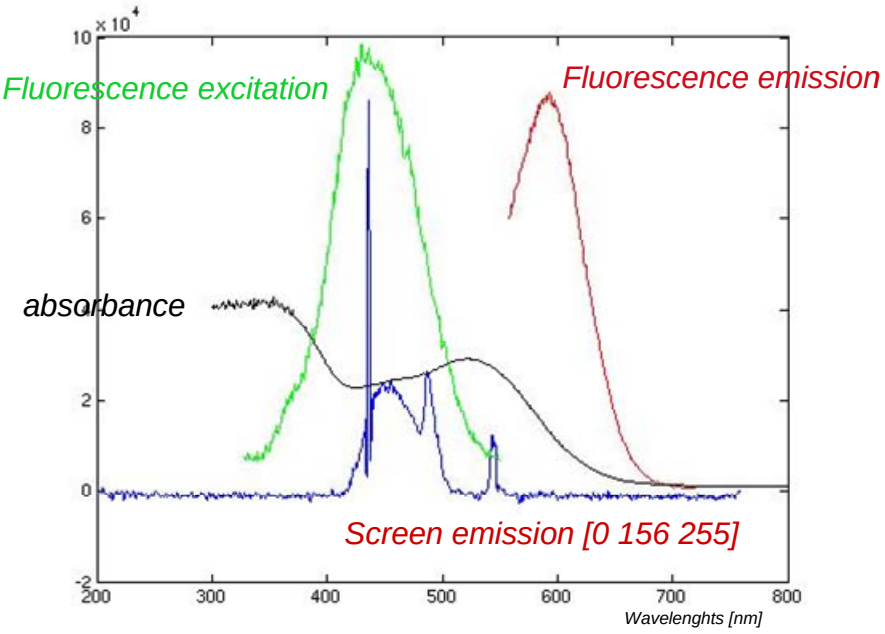

Figure 4.3: LCD emission spectra for a combination of three primary colors with weights: 0, 156, 255 (Blue line); and wine absorbance spectrum (Green line) overlapping.

During this CSPT measurement web camera captures the image of the wine array under an illuminating sequence provided by the screen (a rainbow of 50 colors in this experiment). From this video stream a regions of interest (ROI) for each vial is selected (the white circles in Figure 4.4). For each ROI centered on the vial spot another ROI on a close background is also considered. RGB values of the pixel enclosed by a ROI are averaged, and a fingerprint for each sample is calculated subtracting the RGB sequence of the sample ROI and its complementary background. Background subtraction ensure the elimination of spatial non homogeneities of screen and webcam.

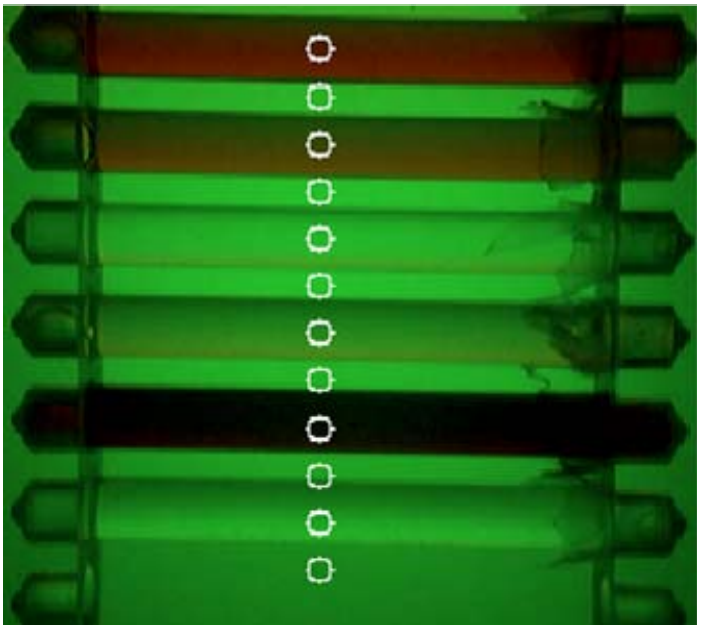

Figure 4.4: RoIs of some wine samples used during the measurements. The samples are in glass tubes, and some of them are filled with water.

Red, green and blue channel signals are concatenated in order described in the First Chapter, then, in this case, the fingerprints are vectors of 150 elements. The fingerprint is the CSPT output, and it is used to form a mulivariate model, using Partial Least Squares (PLS) [7], to estimate analytical parameters of wine.

4.2.3 Reference methods

Wine colour was expressed by standard indicators all them resulting from transmittance spectroscopy measurement. The following parameters were calculated: Intensity, Tonality, Glories' Index, Luminosity, and color Purity. Total polyphenols and antocyanins content was evaluated with the standard method [4] consisting in complicated solutions workable only in dedicated laboratories, that involve many reagents such as H_2SO_4 1N, methanol, Na_2CO_3, H_2SO_4 0,1N, HCl etc, and sophisticated instrumentation such as spectrophotometer.

4.2.4 Results and Discussion

In Table 4.2 the analytical parameters measured by reference standards for the ten categories of wines are shown. As expected during the selection of samples the interval of each parameters is rather wide permitting a reliable calibration of the proposed method.

Sample number	Intensity	Tint	Glories' index dA%	Brillance Y%	Colour purity P%	Polyphenols	Antoyianins
1	**1.233**	**0.581**	**60.385**	**1.278**	**99.816**	**2588,6**	**188,87**
2	**0.083**	**0.784**	**53.879**	**54.433**	**18.439**	**520,34**	**129,36**
3	**0.308**	**1.133**	**28.670**	**12.214**	**70.810**	**1590,8**	**97,02**
4	**0.333**	**0.665**	**56.144**	**9.673**	**64.415**	**1417,4**	**130,65**
5	**0.341**	**0.900**	**41.648**	**9.391**	**70.242**	**1991,8**	**198,57**
6	**0.240**	**0.785**	**51.040**	**18.521**	**56.983**	**1721,4**	**75,029**
7	**0.703**	**0.743**	**49.442**	**2.266**	**96.561**	**2916,9**	**284,59**
8	**0.441**	**0.877**	**43.191**	**6.080**	**83.759**	**1859,4**	**146,18**
9	**1.153**	**0.666**	**52.818**	**0.922**	**99.774**	**1570,3**	**239,96**
10	**1.116**	**0.993**	**30.089**	**0.145**	**99.735**	**1238,4**	**149,41**

Table 4.2: All parameters measured by standard methods.

Since the scope of the experiment here described is to derive a model to estimate the set of parameters from the CSPT fingerprints it is important to evaluate the degree of correlation between samples. Large correlations are found between colour indicators. Correlation

coefficients larger than 0.9 are found between Glories index and tonality and between luminosity and colour purity. On the other hand, it is interesting to note that although optical properties are related to the presence of antocyanins and total polyphenols, colour indicators have a very low correlation with their concentration. This may be explained by the fact that colour is a synthetic indicator of the whole spectra and then it may not take into account precise analytical values.

In Figure 4.5 all the recorded fingerprints are shown. These spectra have been calculated subtracting for each sample the fingerprint of the ROI centered on the sample vial with the fingerprint of the ROI of an immediately close background region. The portion of Figure 4.5 with negative signals are then correspondent to the cases when the light from the sample is more intense than the background. This situation occurs when the sample fluorescence is excited by the screen emission. Beside this straightforward evidence of fluorescence, it has to be considered that absorbance of wine in presence of blue and green light is very large (see Figure 4.1), then also signals barely close to zero are clearly due to wine emission.

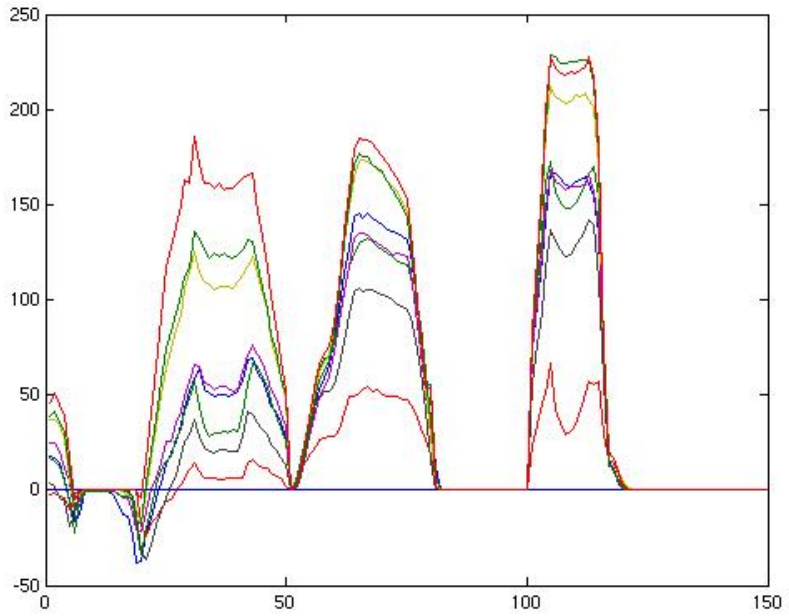

Figure 4.5: Overlapping of CSPT Fingerprints.

Fluorescence is correctly observed in the red channel of webcam and it is observed when the red intensity of the screen is low and blue and green channels are high.

To estimate analytical parameters three different PLS models were built. Each model was optimized to estimate colour indicators, total polyphenols and antocyanins. The values measured by the reference methods have been used to train PLS models.

Each model has been cross-validated by leave-one-out method and the root mean square validation error (RMSECV) has been evaluated as an indicator of the generalized prediction accuracy (Table 4.3). The PLS model achieving the lowest RMSECV was formed by 9 latent variables in the case of colour indicators. In Figure 4.6 the scatter plots for color indicators are shown.

	RMSECV
Intensity	0.2115
Tonality	0.2742
Glories Index	11.4945
Luminosity	17.6855
Colour Purity	7.117

Table 4.3: Cross-validation errors for color parameters.

PLS models estimating the concentration of antocyanins and total polyphenols were optimized following the same methodology used for colour indicators, and the number of laten variables minimizing RMSECV are 6 and 5 for antocyanins and total polyphenols respectively. In Figure 4.7 the scatter plots related to these two quantities are shown. In each plot of Figure 4.6 and Figure 4.7 an error bar of the same magnitude of the RMSECV has been plotted in order to signify the entity of the foreseen uncertainty of estimation.

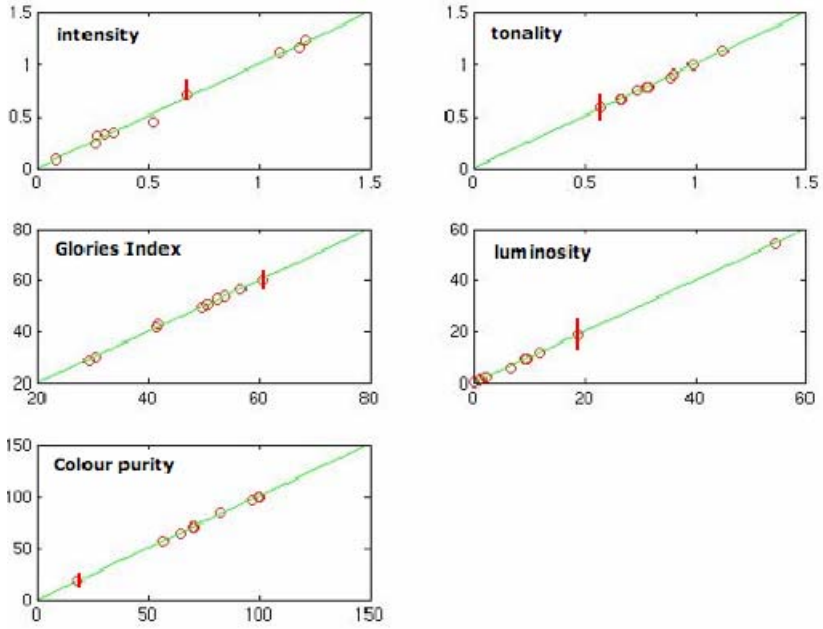

Figure 4.6:Scatter plots of five color indicators: Intensity, Tonality, Glories' index, Luminosity and Color Purity.

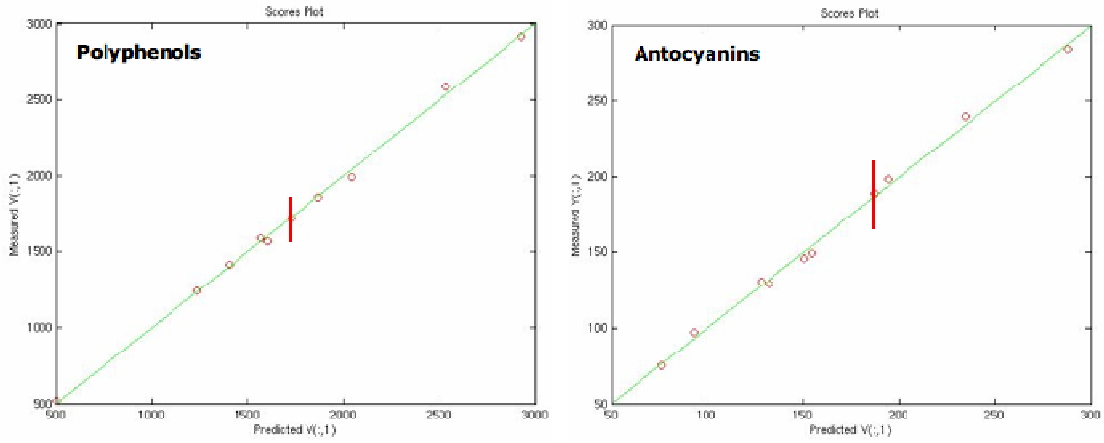

Figure 4.7: Scatter plots of Polyphenols (RMSECV=300) and Antocyanins (RMSECV=60).

Then it has been demonstrated that a simple experimental setup formed by a computer monitor and a webcam provides data that once properly analyzed result in a estimation of colour properties, total polyphenols and antocyans concentration with a resolution comparable with the standard analytical protocols without using any particular reagent and specific and expensive instrumentation. It is also important underlining that a similar

platform not only fully simplify the measurement platform but it is almost present everywhere for oenologists and final users exploitation.

4.3. BILIRUBIN ANALYSIS

4.3.1 Bilirubin in children blood

In the first few days of life, the skin of neonates develops a distinct yellow color due to bilirubin deposition. This icteric episode is known as physiological jaundice and is caused by elevated concentration of bilirubin in blood. The elevation of serum bilirubin is caused by a combination of increased red cell destruction and decreased hepatic bilirubin conjugation. In the jaundiced infant, it is thought that the binding capacity of plasma albumin is exceeded and then, free bilirubin can diffuse into and accumulate within extravascular tissues, such as the central nervous system [8]. In severely jaundiced infants, this can cause acute bilirubin encephalopathy, a clinical diagnosis characterized by stupor, hypotonia and poor sucking in the first few days followed by fever and hypertonia which, in turn, is followed by diminution and disappearance of hypertonia. The chronic encephalopathy that follows the acute phase is characterized by extrapyramidal disturbance, gaze abnormalities and sensorineural hearing loss, but with only infrequent intellectual deficits [9]. To prevent bilirubin encephalopathy or kernicterus in severely jaundiced newborn infants, the infant can be subjected to exchange transfusions that are aimed at preventing further production of bilirubin, or phototherapy that isomerizes unconjugated bilirubin into water-soluble derivates and facilitates their excretion from the body.

Introduction of phototherapy and its ubiquitous use had virtually eliminated bilirubin encephalopathy and kernicterus by the early 1980s [10]. Although the clinical problem appeared to be solved, of particular interest is the method for evaluting bilirubin concentration.

This is largely due to the fact that serum bilirubin values are regarded as the "gold standard" for clinical decision-making in the absence of better indicators [11]. It has been estimated that approximately 50% of newborns are visibly jaundiced [12], but only about

6% of infants develop significant hyperbilirubinmia (serum bilirubin > 220 μmol/L) and receive phototherapy [13]. For this purpose can be useful the exploitation of CSPT-spectroscopy mode, which is a excellent color detector.

4.3.2 Bilirubin experiment description

In this experiment 9 binary mixtures of hemaglobine and bilirubin have been chosen to cover a wide range of concentration. In Figure 4.1 is shown the concentrations plan for these 9 samples at the following Units (mg/cm^3).

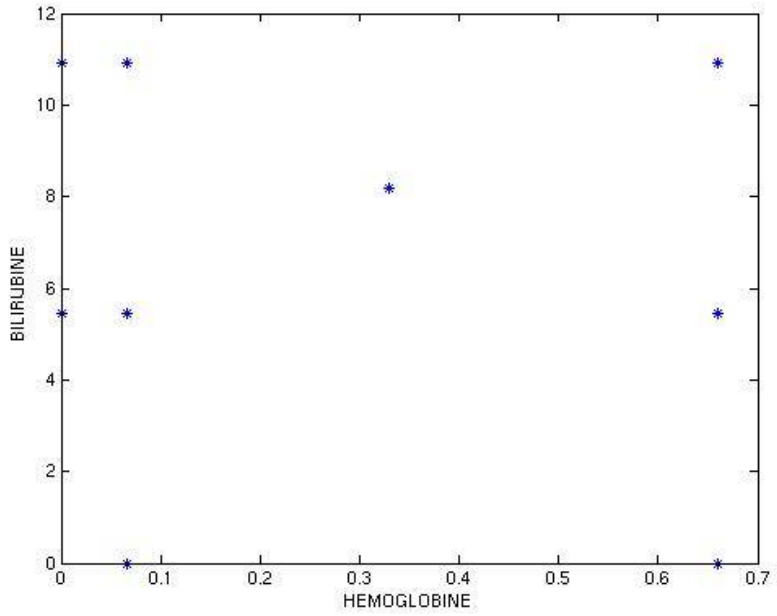

Figure 4.8: Bilirubin and Hemoglobin concentrations plan (mg/cm^3) for samples used during the measurements.

Blood samples are in solution filled capillaries, in random order. Samples are also alternated with empty capillaries and were not arranged in a regular pattern, so regular masks could not be used. The samples were fixed to a sample holder keeping them in between the optical path connecting a computer screen and a webcam. A suitable support properly shielded

from ambient light has been used for keeping tight the geometrical arrangement. In this way all 9 samples were simultaneously measured. The experiments involves a regular LCD screen (Philips 170S4), used as a light source, a Logitech Quickcam pro 4000 operating at a resolution of 320x240 pixels, used as image detector, and a Toshiba SA60-198 laptop. CSPT measurement were performed as described in previous sections, but in this case, for the particular arrangement, a different selection of RoIs has been chosen.

Then a procedure selecting by hand each spot was written in MatLab, and squared average areas (RoIs) were used as can be seen in Figure 4.9. An optical effect limited the extension of the empty capillaries images, not allowing the measure of references.

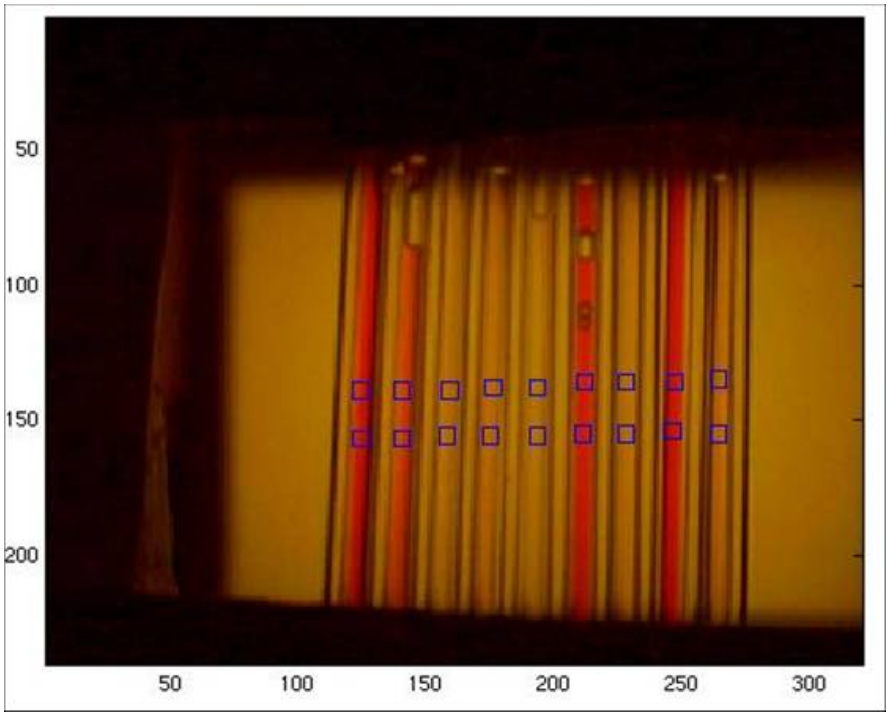

Figure 4.9: A set of blood samples alternated with empty capillaries.

After standard data acquisition by CSPT measurement, for each spot the average of 16 pixels were considered to extract the relative Spectral Fingerprints, that are displayed in Figure 4.10. How it can be seen in Figure 4.9, in this experiment two RoIs for each blood sample have been chosen for evaluating the reproducibility of the measures.

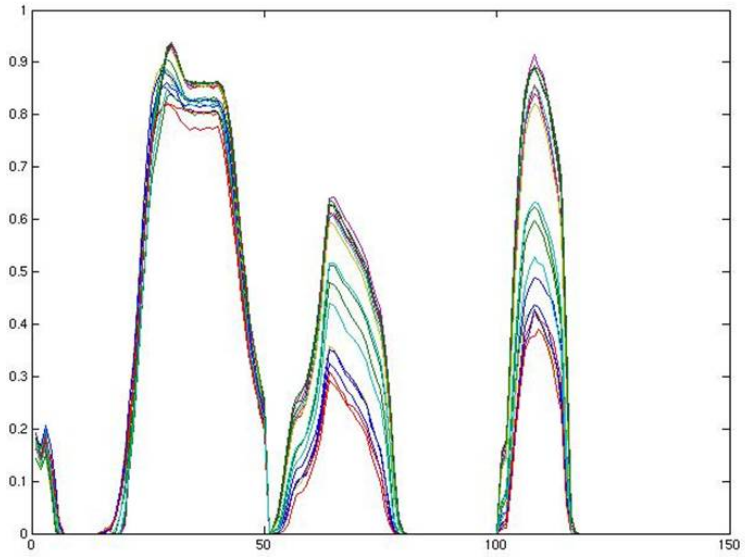

Figure 4.10: Overlapping of all Spectral Fingerprints.

It can be noticed that most of the differences among samples are in the green and blue regions.

4.3.3 Multivariate Analysis of Fingerprints

A PLS model [14] was trained to estimate at the same time the concentration of hemoglobin and bilirubin. The number of latent variables was chosen to minimize the prediction error in a leave-one-out cross-correlation.

Using 6 latent variables has been achieved the following root mean square validation error (RMSECV):

Hemoglobin: 0.024;

Bilirubin: 0.899.

In Figure 4.11 is shown the RMSECV and RMSEC vs latent variable, then the reason of choice of the latent variables number can be understood.

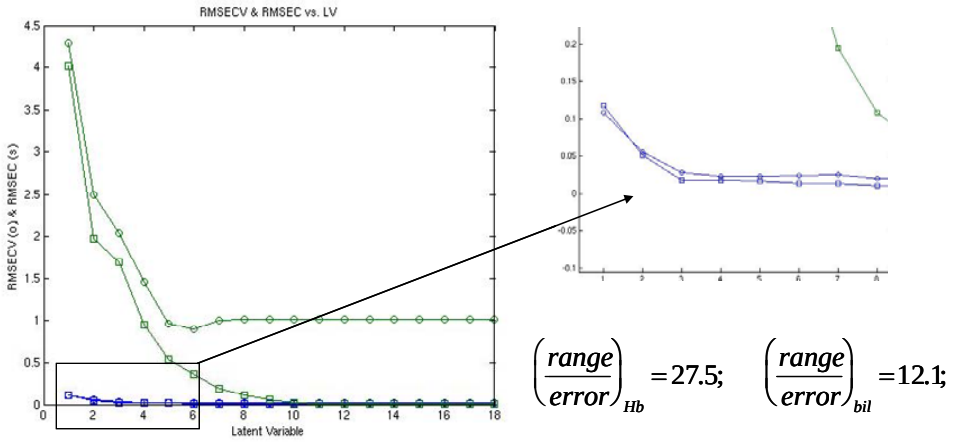

Figure 4.11: RMSECV and RMSEC vs Latent Variable Plan, for the evaluation of Hemoglobin and Bilirubin concentration.

The best results, that have been achieved by using 6 latent variables, are shown in Figure 4.12, where the scatter plots related to these two quantities are displayed.

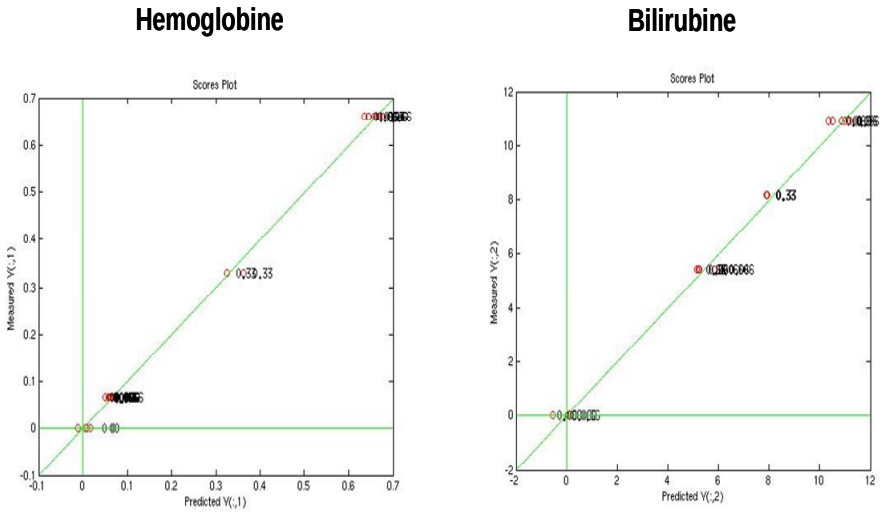

Figure 4.12: PLS model Scatter Plots, for the evaluation of Hemoglobin and Bilirubin at the same time.

PLS model estimating the concentration of Hemoglobin and Bilirubin were optimized by this choice, in this way CSPT has achieved a excellent assessment of these two compounds, as can been easily noticed in the concentrations plan error (Figure 4.13), where the true and

estimated values have been plotted in order to signify the entity of the foreseen uncertainty of estimation.

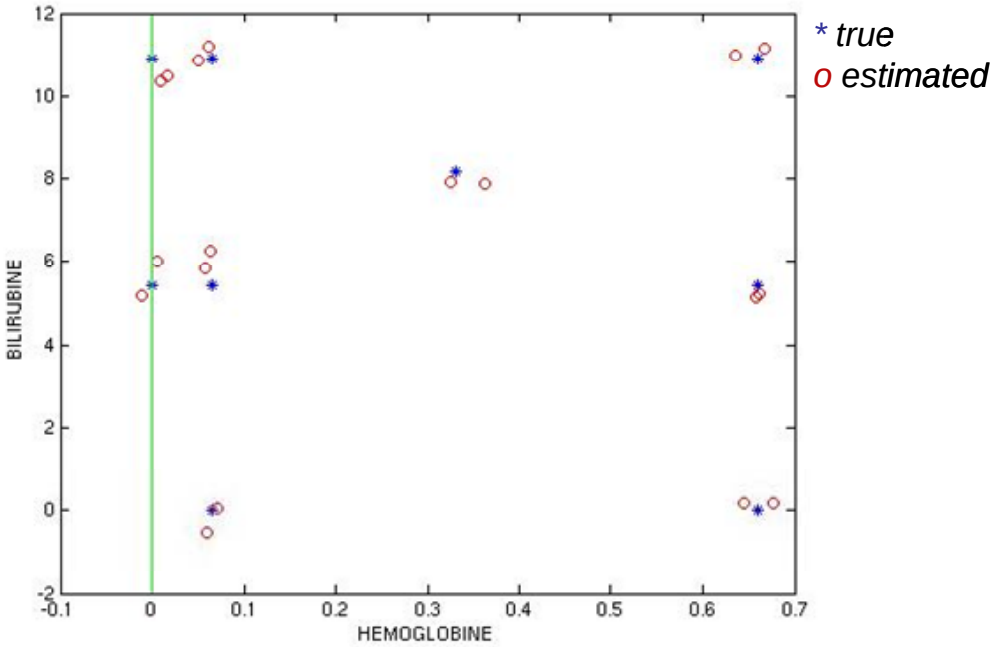

Figure 4.13: Concentrations plane error of Bilirubin and Hemoglobin.

To further underline this good estimation in Figure 4.14 the Score Plot of the first two latent variables of the all fingerprints are shown: the ability of CSPT as a method for practical evaluations is demonstrated, in fact this simple and efficient way to summarize and compare information in complex signals, which explain about 98% of the original information, shows the classification of the considered blood samples for the different tested concentrations. Furthermore it can be noticed that different directions means different contribution of two compounds and that the samples are placed with good orthogonality between hemoglobin and bilirubin samples.

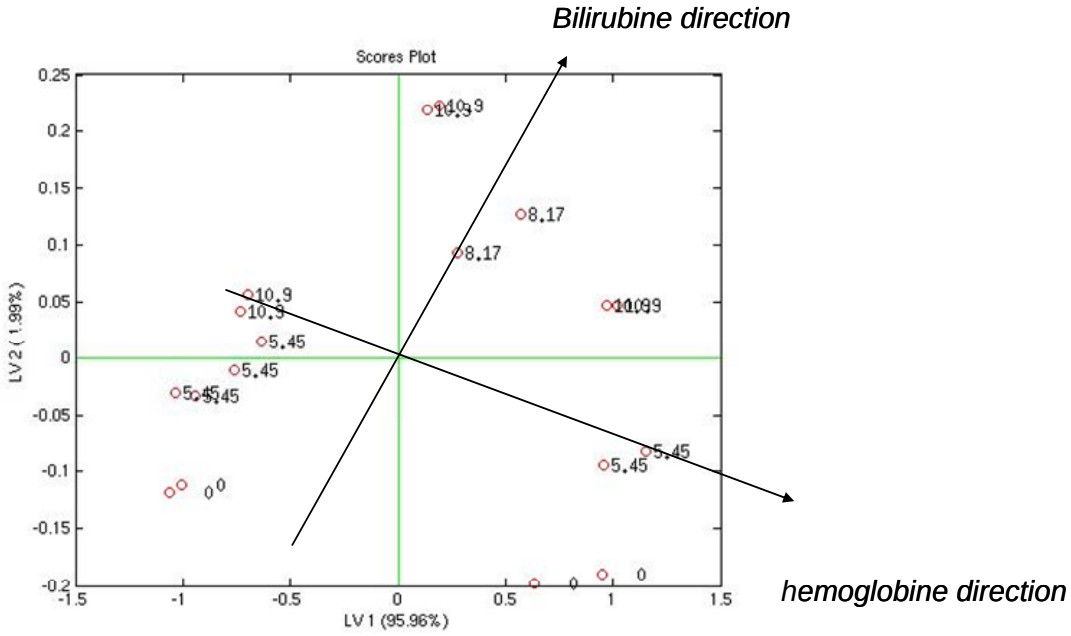

Figure 4.14: Score Plot of first two latent variable.

The BiPlot of the first two latent variable of the PLS-DA model, shown in Figure 4.15, address the correlation of the classification with the 150 loadings (1 to 50 for Red Channel, 51 to 100 for Green Channel and 101 to150 for Blue Channel, of the webcamera used as detector). The loadings of each of the three primary colors are surrounded by a circle. In this graphic, scores that are 100% correlated with a measuring condition lie in the same direction, while perpendicularly oriented elements are not correlated. Thus, become possible identifying the colors that determine the ability of the CSPT fingerprints to distinguish the different compounds. The detection of Hemoglobin, for example, is mainly correlated with the Red and Green channel of Fingerprints. It is also possible to identify a subset of optimum illuminating conditions from Figure 4.15, that could produce a similar , or perhaps even better, result with a shorter color sequence, an important aspect for implementing fast measurements. In fact a great number of loadings are very close to zero, or lie in the same portion of place. In the first case these loadings do not give contribution to haemoglobin and bilirubin detection then these can be removed; in the second case, these kinds of loadings are redundant between them, and only one for each group can be chosen.

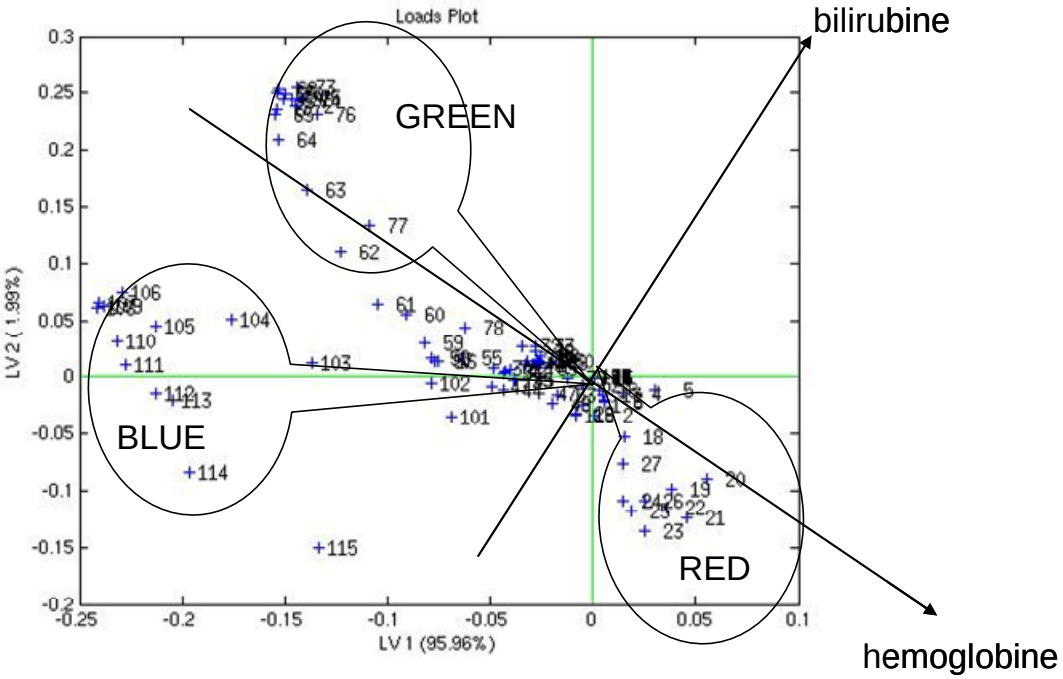

Figure 4.15: BiPlot of first two latent variables.

Then in conclusion, the Computer screen photo-assisted techniques, in further studies also controlled and evaluated via internet, is shown a promising alternative to a generally available instrumental platform for color based medical tests to be performed at primary health care units, pharmacies, service houses for elderly and in individual homes.

REFERENCES

[1] P. Ribéreau-Gayon, Y. Glories, A. Maujean, D. Dubourdieu, Handbook of Enology, Volume 2: The Chemestry of Wine – Stabilization and Treatments, John Wiley & Sons, LTD, 2000.

[2] Y. Glories, La couleur des vins rouges. Ilème partie. Mesure, origine et interpretation. Connaiss. Vigne Vin. 18:253 (1984)

[3] D. Cozzolino, M. Kwiatowksi, M. Parker, W. Cynkar, R. Dambergs, M. Gishen, M. Herdrich, Prediction of phenolic compounds in red wine fermentations by visible and near infrared spectroscopy, *Analytica Chimica Acta*, 513 (2004) 73-80

[4] Di Stefano R., M.C.Cravero,N.Gentilini, ”Metodo per lo studio dei polifenoli dei vini”, L’Enotecnico, 5:83-89 (1989)

[5] J. Bakker, N.W. Preston and C.F. Timberlake, The determination of anthocyanins in aging red wines: comparison of HPLC and spectral methods. Am, J.Enol.Vitic. 37:121 (1986)

[6]. Filippini, S.P.S. Svensson, I. Lundström, Computer screen as a programmable light source for visible absorption characterization of (bio)chemical assays, Chem. Commun. 2 (2003) 240–241.

[7] A. C. Rencher, ‘Methods of Multivariate Analysis’, Wiley-Interscience (2002).

[8] Ahlfors CE. Criteria for exchange transfusion in jaundiced newborns, Pediatrics 1994, 93: 484-494.

[9] Am. Connolly, JJ Volpe, Clinical features of bilirubin encephalopathy. Clin Perinatol 1990; 17: 371-379

[10] LM Gartner, CS Catz, SJ Jaffe, Noanatal bilirubin wokshop, Pediatrics 1994; 94: 537-539.

[11] RL Poland, In search of a "gold standard" for bilirubin toxicity. *Pediatrics* 1992; 89: 823-824.

[12] A. Green**,** I. Morgan, Neonatology and clinical biochemistry. London: Association of Clinical Biochemists, Royal Society of Chemists, 1993

[13] HM. Lewis, RHA Campbell, Hambleton G. Use and abuse of phototherapy for physiological jaundice of newborn infants. *Lancet* 1982; 2: 408412.

[14] B.R. Kowalski and S. Wold; in *Handbook of statistics Vol. 2*, P.R. Krishnaiah and L.N. Kanal eds., North Holland Publ. (Amsterdam, The Netherlands), 1982 pp. 673 – 697.

CHAPTER 5

Further Applications

INTRODUCTION

In this last Chapter some of new preliminary measurements on particular CSPT based on prototypes will be shown. In this moment there are many new measurements that are being developed on different or integrated CSPT platforms, for this reason and for synthesis motive only some of preliminary results will be demonstrated.

5.1. A HYBRID SENSOR ARRAY BASED ON OPTICAL AND MASS TRANSDUCERS

As well as we have seen, Chemical Sensors are devices combining together a chemically sensitive material and a basic transducer. In many cases the kind of transducer is almost obliged, such in the case of metal-oxide semiconductor where the sensing mechanism is better captured measuring the electric conductivity. On the other hand, organic materials offer a manifold of possible transduction mechanisms, and each transduction strategy is also expected to modify the sensing performance in particular in terms of selectivity [1, 2].
Among the organic materials those based on solid-state films of metalloporphyrins have been investigated in recent years for the very high flexibility of the molecule that can be conveniently modified in order to orient the selectivity towards different compound classes. These materials have been used with a number of different transducers measuring e.g. mass, work function, and optical properties [3].
These studies revealed that, since different properties are taken into consideration, each transducer captures a different portion of the interactions that can take place between metalloporphyrin films and volatile compounds. It is then clear that a multiple transduction of the same chemical interaction can give rise to an increased selectivity resulting in a better discrimination either between individual compounds or between similar complex mixtures (odours).

The integration of multiple transducers into a single array has been often hampered by the complexity of transducers. This is the case of integration of optical sensors with other techniques.

As has been demonstrated in the previous Chapters, the recognition of the unexpected properties of consumer devices (CSPT) offered recently the possibility to greatly reduce the complexity of optical measurements [4]. Then in this Section, the integration of quartz microbalance [5] and CSPT [6] based sensor arrays will be discussed, demonstrating that in this hybrid array the discrimination is increased with respect to the use of a single technique.

5.1.1 Measurements Description

Four cross-sensitive materials were considered in the example illustrated here. Three were based on tetraphenylporphyrins (TPP) [7] each functionalized with a different metal atom: Mn, Zn, and Co [8]. The fourth material is based on biladiene [9], a precursor in the porphyrin synthesis route (Figure 5.1).

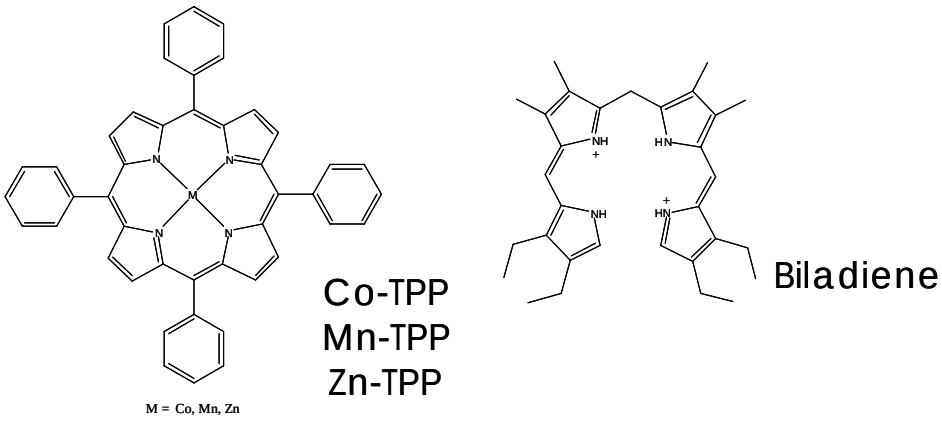

Figure 5.1: Structures of the sensing layers exploited in the experiment.

These molecules were used to coat four QMB (AT-cut, 20MHz of fundamental frequency) and a glass substrate. The QMB and the glass substrate were accommodated in a measurement cell endowed with a gas inlet and outlet. The cell was provided with a glass

lid allowing for the measurement of the optical properties of the sensitive layers deposited onto the glass substrate (Figure 5.2).

For QMB the frequency of the signal generated by oscillators driven by the sensors were measured.

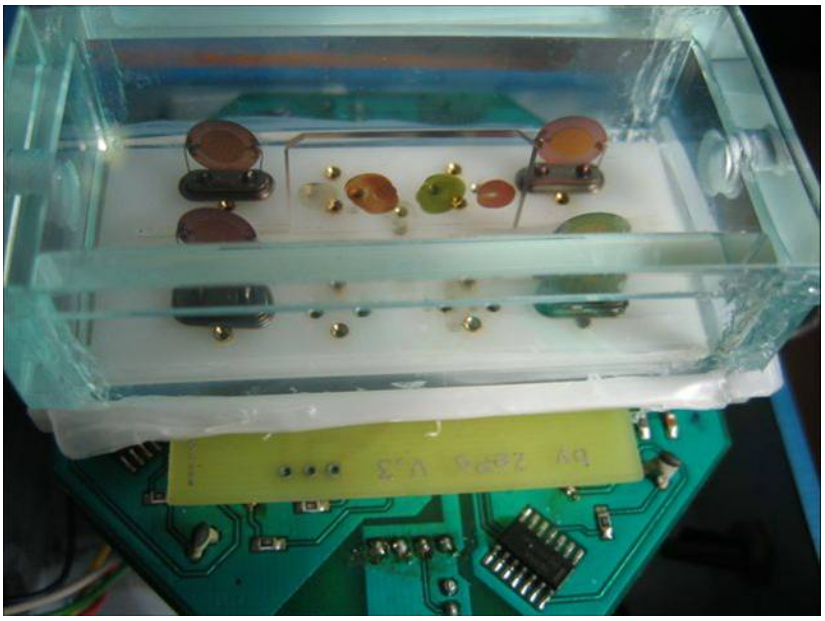

Figure 5.2: Measurements Cell.

CSPT measurement were performed using a sequence of 25 colours combining the red, green, and blue channels of the computer screen. Sensor arrays were exposed to vapours of triethylamine (Et_3N), ethanol (EtOH), and water (H_2O) diluting their saturation pressure at room temperature with nitrogen to the concentrations 10%, 15%, and 20%, respectively.

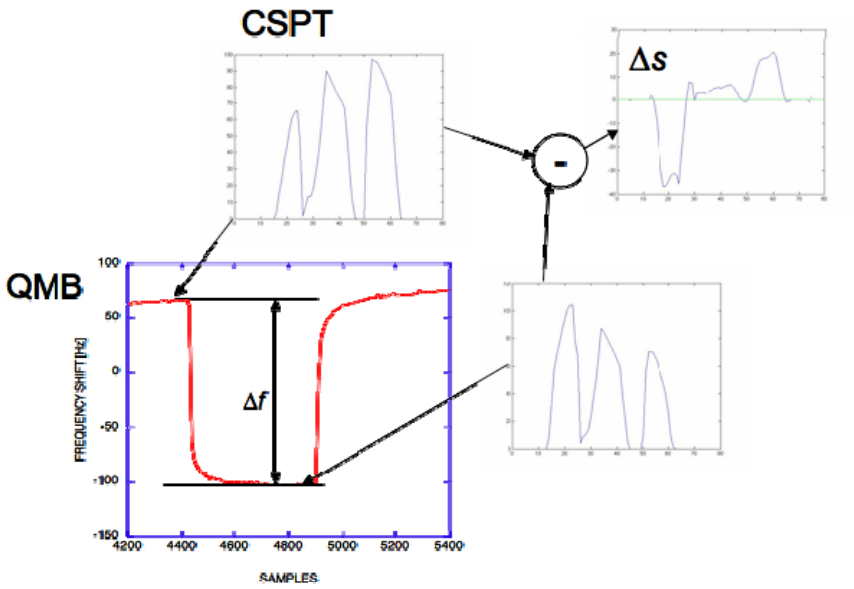

Figure 5.3: Measurement strategy: CSPT spectra were taken in coincidence of the steady state QMB signals.

The measurement strategy is shown in Figure 5.3. CSPT spectra were measured before the sample injection and when the QMB sensors reached the steady condition. Differences between the spectra taken in the two conditions were considered as the CSPT signature of the measurement. Figure 5.4 shows the collected fingerprints calculated as the difference between exposures to test gas and pure nitrogen.

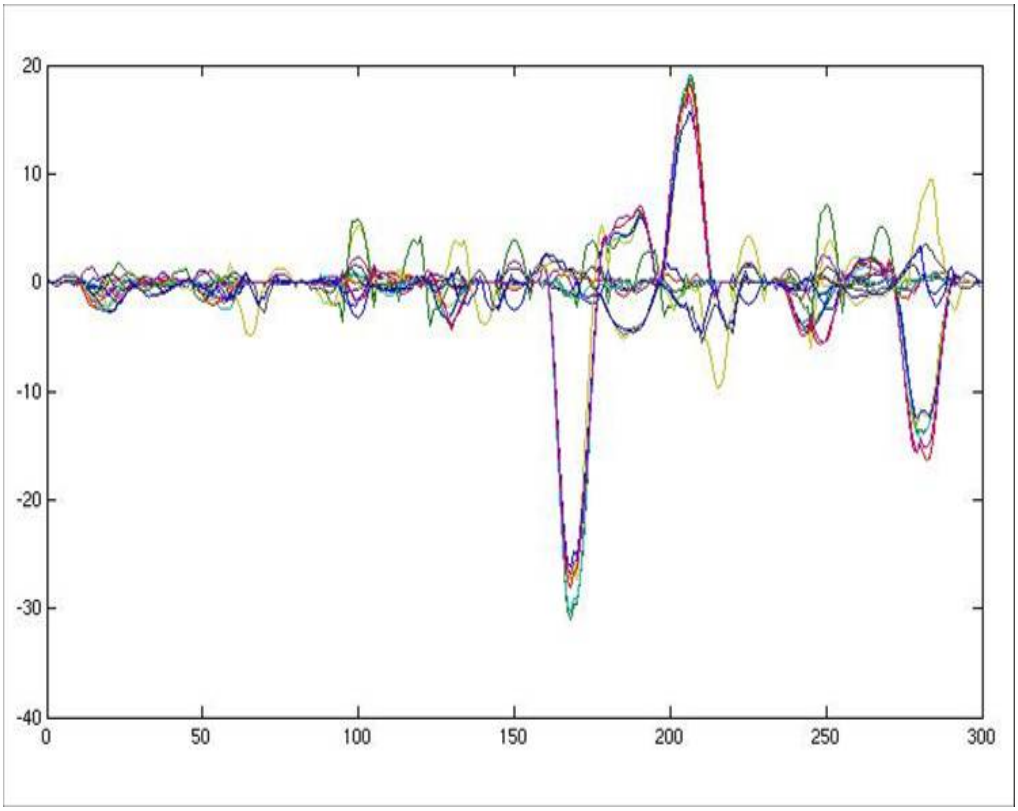

Figure 5.4: Overlapping of all CSPT-Fingerprints

Sensor signals were analyzed using PCA [10, 11]: a very basic tool to inspect multidimensional data. All Data Analysis have been performed in MatLab, PCA has been calculated using the MATLAB PLS TOOLBOX 2.0 (Eigenvector Research Inc.).

5.1.2 QMB features, CSPT-fingerprints and Data Fusion PCA based on Analysis

Figure 5.5 shows the the first two Principal Components of PCA analysis of QMB data. In this Biplot triethylamine (Et_3N) is clearly separated from the other two compounds that are rather confused with each other.

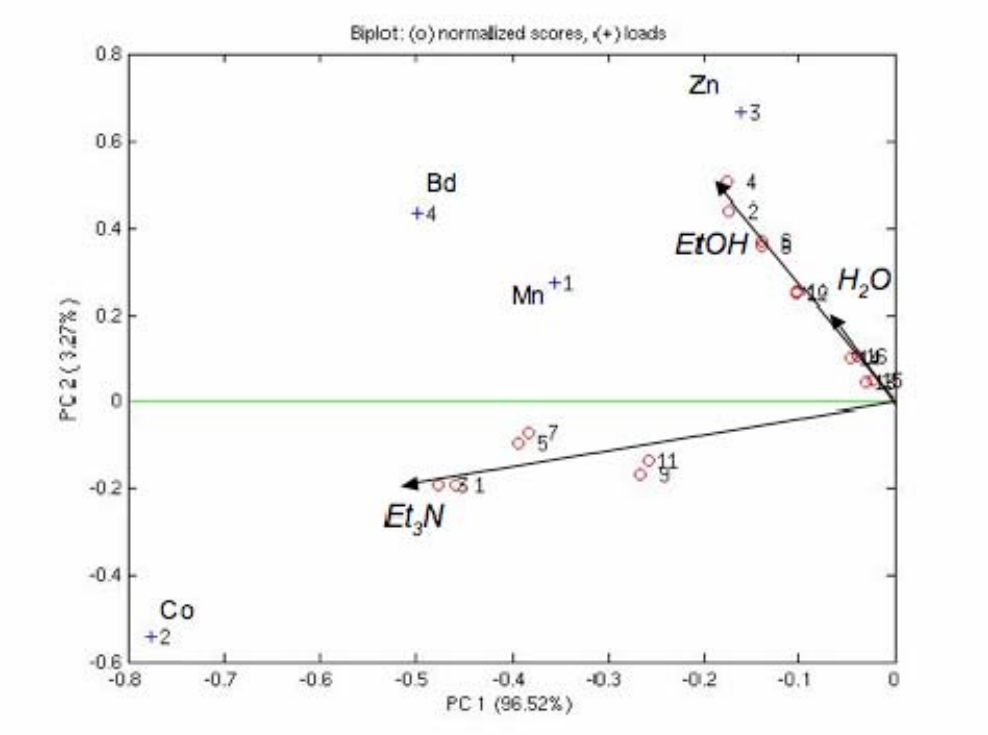

Figure 5.5: Biplot of first two principal components of QMB data.

It is important to observe that the Et_3N axis is at almost 90° from the other two coincident axis. The main role in the separation is played by CoTPP and ZnTPP, as can be seen observing their relative loadings. Figure 5.6 shows the same kind of analysis carried out with CSPT data. In this case, net separation between Et_3N and H_2O occurs while the response to EtOh is very small, confirming previous findings as well as it has been shown in Third Chapter [4].

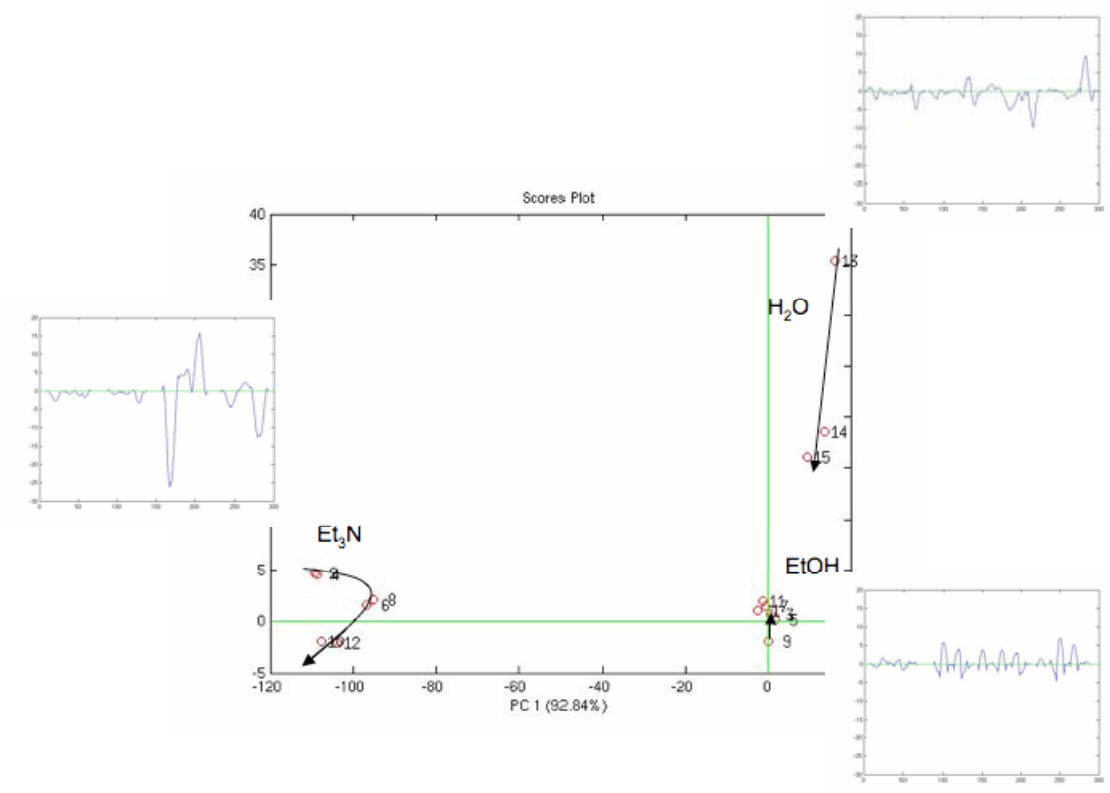

Figure 5.6: Score plot of the first two principal components of CSPT data. For each compound an example of the CSPT spectra changes is also shown.

PCA Loadings indicate a strong contribution of biladiene in the detection of Et_3N while Mn and Co give a dominant contribution to water vapour detection, as can be seen in Figure 5.7.

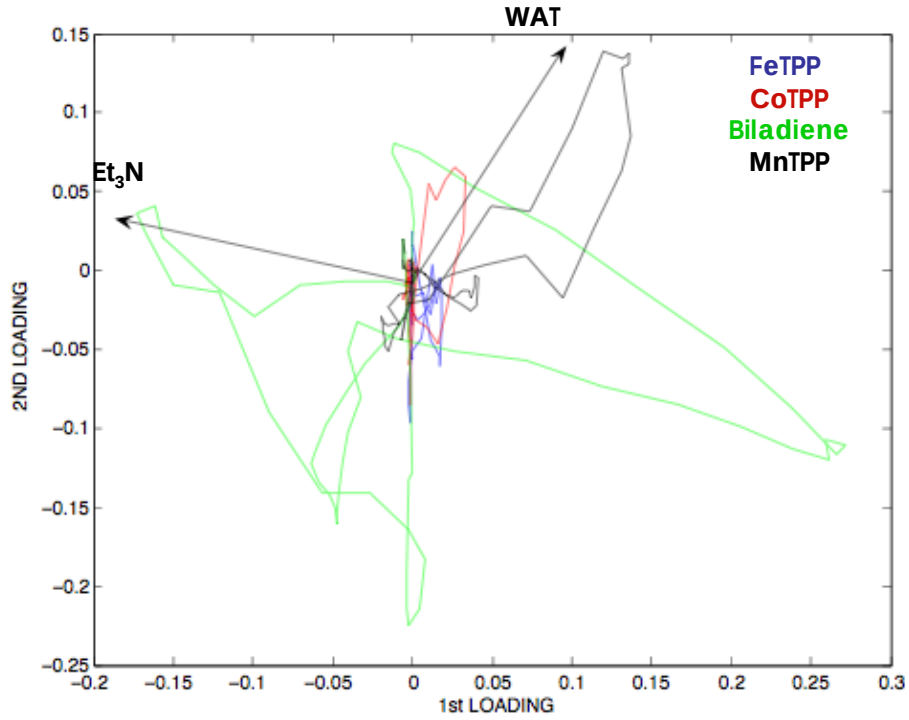

Figure 5.7: CSPT Loadings.

As an example of integration of both the arrays into a hybrid arrays we show the merging of scores of the PCA calculated for each array. Figure 5.8 shows the biplot of the fused data. High level data fusion, obtained fusing PCA scores from both the datasets shows a perfect separation between the three compounds.

This behavior indicates the complementarity of the two transducers putting in evidence that in order to exploit the wide richness of interactions of a complex sensing layer, such as porphyrins, more than one transducer is necessary.

It is interesting to note that QMB and CSPT shares the same first component, namely the largest part of responses depend on the sensing layer while the second components carrying different information is peculiar of the transduction technique. In this case, for instance the detection of water and ethanol and their separation is due to CSPT and QMB respectively.

In the further studies we are going to perform a complete characterization of the combined array by measuring the response of the array to a large set of compounds testing different interaction mechanisms.

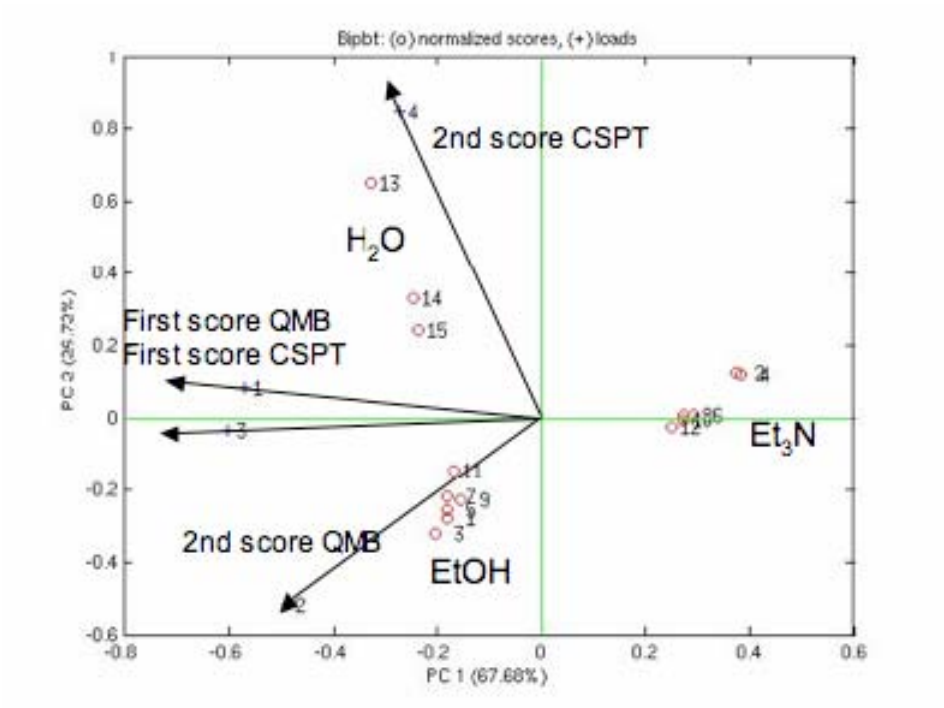

Figure 5.8: Biplot of PCA calculated on the merged scores.

5.2. A PROTOTYPE OF CSPT PLATFORM FOR MOBILE TELEPHONES

The system here illustrated, based on computer peripherals, can be easily scaled to any device endowed with a programmable screen and a camera such as cellular phones offering for the first time the possibility to fulfil the sensor expectation of diffused and efficient analytical capabilities. In this Section a first developing of CSPT platform on a wireless system, a mobile phone, will be shown. The aim of measurements is to demonstrate the possibility of performing the CSPT on a wireless system to detect volatile compounds. In these measurements it is also pointed out the possibility of exploiting a environmental light like light source for the CSPT, in fact as been shown in the First Chapter, the illuminating sequence provided by a programmable area of a LCD screen is essentially redundancy [12]. The only aim of this redundancy colors sequence has been achieving better measurements than ones performed using the only three primary colors, because consumer devices exploited in the CSPT system are noisy and randomly assembled instrumentations. Using this method has been demonstrated a improvement of CSPT performances. But in this case, a threechromatic filter of environmental light has been shown enough to detect volatile molecules.

5.2.1 Measurements description

For this purpose a Nokia N70 mobile phone has been used to implement the CSPT. There have been specific modifications for implementing the CSPT platform for this particular mobile phone. First of all the measurement cell has been adapted to the webcam of the Nokia N70, and has been decreased in the dimensions and changed in the geometrical shape (Figure 5.9).

Figure 5.9:CSPT prototype for mobile phone.

For these preliminary measurements only two CIMs strips have been selected for their cross-sensitivity properties respect to the compounds under investigation: (5,10,15,20-tetraphenylporphyrin)zinc ([Zn(tpp)]) and and 2,3,17,18-tetraethyl-7,8,12,13-tetraamethyl-a,c-biladiene dihydrobromide (BD) dispersed in a polyvinylchloride (PVC) matrix [13] and spotted on a glass slide (Figure 5.10).

Figure 5.10:Two different strips of CIMs spotted on a side of a round glass.

A threechromatic filter (Red, Green and Blue), after an spectral characterization by a spectrophotometer for choosing the best matching ones, has been applied in front of

measure cell (Figure 5.11). In this way the two CIMs strips are orthogonal to the three colored filters, and so becomes possible making the measure only by a simple picture instead of a video stream [14]. In fact in the same picture there are information about all the three primary colors over all the CIMs, because they are orthogonally overlapped at the same time.

Figure 5.11: Three colored filters (Red, Green and Blue), applied on the external side of measurements glass. On the other side are visible the two CIMs strips.

In the Figure 5.12 is shown a prototype of this kind of CSPT platform within a Nokia N70 cellular phone.

Figure 5.12: A CSPT prototype in front of the webcam of a Nokia N70 mobile phone.

The experiments have been made using a mass flow control system to mix the volatile compounds carried by a nitrogen flux.

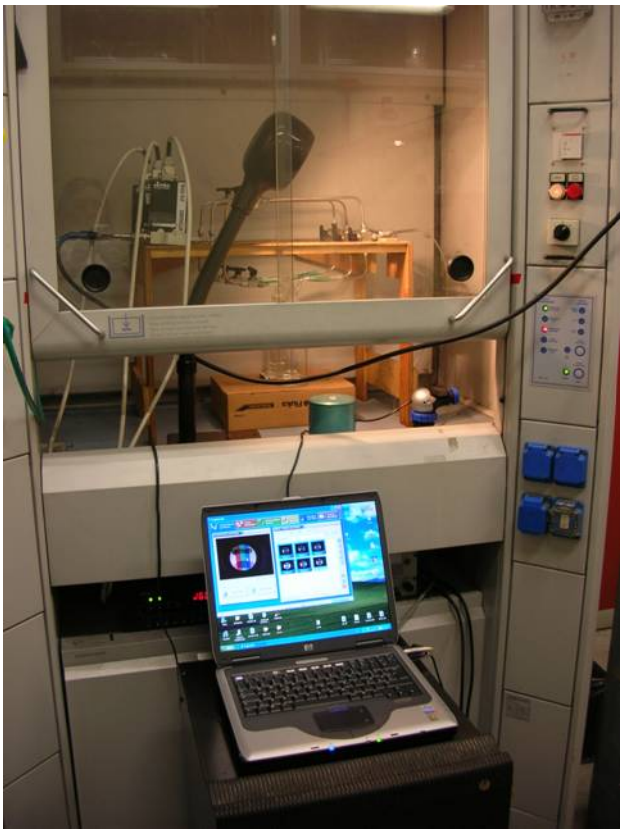

Figure 5.13: Experiments setup: a mass flow control system, a Nokia N70 within a CPT platform and a laptop computer for remote data elaboration.

A software written by me in Visual Basic for the Nokia N70, controls the automatic data acquisition, and sends them to a remote laptop for data elaboration. We are going to perform a complete characterization of this CSPT platform by measuring the response of the array to a large set of compounds. In this Section only the primary best results for the detection of Triethylamine are reported. The array was exposed to different concentrations of TEA from 1% to 20%, showing a good sensitivity, how can be seen simply watching the Figure 5.14 (the differences are also visible by human eye). During all the measurements the array has shown a good reversibility.

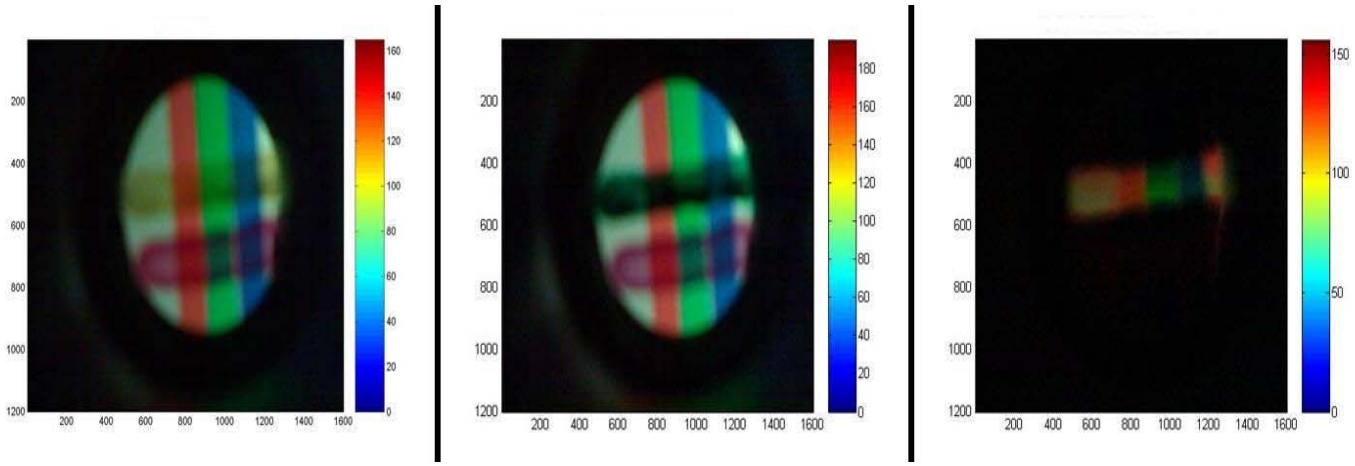

Figure 5.14: Pictures of the array of the CIMs overlapped to the three color filters; a) a picture upon nitrogen flux; b) a picture upon exposure to 10% of TEA; c) colors difference between previous two photos.

REFERENCES

[1] A. D'Amico, C. Di Natale, R. Paolesse, A. Macagnano, Metalloporphyrins as basic material for volatile sensitive sensors. *Sensors and Actuators B* 65 pp 209-215, 2000

[2] C. Di Natale, R. Paolesse, D.. Salimbeni, A. Macagnano, A. Mantini, A. D'Amico; Optoelectronic nose based on absorbance variations in porphyrin films, *Proc. Of the 5" International Symposium on Olfaction and Electronics Nose*, Baltimore, MD, USA, 30 Sept. 1998

[3] R. Paolesse, F. Mandoj, C. Di Natale, Porphyrins based chemical sensors, in Nalwa (ed.) *Encyclopedia of nonoscience*, APS, 2003

[4] D. Filippini, A. Alimelli, C. Di Natale, R. Paolesse, A. D'Amico, I. Lundström; Chemical sensing with familiar devices, Angewandte Chemie Int. Ed. 45 (2006) 3800-3803

[5] Di Natale C, Paolesse R, Macagnano A, Mantini A, Goletti C and D'Amico A. *Sens. Actuators, B* 1998; B52: 162-168.

[6] D. Filippini, S.P.S. Svensson, I. Lundstrom, Computer screen as a programmable light source for visible absorption characterization of (bio)chemical assays, Chem. Commun. 2 (2003) 240–241.

[7] R. Paolesse in The Porphyrin Handbook, Vol. 2 (Eds.: K. M. Kadish, K. M. Smith, R. Guilard), Academic Press, San Diego, 2000, p. 201.

[8] C. Di Natale, R. Paolesse, A. Macagnano, A. Mantini, P. Mari, A. D'Amico, Qualitative structure-sensitivity relationship in porphyrins based QMB chemical sensors, *Sensors and Actuators B* 68 (2000) 319-323.

[9] R. Paolesse, A. Froiio, S. Nardis, M. Mastroianni, M. Russo, D. J. Nurcob and Kevin M. Smith, Novel aspects of the chemistry of 1,19-diunsubstituted a,cbiladienes, Journal of Porphyrins and Phthalocyanines, 2003; 7: 585-592, Published at http://www.u-bourgogne.fr/jpp/

[10] B.R. Kowalski and S. Wold; in *Handbook of statistics Vol. 2*, P.R. Krishnaiah and L.N. Kanal eds., North Holland Publ. (Amsterdam, The Netherlands), (1982) pp. 673 – 697.

[11] C. Di Natale, Lectures Notes of Sensors and Detectors at the University of Rome 'Tor Vergata'.

[12] Filippini D. and I. Lundström, Preferential color substances and optimized illuminations for computer screen photo-assisted classification. Analytica Chemica ACTA, 557 (1-2), January 2006, 393-398

[13] C. Behringer, B. Lehmann; J.-P. Haug, K. Seiler, W.E. Morf, K. Hartmann, W. Simon; Anal. Chim. Acta 1990; 233; 41-47

[14] D. Filippini, I. Lundstrom, Measurement strategy and instrumental performance of a computer screen photo-assisted technique for the evaluation of a multi-parameter colorimetric test strip, Analyst. 2006 Jan;131(1):111-7. Epub 2005 Nov 23.

List of publications

Papers related to the thesis subject

Referenced Journals

- A. Alimelli, G. Pennazza, M. Santonico, R. Paolesse, D. Filippini, A. D'Amico, I. Lundstrom, C. Di Natale; "Fish Freshness Detection by a Computer Screen Photoassisted Based Gas Sensor Array", *Analytica Chimica Acta* 582 2007 320-328.
- D. Filippini, A. Alimelli, C. Di Natale, R. Paolesse, A. D'Amico, I. Lundström; "Chemical sensing with familiar devices", *Angewandte Chemie Int. Ed. Engl* 45 2006 3800-3803
- J. Spadavecchia, R. Rella, P. Siciliano, A. Manera, A. Alimelli, R. Paolesse, C. Di Natale, A. D'Amico; "Optochemical vapour detection using spin coated thin film of ZnTPP", *Sensors and Actuators B* 115 2006 12-16
- D. Filippini, C. Di Natale, R. Paolesse, A. Alimelli, A. D'Amico, I. Lundström, "Modeling of computer screen photo-assisted excitation-emission fingerprints"-*Applied Physics Letters*, submitted
- A. Alimelli, R. Paolesse, S. Moretti, L. Ciolfi, D. Filippini, A. D'Amico, I. Lundstrom, C. Di Natale; "Computer Peripherals as Analytical Instruments: the case of red wine", *manuscript in preparation*

International conferences

- Di Natale, D. Filippini, A. Alimelli, G. Pennazza, M. Santonico, A. D'Amico, R.Paolesse, I. Lundström; Ubiquitous chemical sensing for ubiquitous environments; *ICRA 07 Workshop on Robotic Olfaction*, Rome 14-4-2007
- D. Filippini, C. DiNatale, R. Paolesse, A. Alimelli, A. d'Amico, I. Lundström,"Home and Global (Bio) Chemical Sensing with Computer Screen Photo-Assisted Techniques", - *11th World Congress on Internet in Medicine* (MEDNET 2006) Toronto (Canada) 13-20 Oct. 2006
- C. Di Natale, G. Pennazza, M. Santonico, A. Alimelli, R. Paolesse, A. D'Amico, D. Filippini, I. Lundstrom, "A hybrid sensor array based on optical and mass transducers", - *Eurosensors XX*, Goteborg (Sweden) 17-20 Sep 2006
- Alimelli, R. Paolesse, A. D'Amico, D. Filippini, I. Lundström, C. Di Natale; "Fish Freshness Identification by a Computer Screen Photoassisted Sensor Array", - *XI International Meeting on Chemical Sensors*, Brescia (Italy) 16-19 Jul 2006
- D. Filippini, C. Di Natale, R. Paolesse, Alimelli, A. D'Amico, I. Lundström, "Disposable e-nose based on spectral fingerprinting using a computer screen photo assisted technique", - *XI International Meeting on Chemical Sensors*, Brescia (Italy) 16-19 Jul 2006
- F. Mandoj, A. Alimelli, D. Filippini, G. Verrelli, S. Nardis, A. Micozzi, C. Lo Sterzo, A. D'Amico, R. Paolesse, I. Lundström, C. Di Natale, "Zinc-porphyrin conjugated polymer: a novel and versatile sensing material", - *XI International Meeting on Chemical Sensors*, Brescia (Italy) 16-19 Jul 2006
- D. Filippini, A. Alimelli, C. Di Natale, R. Paolesse, A. D'Amico and I. Lundström, "CSPT fingerprinting of molecular interactions with porphyrins", - Journal of Porphyrins and Phthalocyanines 10 2006 448 *4th International Conference on Porphyrins and Phthalocyanines* Rome (Italy) 2-7 Jul 2006

- D. Monti, R. Paolesse, M. Stefanelli, A. Alimelli, C. Di Natale, A. Macagnano, A. D'Amico; "Development of chemical sensors based on amphiphilic porphyrin aggregates", - *Synthetic Receptors 2005* Salzburg (Austria) 7-9 Sep. 2005
- C. Di Natale, R. Paolesse, A. Alimelli, A. Macagnano, A. D'Amico, "Development of Porphyrins based sensors to measure the biological damage of carbon monoxide exposure" - *IEEE SENSORS CONFERENCE* Toronto 22-24 October, 2003

National Conferences

- A. Alimelli, R. Paolesse, A. D'Amico, C. Di Natale,, D. Filippini, I. Lundström, "Development of chemical sensors based on computer screen photoassisted technology" - *AISEM 2006* Lecce February 8-10 2006

Papers related to other scientific activities

Referenced Journals

- R. Paolesse, C. Di Natale, A. D'Amico, E. Martinelli, A. Alimelli, M.G. D'Egidio, G. Aureli, C. Fanelli, A. Ricelli; "Detection of fungal contamination of cereal grain samples by an electronic nose", *Sensors and Actuators B* 119 2006 425-430

International conferences

- M.Stefanelli, D.Monti, A. Alimelli, G.Pomarico, A. D'Amico, C. Di Natale, R.Paolesse, "Development and testing of new sensitive material based on metalloporphyrin-resorcinarene coniugate", - *XI International Meeting on Chemical Sensors*, Brescia (Italy) 16-19 July 2006
- G. Pomarico, R. Paolesse, A. Alimelli, E. Martinelli, A. Macagnano, E. Sgreccia, C. Di Natale, A. D'Amico, "Exploitation of 5,10,15,20 – Tetrakis (2,6-dimethoxyphenyl) porphyrin metal derivatives as coating material of quartz microbalances", - *4th International Conference on Porphyrins and Phthalocyanines* Rome (Italy) 2-7 Jul 2006
- M. Stefanelli, D. Monti, A. Alimelli, G. Pomarico, A. D'Amico, C. Di Natale, R. Paolesse, , "Development and testing of new sensitive material based on metalloporphyrinresorcinarene conjugated", - *XI International Meeting on Chemical Sensors*, Brescia (Italy) 16-19 July 2006
- *A. Alimelli, S. Nardis, I. Di Leonardo, F.M. Bucarelli, G. quaglia, G. Pennazza, R. Paolesse C. Di Natale, D'Amico,* "Optimization of coffe roasting time and blends preparation with an electronic nose", - Eurosensors XIX Barcelona Sep 2005

- R. Paolesse, C. Di Natale, E. Martinelli, A. Alimelli, M.G.D'Egidi, G. Aureli, C. Fanelli, A. D'Amico; "Exploitation of an electronic nose for the detection of fungal contamination of grain", - *ISOEN 2005* Barcelona 11-14 April 2005
- B. Crociani, S. Antonaroli, C. Di Natale, R. Paolesse, S. Nardis, A. Marini, A. Alimelli, A. D'Amico; "Exploitation of Rh(I) complexes for high sensitive carbon monoxide sensors", *Eurosensors XIX* Barcelona Sep 2005

National Conferences

- *M. Stefanelli, D. Monti, G. Pomarico, A. Alimelli, R. Paolesse, "*Resorcinarene-porphyrin conjugate: a new ditopic receptor for chemical sensors", - *AISEM 2006* Lecce February 8-10 2006
- M.Mastroianni, R. Paolesse, A. Alimelli, , C. Di Natale, A. D'Amico, "Exploitation of substituted porphyrin films for gas sensors development", - *AISEM 2006* Lecce February 8-10 2006
- R. Paolesse, A. Alimelli, S. Nardis, G. Pomarico , E. Sgreccia, A. Macagnano, E. Martinelli, C. Di Natale, A. D'Amico, "Exploitation of 5,10,15,20-tetrakis (2,6 dimethoxyphenyl) porphyrin metal derivatives as coating material of quartz microbalances", - *AISEM 2006* Lecce February 8-10 2006
- R. Paolesse, S. Nardis, A. Alimelli, E. Martinelli, C. Di Natale, A. D'Amico , M. G. D'Egidio, G. Aureli, M. Epifani, A. Ricelli, C. Fanelli, "Detection of fungal contamination of cereal grain samples by an Electronic Nose" - *AISEM 2005* Firenze 15-17 February 2005
- S. Antonaroli, A. Marini, R. Paolesse, B. Crociani, A. D'Amico, A. Alimelli, C. Di Natale, "Development of chemical sensors based on Rh(I) and Pd(II) Complexes", - *AISEM 2004* February 8-11 Ferrara